

# Soft Actuators for Soft Robotic Applications: A Review

Nazek El-Atab, Rishabh B. Mishra, Fhad Al-Modaf, Lana Joharji, Aljohara A. Alsharif, Haneen Alamoudi, Marlon Diaz, Nadeem Qaiser, and Muhammad Mustafa Hussain\*

Soft robotics technologies are paving the way toward robotic abilities which are vital for a wide range of applications, including manufacturing, manipulation, gripping, human-machine interaction, locomotion, and more. An essential component in a soft robot is the soft actuator which provides the system with a deformable body and allows it to interact with the environment to achieve a desired actuation pattern, such as locomotion. This Review article aims to provide researchers interested in the soft robotics field with a reference guide about the various state-of-the-art soft actuation methodologies that are developed with a wide range of stimuli including light, heat, applied electric and magnetic fields with a focus on their various applications in soft robotics. The underlying principles of the soft actuators are discussed with a focus on the resulting motion complexities, deformations, and multi-functionalities. Finally, various promising applications and examples of the different soft actuators are discussed in addition to their further development potential.

## 1. Introduction

The compliant, continuum, and configurable robotics field in general has gained growing interest in the past years especially with the exciting advances in artificial intelligence technology,<sup>[1]</sup>

Dr. N. El-Atab, R. B. Mishra, M. Diaz, Dr. N. Qaiser, Prof. M. M. Hussain  
 mmh Labs  
 Electrical Engineering, Computer Electrical Mathematical Science and Engineering Division  
 King Abdullah University of Science and Technology (KAUST)  
 Thuwal 23955-6900, Saudi Arabia  
 E-mail: Muhammad.Hussain@kaust.edu.sa, mmhussain@berkeley.edu

R. B. Mishra  
 Center for VLSI and Embedded System Technology (CVEST)  
 International Institute of Information Technology (IIIT)  
 Hyderabad, Telangana 500032, India

F. Al-Modaf, L. Joharji, A. A. Alsharif, H. Alamoudi  
 Department of Engineering  
 King Abdulaziz University (KAU),  
 Jeddah 21589-80200, Saudi Arabia

Prof. M. M. Hussain  
 Electrical Engineering and Computer Sciences (EECS)  
 University of California  
 Berkeley, CA 94720, USA

 The ORCID identification number(s) for the author(s) of this article can be found under <https://doi.org/10.1002/aisy.202000128>.

© 2020 The Authors. Published by Wiley-VCH GmbH. This is an open access article under the terms of the Creative Commons Attribution License, which permits use, distribution and reproduction in any medium, provided the original work is properly cited.

DOI: [10.1002/aisy.202000128](https://doi.org/10.1002/aisy.202000128)

which could enable various valuable applications ranging from manufacturing to safety and healthcare.<sup>[2,3]</sup> Soft robots are of notable interest because, unlike their rigid counterpart, they can easily deform while being mechanically resilient,<sup>[4,5]</sup> adapt to the outer environment without harm to humans,<sup>[6]</sup> and finally, enable low-cost manufacturing.<sup>[7]</sup> For robots to interact with the outer environment and complete tasks, a set of sensors and actuators need to be integrated into the system. Soft robots, in specific, present additional challenges because their sensing and actuation devices are generally highly integrated within the body of the robot and its whole functionality. These challenges become even more critical when the soft robot is scaled down to sub-centimeter size as the sensing, power, and data analysis units are moved off-board. As a result, miniaturized soft actuators that respond to various stimuli and show large deformations in addition to mechanical resilience are crucial. These would be particularly promising for application in artificial muscles, microrobots, and micro-manipulators.<sup>[8–10]</sup>

Active and soft materials are promising for this task as they can be actuated through various external stimuli, such as photons, thermal, magnetic and/or electric field. Such materials range from particles, to polymers (either electroactive or shape memory), papers, fluids, shape memory alloys (SMAs), liquid metals, hydrogels, 2D materials, or a combination of these.<sup>[6–25]</sup> Nevertheless, some materials can be more suitable for a specific set of applications than others; for instance, materials stimulated by the near-infrared (NIR) spectrum are promising for biomedical applications, whereas sunlight-stimulated materials are suitable for nature-inspired soft robots used in outside environments. Various useful metrics are generally used to assess the performance of the actuators; these include the generated stress and strain, Young's modulus or measured stiffness, in addition to their power, work, energy, and force density. In this Review article, however, we focus on the application of the soft actuators in soft robotics where the reported metrics include mode and speed of actuation (or locomotion), power, voltage, current (of the driving signal), lifting force, and weight among others.

In this Review article, different active materials that have been developed and used in soft actuators for soft robotics are discussed and grouped by the stimulus that generates the actuation response as shown in **Figure 1**. The physics of operation, resulting deformations, mechanical resilience, and their pros and cons are presented with a focus on the applications of the different soft

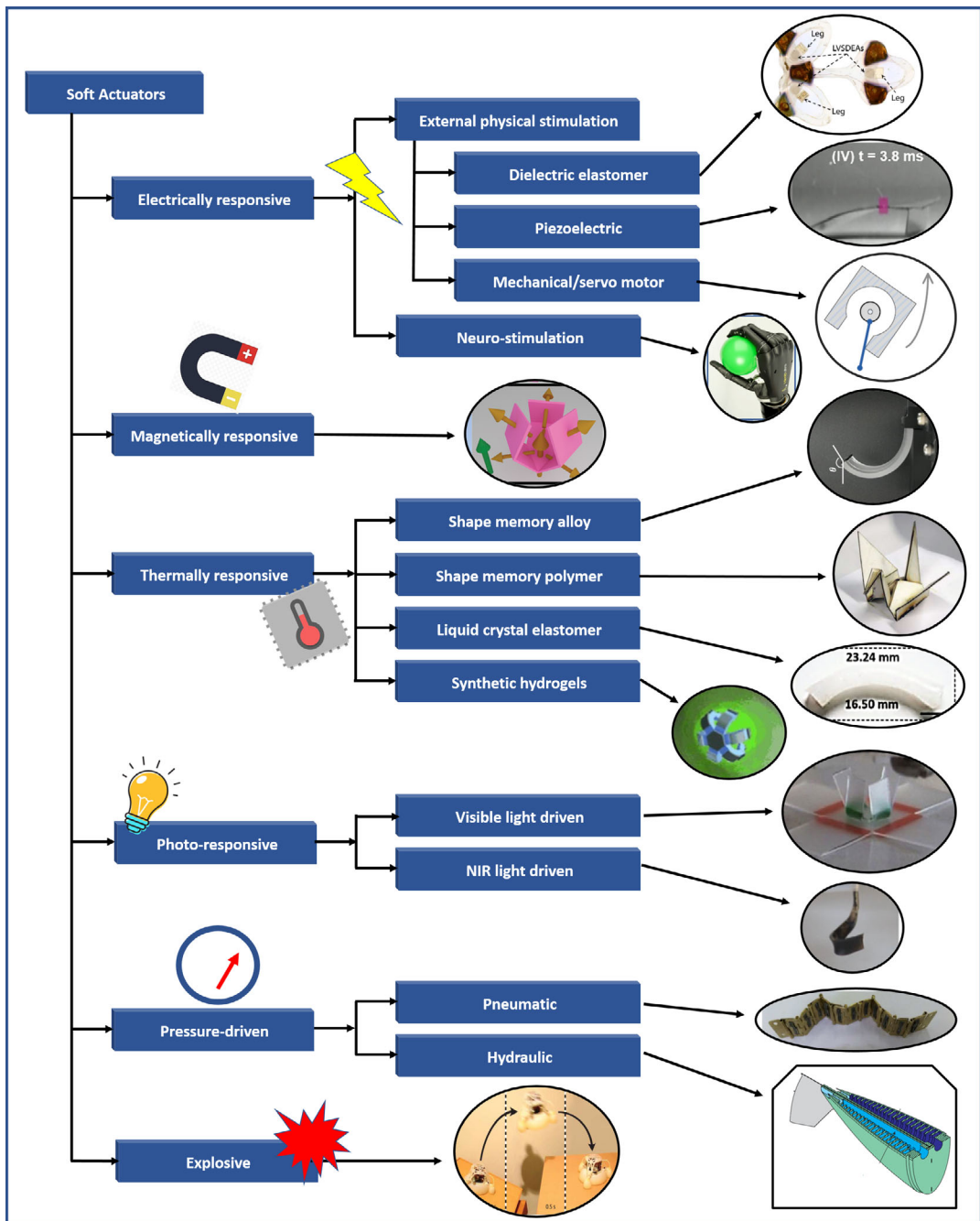


**Figure 1.** Chart showing the different classes of soft actuators discussed in this review article and divided based on the stimulation type.

actuators. The suitability of each material in different applications is explained with detailed examples. Finally, the further development potential of the presented soft actuators is analyzed.

### 1.1. Why Rigid to Soft Actuators?

The advancements in integrated circuit (IC) technology emerged micro-electro-mechanical systems (MEMS) which made the integration of sensors/actuators with printed circuit boards (PCBs) possible. The remarkable article entitled *Silicon as*

*Mechanical Material* by K. E. Petersen et al.,<sup>[26]</sup> suggested that silicon is the basic material for MEMS to be able to design highly precise and reliable miniaturized versions of sensors/actuators. The sensors/actuators consist of mechanical and electrical elements whose output/operation vary under different physical, chemical and/or biological stimuli. The micro-mechanical elements in MEMS which can be batch-fabricated include cantilevers, diaphragms/plates, joints, springs, grippers, switches, gears, rotary motors and resonators, and have different attractive features in terms of compatibility, performance, and

sensitivity.<sup>[27,28]</sup> The MEMS market is very revolutionized, however, it requires clean-room fabrication facilities which increases the cost and development time of sensors/actuators. Moreover, the MEMS-based devices are naturally rigid which poses a major challenge for application on unconventional and unstructured surfaces, nevertheless, flexibility and compliance are needed due to the wide range of potential applications in electronic skin, soft robotics, and implantable/wearable devices in the modern era.<sup>[28–32]</sup> As a result, several active, soft, flexible, and stretchable materials have shown potential in soft actuation applications as will be discussed in this Review article. The considered active materials and corresponding stimuli in this Review article are shown in Figure 1.

## 2. Overview of Methods for Soft Actuators

### 2.1. Electrically Responsive Actuation

There exist plenty of soft, flexible, and stretchable materials which are capable of transforming electrical energy into mechanical energy. These include liquid metals, memory alloys, polymers, fluids, gels, paper, and even carbon-based materials, such as stand-alone carbon nanotubes (CNTs). The electronic signals that drive the actuators enable simple and fast modulation of the signal phase, magnitude, and frequency. In addition, as these actuators are compatible with traditional electronic devices, they can be easily integrated with energy devices and electric drivers. The range of applications is unlimited; some of the greatest research fields are found in artificial muscles,<sup>[33–35]</sup> microrobots,<sup>[36,37]</sup> microscale object manipulation,<sup>[38]</sup> and microfluidic systems.<sup>[39–41]</sup> In the following, we will discuss the two specific types of electrically responsive actuators that have been widely used—dielectric elastomers and servomotor-based mechanical actuators. Finally, neural-stimulated actuators, which are considered electrical responsive actuators, will be introduced and explained.

#### 2.1.1. Dielectric Elastomer Actuators

The operation of dielectric elastomer actuators (DEAs) is based on Coulombic attraction between two flexible electrodes with a potential difference that are located on separate ends of a compressible membrane. DEAs are very flexible, show high energy density, high strains, exhibit self-sensing characteristics, have accurate simulation models,<sup>[42]</sup> and have been demonstrated to be as useful as biological muscles.<sup>[35,43]</sup> Moreover, the performance of DEAs is in function to the steadiness, the breakdown voltage, and the dielectric constant of the elastomer. Nevertheless, DEAs' disadvantages consist of the large voltages required to operate them (in kV) and leakage currents, both of which result in easier to reach electrical breakdown.<sup>[44,45]</sup>

Acrylic elastomers, silicones, polyurethanes (PUs), and rubber are typical membrane materials with varying performance characteristics. Acrylic elastomers, which include the very common VHB4910 elastomer, can achieve quite large deformations; however, they are enormously viscoelastic, which could limit the actuators bandwidth. Silicone-based and PU-based elastomers show faster reaction and have the ability to be cast into various

shapes and softness; however, the produced strain is significantly lower. Moreover, generally, silicone-based elastomers exhibit reduced permittivity that results in a higher required activation voltage as compared with PUs and acrylic elastomers.<sup>[46]</sup> Currently, a lot of research is being conducted to enhance DEA performance in terms of increasing the dielectric constant of the membrane by either embedding microparticles<sup>[45,47]</sup> or developing completely organic elastomers.<sup>[41]</sup>

DEAs could be used in different ways, including stacking, folding, framing, inflating, or rolling them. They can also be bent, expanded or buckled, which increases their range of applications. For instance, Jung et al. stacked millimeter-sized actuators along a robot length, and thus were able to show an annelid-like robot.<sup>[44]</sup> Using a similar technique, Shintake et al. demonstrated multipurpose electro-adhesive soft grippers,<sup>[45]</sup> whereas Shian et al. showed the capability to nonuniformly deform the surface of a thin sheet of dielectric elastomer in a controllable and reversible manner.<sup>[48]</sup> Moreover, when the DEA is integrated with a buckling frame, quite large and often quicker deformations can be achieved.<sup>[49–52]</sup> Duduta et al. used a multilayer fabrication technique to achieve a crawling soft robot using DEAs. Such actuators were prepared without having to prestretch them, which eliminates or reduces the requirement for rigid parts. The process for developing multilayer actuators is based on a sequence of steps where initially the precursor is spin-coated, then elastomer is cured under UV, and finally the electrodes are stamped. The DEAs consists of three unique precursors (A, B, and C) which exhibit different electromechanical characteristics. The A and C components consist of urethane acrylic copolymers, whereas the B component is a polybutadiene acrylic copolymer. Made using this fabrication process, inchworm robots have been reported as the quickest DEA-based systems to date. These robots demonstrated traveling speeds faster than 1 body length per second with a strain in the material-actuated state of less than 3% under an applied field of  $50 \text{ V } \mu\text{m}^{-1}$ . Most notably, the reported systems are soft and deformable with very few rigid components. This has been achieved by stacking five layers of elastomers that resulted in a faster response time, higher energy density, and lower actuation voltage than the previously reported unimorphs which use only one distinct type of elastomer.<sup>[52]</sup>

In terms of fabrication, advancement in roll-to-roll processing has been utilized to fabricate rolled DEAs which are advantageous in terms of showing design enhancement, high electro-elastomer to weight ratio, compactness, and configurability which is needed to achieve various actuation modes. The spring-rolled DEAs shown in Figure 2a–c with single- and multi-degrees of freedom (DOF) perform different functionalities including actuation, sensing, and load bearing which are crucial capabilities for designing robotic hands and robotic legs of walking robots.<sup>[53,54]</sup> The spring-rolled actuators exhibit large strains over a high-pressure range, allow different electrodes corrugation, and enable mass production with low cost due to the roll-to-roll processing; however, they suffer from the pre-stress generated in the spring-roll shape in addition to showing smaller bandwidth of around 10 Hz. Sarban et al. presented tubular architecture-based DEAs with a semi-automated fabrication process as shown in Figure 2d–f, which involves two stage of processes, i.e., coating and assembly.<sup>[55]</sup> In coating stage, the fluid

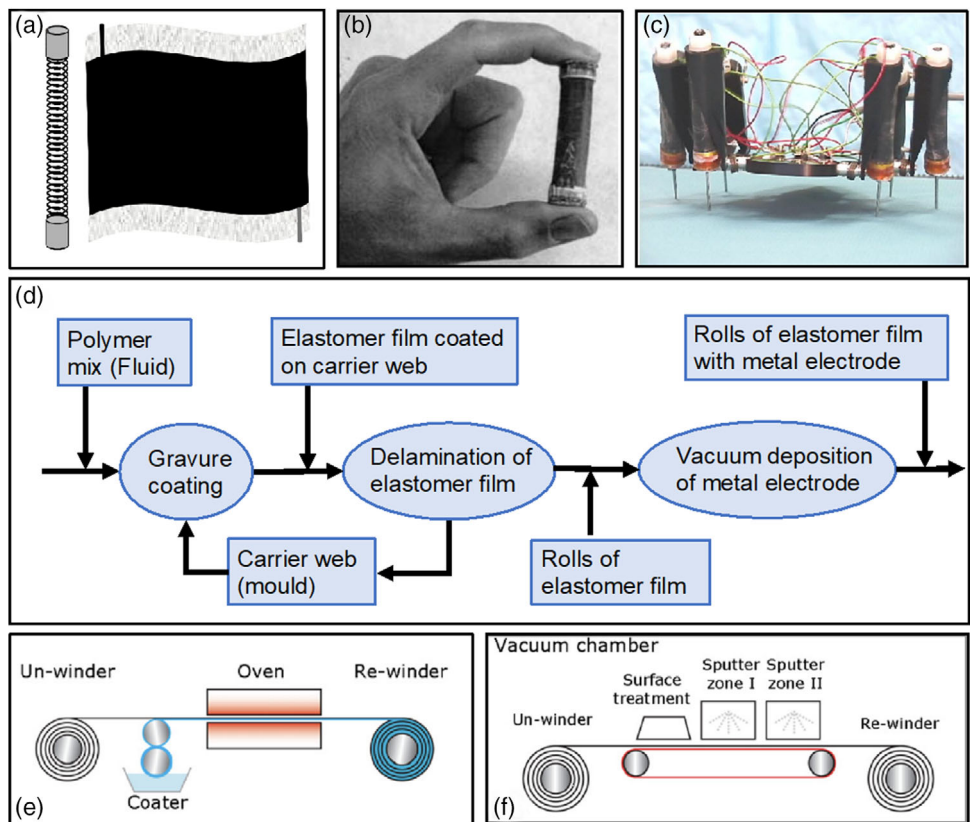


**Figure 2.** a) Schematics of spring roll's fabrication process. Reproduced with permission.<sup>[53]</sup> Copyright 2002, SPIE. b) Fabricated spring roll with axial tensile strain. Reproduced with permission.<sup>[54]</sup> Copyright 2003, Elsevier. c) Digital photograph of walking robot's leg with six spring rolls. Reproduced with permission.<sup>[53]</sup> Copyright 2002, SPIE. d) Fabrication process steps of tabular DEAs. Reproduced with permission.<sup>[55]</sup> Copyright 2011, Elsevier. Schematics of e) coating and f) metallization step process. Reproduced with permission.<sup>[55]</sup> Copyright 2011, Elsevier.

polymer is mixed and processed for gravure coating. The elastomeric film is then coated onto the carrier and later delaminated. This process would be repeated n-times as a closed-loop process for molding. Next, the delaminated elastomer film is proceeded for roll-to-roll manufacturing of elastomer layers where the vacuum deposition process is utilized for the fabrication of metallic electrodes (Figure 2f). Zhao et al. simulated different designs of rolled DEAs (i.e., actuator's geometry, thickness of elastomer, and number of turns, etc.) using COMSOL Multiphysics Software and fabricated compact-rolled DEAs for both axial and radial displacement free motion and blocked motion.<sup>[56]</sup> The performance of DEAs at 200 Hz bandwidth, 1 N blocked force, and 1 mm displacement is reported to be capable of performing 50 000 operations. The roll-to-roll fabrication step consists only two basic steps, i.e., multilayering and rolling processes. In the multilayering process, the thin sheet of elastomer is spin-casted on acrylic sheet which acts as substrate and is then thermally cured. In rolling process, the large strips of multilayered elastomer are rolled to form a hollow cylindrical shape of actuator. The fabricated DEAs were experimentally characterized by applying a voltage that varies linearly from 0 to 1 kV after each 10 s. The actuators are found to perform linear forced and free displacements with negligible degradation in performance up to 50k cycles.

While polymeric DEAs generate high actuation strain (>100%) with high efficiency (>80%), however, they generally show the potential of failure due to the applied high electric fields in addition to aging. To overcome this, DEAs can be based on liquid elastomers which show self-healing properties and not solely polymeric solids. Acome et al. used liquid elastomers to develop a high-performance soft transducer which mimics muscle and is known as hydraulically amplified self-healing electrostatic (HASSEL) actuators. HASSEL actuators are based on an electrohydraulic method that merged the versatility of soft fluidic actuators and the muscle-comparable performance of dielectric actuators with self-sensing abilities. However, HASSEL actuators are different than soft fluidic actuators in which fluid flow in the channels lead to losses of actuation efficiency. In HASSEL actuators, liquid dielectrics are embedded in a soft structure, where application of electrostatic forces results in a hydraulic pressure. Repeated self-healing after multiple breakdowns is possible due to the use of liquid dielectrics in HASSEL actuators. Figure 3a shows the operation principle of a HASSEL actuator, which includes an elastomeric shell that is partly coated with two electrodes and filled with the dielectric liquid. When a voltage drop is applied between the electrodes, an electric field is generated through the dielectric liquid. The obtained electrostatic Maxwell stress applies pressure and causes the displacement

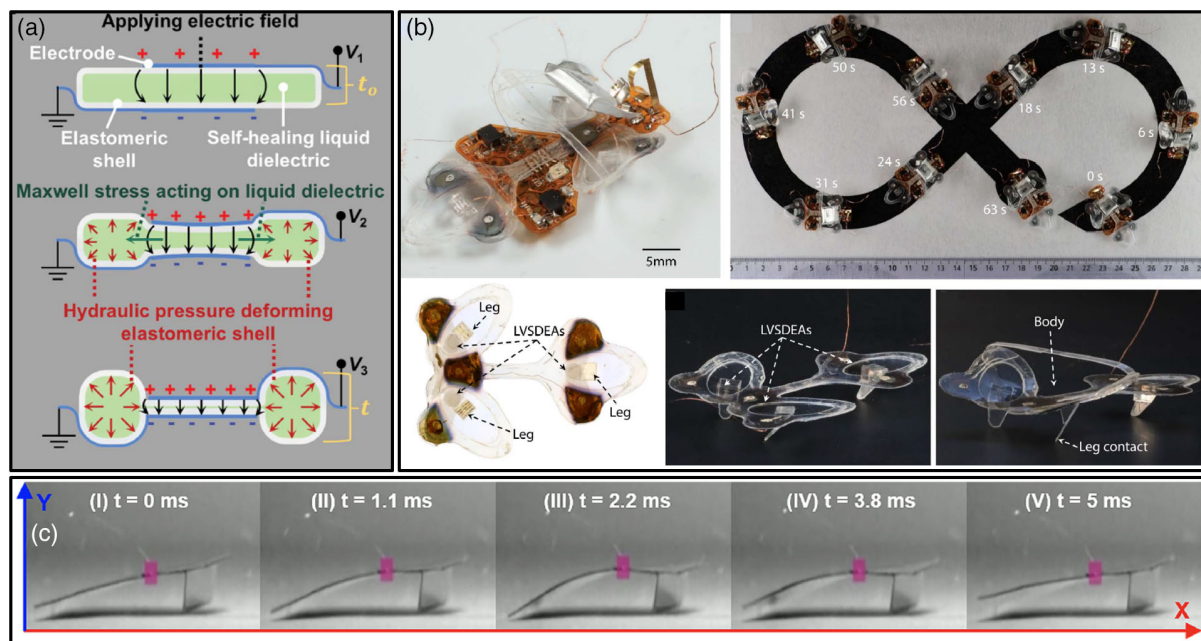


**Figure 3.** Demonstrated electrically responsive actuators using dielectric elastomers or piezoelectric materials. a) HASEL actuator schematic shown at three different voltages in which  $V_1 < V_2 < V_3$ . Reproduced with permission.<sup>[57]</sup> Copyright 2018, American Association for the Advancement of Science (AAAS). b) Insect-sized autonomous untethered soft robot based on stacked layers of DEAs. Reproduced with permission.<sup>[58]</sup> Copyright 2019, AAAS. c) The movement of the piezoelectric based robot in one cycle. Reproduced with permission.<sup>[59]</sup> Copyright 2019, AAAS.

of the liquid dielectric from the volume between the electrodes to surrounding area. When the voltage increases from  $V_1$  to  $V_2$ , the actuation strain slightly increases. When voltage exceeds a threshold  $V_3$ , the electrostatic force starts to surpass the mechanical restoring force which causes the electrodes to pull together abruptly. The design of the HASEL can be customized to achieve various actuation modes, such as the mode needed for soft fluidic actuators. Due to the applied voltage drop, HASEL actuators can also self-sense the deformation. Strain values up to 124% were reported in addition to  $614 \text{ W kg}^{-1}$  peak specific power during contraction while the specific work during contraction was  $70 \text{ J kg}^{-1}$ . A robust performance of the actuator was demonstrated where a negligible degradation in the performance was observed when performing a cycling test up to 1 million cycles with a strain of 15%. Nevertheless, it should be noted that large voltages (11 kV) are still required to achieve high-enough electrical fields for actuation. Moreover, it should be noted that the shell layer of the HASEL actuator is based on an elastomeric layer which requires further characterization and reliability testing against electrical aging.<sup>[57]</sup>

To overcome the high-voltage problem, Ji et al. demonstrated low-voltage stacked DEAs (LVSDDEAs) which require less than 450 V to operate. The actuators were used to drive a 40 mm long three-legged robot which is soft, autonomous, and wireless. The scale of the robot is similar to that of insects and thus it was called DEAnsect, as shown in Figure 3b. The DEAnsect design is based on a 3.5 cm wide flexible frame which supports three legs that allow forward-movement, in addition to right and left movements. Although tethered to a power source, the robot showed a speed of  $30 \text{ mm s}^{-1}$  and while untethered,  $12 \text{ mm s}^{-1}$

is achieved. The DEAnsect is also very lightweight (around 1 g) consisting of a 190 mg body carrying the 780 mg flexible electronics. Strain values up to 25% were demonstrated with no impact on the electrodes surface resistance. The LVSDDEAs are integrated on the robot legs, whereas the remaining integrated on-board electronics, such as sensors, battery and control devices, enable the system to autonomously respond to the outer environment. It is worth to note that, to date, the DEAnsect is the only wireless soft robot which can autonomously navigate a path with an actuation that is responsive to environmental conditions.<sup>[58]</sup>

### 2.1.2. Piezoelectric-Based Actuators

Piezoelectricity is a property of material where a voltage or electric charge is produced by the application of mechanical or vibrational forces, and inversely, where a mechanical deformation is achieved when applying an electric field.<sup>[60]</sup> Thus, piezoelectric materials can be used to achieve actuation. Nevertheless, to date, the demonstrated piezoelectric materials in soft robots require large voltages that can limit their applications. In fact, the piezoelectric effect under an AC voltage has been used for enabling a polyvinylidene fluoride (PVDF) layer to extend and contract which results in shape change in the soft robot. Wu et al. demonstrated a 3 cm × 1.5 cm robot which has a curved body and a leg structure at the front. Five states of movement were achieved. In the first state, when  $-60 \text{ V}$  is applied, the body of the robot is extended and the front leg is in the ground-touching posture. During the second state, when the applied voltage is almost 0 V, the robot recovers its initial shape but with

the front leg still in the ground-touching posture. In the third state, where  $>60$  V voltage is applied, the body contracts while both of the front leg and abdomen of the robot are in the ground-touching posture, as shown in Figure 3c. States 1–3 enable the forward movement of the soft robot, whereas states 3–5 enable its backward movement. The robot is shown to climb slopes and carry loads which are six times its weight at about one-sixth of its original speed (20 body lengths per second).<sup>[59]</sup> Ma et al. also used piezoelectric actuation to achieve a flapping-wing robot with 3 cm wingspan. The flapping-wing robot is only 80 mg and exhibits high-power density piezoelectric flight muscles which are able to produce  $>1.3$  mN of lift force. To produce bidirectional forces, voltage-driven piezoelectric bimorphs were used. To generate the motion of the wing-flapping, a four-bar linkage acts as a lever arm to amplify the small displacement of the piezoelectric flight muscle. When the flapping motion, along with the passive pitch rotation of the wings are averaged over a full stroke cycle, a downward propulsive force is generated. Nevertheless, the applied voltage for the actuation was not reported.<sup>[61]</sup>

#### 2.1.3. Mechanical Servomotor-Based Actuators

Although different stimulus-responsive materials have been used to enable actuation, the easiest and most straightforward method to achieve actuation based on electrical stimulation is through the use of a servomotor which is connected to soft parts. Nevertheless, the clear disadvantage of servomotors is that they are rigid and bulky components and thus limit the flexibility and softness of the complete system. Servomotor-based soft robots have been reported which can achieve various actuation modes such as flying and jumping.<sup>[48–54,62–69]</sup> For instance, Chang et al. studied the kinematics of pigeon feathers (with stiffness of  $100 \text{ N m}^{-1}$ ) in an attempt to develop the principles of operation for a robot with soft-feathered wings. Using the right and left wrist in addition to the finger joints as four independently controlled DOF, the authors modeled how the birds articulate their feathered wings during flight. Using this model and with the help of servomotors to achieve actuation, a biohybrid wing is developed that has 40 under-actuated real pigeon feathers which are robust, soft, and ultralight in comparison with previously reported carbon-based and glass fiber-based robotic feathered wings. The operation and efficiency of the feathered wing was tested and confirmed under aerodynamic pressure. A more advanced version of this robot was developed, called PigeonBot, which uses asymmetric wing platform to enable the robot to turn during flight and which responds well to control inputs up to around 5 Hz. The study of the effect of the discrete feather elements on the flight actuation in birds enabled the development of a feathered robot with the minimum number of sensors and actuators allowing for a lighter, cheaper, and more reliable design.<sup>[63]</sup>

In another application, servomotors have been used to achieve continuous jumping actuation in a cubic system. Li et al. reported that by covering the cubic system with silicone foam and creating a hole on every face in addition to integrating an elastic strip, jumping actuation in two directions and at any orientation can be enabled. The jumping actuation is achieved by winding up and freeing the elastic strip which has a 200 GPa

Young's modulus and a yield strength of 400 MPa. In fact, the elastic strip stores energy through the rotor and then delivers mechanical energy upon release, as shown in Figure 4a. The rotor, 20 mm in size and 200 g in mass, can produce 20 Nm torque and is driven using a 9 V DC motor which enables rotation in the direction of all of the cubic diagonal axes, and therefore allows the system to follow a trajectory. The robot is shown to have the capability of jumping around 20 cm in height and traveling over 30 cm in distance. Two versions of the autonomous cubic system were prepared—one is rigid and one is encapsulated with the soft silicone. The results showed that the soft cubic system enables longer travels using a single jump due to the bouncing and self-spinning behaviors resulting from the soft body. Nevertheless, this means that the motion of the soft robot was more scattered than that of its rigid counterpart.<sup>[70]</sup>

Servomotors have also been used in the development of an octopus-like robot which can swim. Calisti et al. mimicked the main characteristics of an octopus using soft limbs fabricated on steel and nylon cables attached to a silicone-based cone. The different limbs are connected and actuated using a DC servomotor through a rotational joint, as shown in Figure 4b. The limb exhibits shortening and elongating capabilities under water. A crawling speed of  $200 \text{ mm s}^{-1}$  and grasping capability of masses up to 135 g are reported. In addition, the octopus included multiple limbs to enhance the reliability of the system in case of component failure, in addition to enhancing functionality, such as ability to grab multiple objects at one time.<sup>[71]</sup>

#### 2.1.4. Neuro-Stimulation-Based Actuators

Neurons communicate via both electrical and chemical signals. The electrical signals can be sensed and used to actuate different devices, especially prosthetics. To date, the following has been concluded from neuroprosthetics research: 1) The most reliable method to extract motion intention for an upper limb from the prosthetic user is to decode the electrical activity of the muscle.<sup>[72–86]</sup> 2) By stimulating the peripheral nerves electrically,<sup>[79,80,87]</sup> close-to-natural sensations can be provided to the brain including pressure, object shape, stiffness, and texture.<sup>[79,80,87–100]</sup> 3) The sensations evoked by nerve-cuff electrodes and interface nerve electrodes are stable for a duration of 24 months.<sup>[79,81]</sup> 4) Users are quite satisfied from the sensors feedback and experience considerable relief from pain of the phantom limb.<sup>[90]</sup> 5) The feedback from the sensors provides the user with a sense of prosthetic limb ownership.<sup>[86,91]</sup> Nevertheless, commercial-grade myoelectric prostheses generally show efferent control only, which is achieved via the measurement of muscle activity from the area of the forearm in addition to the collection of the movement intentions from the prosthetic user,<sup>[64]</sup> while afferent data is not available. Therefore, amputees who use such systems usually complain about the necessity to depend on visual signals during day-to-day usage of prosthesis.<sup>[72,73]</sup>

To this end, D'Anna et al. developed a hybrid methodology to restore multimodal sensing data to the users who suffer from transradial amputation; information about finger location was provided through intra-neural stimulation-based sensory substitution, and data about the tactile sensation was obtained

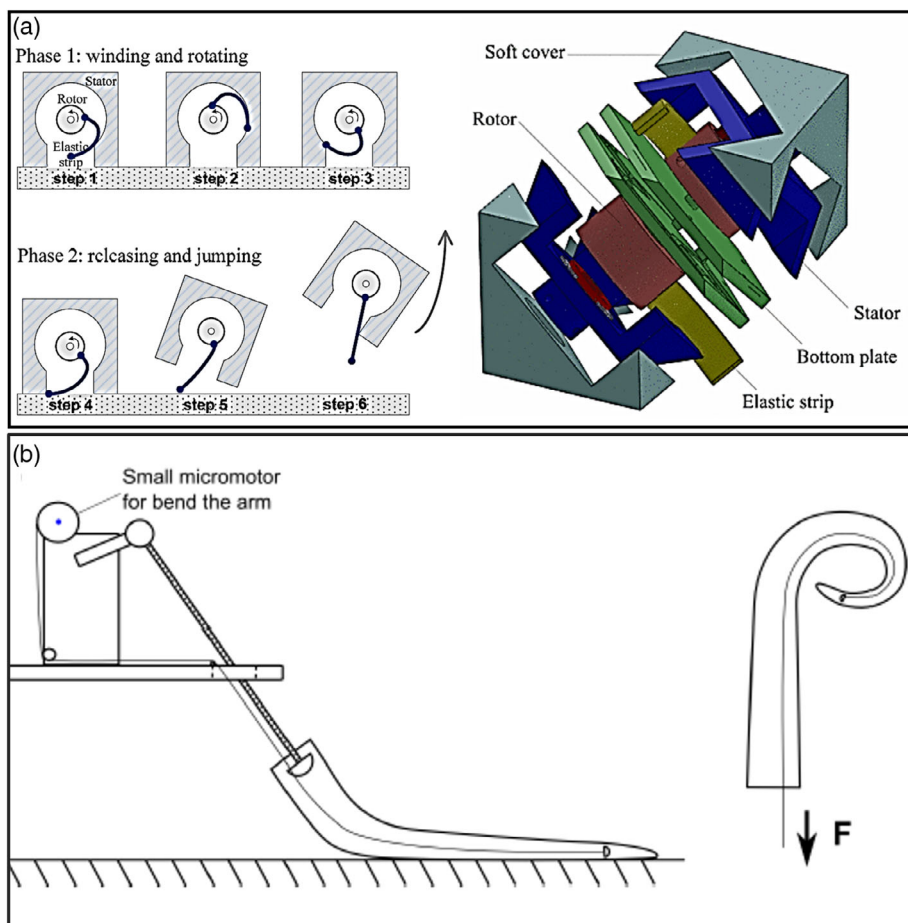


**Figure 4.** Examples of servomotor-based actuators. a) The jumping mechanism of a cubic system with an embedded elastic strip and rotor. Reproduced with permission.<sup>[70]</sup> Copyright 2015, IEEE. b) Schematic of arm bending system. The left picture shows the small micromotor which pulls the cable that is embedded in the side of the arm. On the right, when pulled, the cable exerts a distributed load to a side of the arm, providing bending with increasing curvature from the base to the tip. Reproduced with permission.<sup>[71]</sup> Copyright 2012, IEEE.

via a somatotopic methodology performed at the stump. More specifically, data about the joint angle was provided by safe neural pathways via intra-neural stimulating the peripheral nerves available in the amputee's stump. Surface electromyographic electrodes based data were acquired using a 1 kHz sampling frequency, whereas the injected current levels for each stimulation site were limited to 120 nC which is the chemical safety limit. Actuation speed achieved using electronic components embedded within the soft prosthesis was studied. The experimental results confirm that the two data streams can be used concurrently resulting in high performance during task execution. These findings contribute toward refined bidirectional electronic limbs that transfer more detailed multimodal sensations. Future efforts should be focused on the restoration of the position or angle data across specific joints, including wrist and elbow, which would have considerable impact on functional results.<sup>[92]</sup>

Moreover, Zollo et al. confirmed that sensorimotor integration can be recovered using neural electrodes in addition to routing the sensors input to enable real-time and closed-loop control of the electronic limb (hand) during tasks of manipulation and

grasping. Implanting neural electrodes in a young woman suffering from hand amputation provided close-to-natural sensations about slippage and force, vital for considerably enhancing the user's skills of prosthesis manipulation. The actuation in this case was also provided using rigid electronic components embedded within the soft prosthesis, as shown in Figure 5. The slippage sensation was deduced using a stick-slip model from the vibrations in the force signals collected by the sensors which are integrated in the prosthetic hand. Data on force and slippage was converted into electrical stimuli (via rectangular biphasic pulses with 150 µA current amplitude, 50 Hz frequency, and 80 µs pulse width); this allowed the user to efficiently control the stability of the grasp function, regulate the force level, and impede dropping of the object. The key goal of the stick-slip model was to deeply assess the slippage mechanism in healthy users, and then deduce slippage stimulation approach for the amputee. In an experiment, cuff and intraneuronal electrodes were implanted into the ulnar and median nerves of an amputee's residuum for the stimulation of surface and deep nerve fibers during an 11-week study. The sensors output provided by the biomechatronic hand during manipulation and grasping tasks

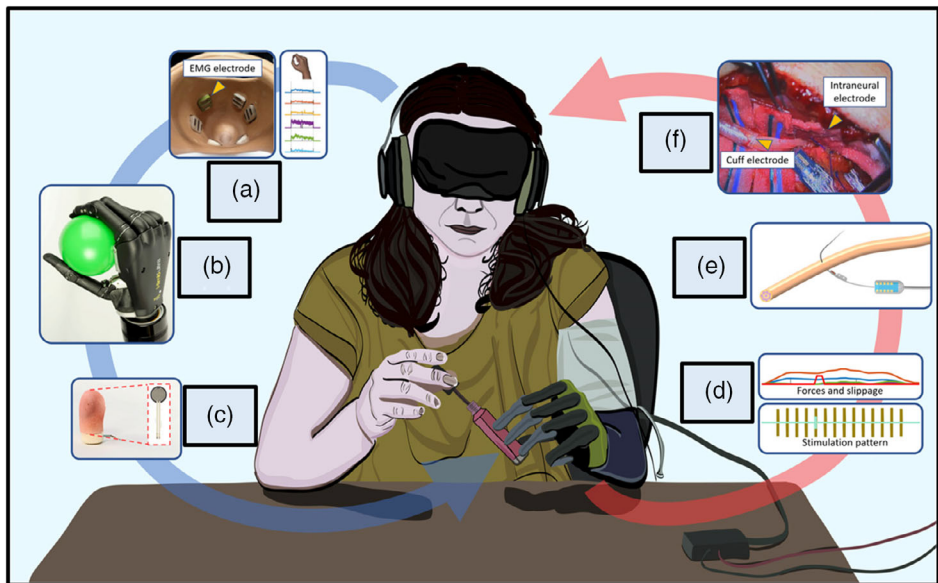


**Figure 5.** Real-time force-and-slipage closed-loop control of hand prosthesis with neural feedback. The sensory output produced by a biomechatronic hand with embedded force sensors was routed back through neural stimulation to evoke close-to-natural force and slippage feedback. a) Participant's intention was decoded by the muscular activity through sEMG sensors in the socket and a pattern recognition algorithm that classified the gesture and the force level. b) Position and force control was implemented on a biomechatronic prosthetic hand for performing the task. c) The hand fingers with force-sensing resistors read the applied forces and detect slippage. d) The measured force applied to the grasped object and the detected slippage are encoded in force and slippage stimulation patterns. e) Force and slippage sensations are delivered to the participant by means of cuff and intraneural electrodes. f) Photograph of the surgical intervention for implanting cuff and intraneural electrodes in ulnar and median nerves. Reproduced with permission.<sup>[74]</sup> Copyright 2019, AAAS.

was transferred to the user through neural stimulation to generate close-to-natural feedback about force and slippage in real time.<sup>[74]</sup>

A synthetic analogue inspired by the human perceptive system was developed by Thuruthel et al. using polymeric actuators. The system builds models using a repetitive and unorganized sensor topology integrated within a soft actuator, a vision-based motion detection system and a machine learning methodology. The system allows the modeling of an unknown soft actuated system. First, the actuators were fabricated using 3D-printed molds in which polymeric silicone was casted silicone; next the sensors based on conductive CNTs were embedded and bonded to the bottom end of the actuator; then actuator chambers were molded and sealed off by encapsulating them with extra silicone and silicone tubing was inserted into the chambers to enable their inflation. Maximum sampling rate of 10 Hz was used. The sensors wires were solder-connected to a PCB which achieved mechanical stability to the electronics interconnections with header pins. Nevertheless, the soft actuator system was relatively large (120 mm × 35 mm × 25 mm).<sup>[75]</sup>

## 2.2. Magnetically Responsive Actuators

Magnetic stimulation is considered interesting especially because of the easiness in quickly and accurately controlling the magnetic field direction and magnitude, in addition to its ability to penetrate most materials. Polymers, gels, papers, and fluids have been used as the medium to incorporate magnetic particles and fillers such that they can be actuated when

an external magnetic field is applied. The insertion of discrete magnetic fillers into soft compounds results in a magnetization profile with variable magnitude and direction.<sup>[93–97]</sup> When exposed to a magnetic field, the magnetic fillers seek alignment with the field resulting in generation of different actuation modes such as deformation, bending, elongation, and contraction. These actuation modes are generally generated when the field spatial gradients interact with the magnetic fillers. However, in small areas, both the field and its spatial gradients can be created independently allowing for two independent actuation modes needed for complex motions.<sup>[98]</sup> Various distortion patterns can be created by modifying a number of parameters, including the actuating signals, the magnetization profiles, and the stiffness and shape of the materials. The ability of magnetic fields to penetrate a wide range of materials makes this type of actuator promising for applications restricted to enclosed areas such as targeted drug delivery, microfluidics, and microsurgery.<sup>[98–103]</sup> Moreover, such actuators have fast response time, compared with other modes of actuation, where speeds of 100 Hz have been reported.<sup>[104–109]</sup> Therefore, magnetic actuators have been successfully used in the development of various crawling devices, swimmers, and micropumps.<sup>[94,110–114]</sup> Nevertheless, it should be noted that external magnetic coils, which are used to generate magnetic fields, are generally bulky and consume a lot of power, whereas the regions where the magnetic field is strong enough and controllable are usually small.

Ferromagnetism can also be used to achieve actuation. In fact, Kim et al., use ferromagnetic materials to demonstrate a sub-millimeter-sized soft robot which can steer and navigate

in all directions using magnetic actuation. The actuation is in fact enabled through the programming of ferromagnetic domains within the system body where a soft hydrogel skin is coated on its surface. The robot body consists of a soft polymeric matrix with embedded ferromagnetic microparticles with a Young's modulus of 1.4 MPa and uniform magnetization of  $M = 128 \text{ kA m}^{-1}$ , thus, it can be scaled down to a couple hundred micrometers. The hydrogel skin is used to significantly reduce friction. The ferromagnetic soft actuator is demonstrated to be able to navigate through various complex regions, such as a tortuous cerebrovascular phantom with multiple aneurysms. In addition, the ability of the actuator to steer a laser and focus on specific small regions within a complex environment is

reported, as shown in **Figure 6a**. However, even though the soft robot is within the submillimeter scale, a larger scale cylindrical permanent magnet (5 cm in size placed at a distance of 4–8 cm) is used to generate the needed magnetic fields (20–80 mT).<sup>[115]</sup>

Moreover, magnetic soft robots generally use patterned magnetization to generate quick deformations and various actuation modes needed for the different applications, such as drug delivery and object manipulation. Nevertheless, the existing methods available for patterning magnetic fillers in flexible soft materials are limited. As a result, different modes of deformations are still not possible using the existing patterning methods (such as microrobots with programmable shapes) as they do not allow the precise patterning of discrete 3D magnetic fillers in planar

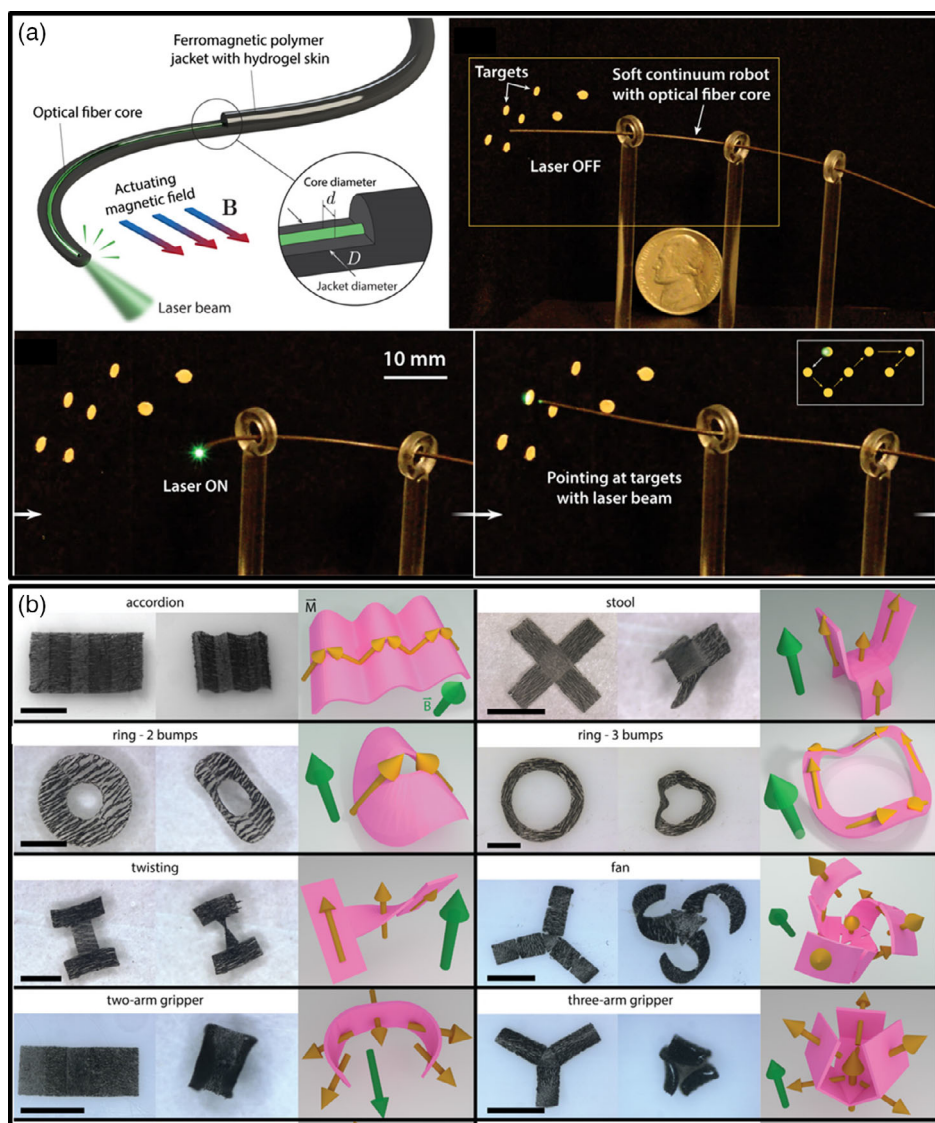


**Figure 6.** Demonstrated magnetically responsive actuators. a) Schematic illustration of the ferromagnetic soft continuum robot with an optical fiber and experimental setup for demonstrating steerable laser delivery. The outer diameter of the demonstrated prototype is 500  $\mu\text{m}$ . Reproduced with permission.<sup>[115]</sup> Copyright 2019, AAAS. b) Flexible magnetic planar structures that have distributed 3D magnetization profiles. Yellow arrows represent the direction of local magnetization, and green arrows represent the direction of the actuating magnetic field. The materials are about 80  $\mu\text{m}$  thick. All the items presented reversible and rapid transformation between the original shape and the folding shape. Scale bars, 2 mm. Reproduced with permission.<sup>[116]</sup> Copyright 2019, AAAS.

soft materials. The only patterning technique that does allow this is manual microassembly of the magnetic fillers which results in costly, time-consuming, and difficult fabrication, especially when the soft robot size is reduced to below the centimeter scale and when the number of components is increased. To overcome this challenge, Xu et al. developed a technique for patterning magnetic microparticles embedded within a biocompatible elastomer. This approach is based on precise reorientation of the magnetic fillers and selective UV light exposure to program the microparticles in the planar elastomer with random 3D orientation in a small-sized area down to 100 micrometers. Using this technique, numerous planar microrobots with different sizes, geometries, and magnetization profiles can be developed using one precursor in a single process, as shown in Figure 6b where the material thickness is around 800  $\mu\text{m}$  while the applied magnetic field is 20 mT, which can be generated by a general electromagnetic coil system. As a result, new modes of actuation and deformation can be achieved that were previously unobtainable, such as multi-legged paddle crawling. A swimming actuation was also demonstrated under a 9 mT rotating field at 20 Hz, resulting in average speed of 3.38  $\text{mm s}^{-1}$  which presents 78.6% body length. Moreover, using this technique, the authors demonstrated a multi-arm structure which turns into a hollow sphere when a magnetic field is applied. Finally, the authors developed a physics-based model which can be used to forecast the shape deformations when a magnetic field is available.<sup>[116]</sup>

To reduce the cost of the actuator, inexpensive substrates are used such as paper.<sup>[117–119]</sup> Ding et al. demonstrated a paper-based actuator which performs a specific actuation in the presence of an external magnetic field. Different types of papers including soft tissue, cleanroom, Whatman-1 filter, printer, and newspapers were tested where they were coated with ferrofluids (a colloidal magnetic fluid) until saturation and next, they were placed into microwave oven for curing. In fact, the magnetic and mechanical properties of the actuator can be customized by modifying the concentration of the absorbed ferrofluids or using different types of cellulose-based papers with different thicknesses and porosities. The cured paper is further micromachined using laser cutting tool to form cantilevers which are next coated with a parylene layer deposited using chemical vapor deposition (CVD) technique, as shown in Figure 7a. The parylene layer enhances the impermeability of the cantilever to humidity and some gases in addition to enhancing its mechanical stiffness. The cantilevers were tested under different magnetic fields generated using a commercial electromagnet where a maximum bending angle of 40° (equivalent loading of 1.8 mg, with a spring constant of 2.67  $\text{N m}^{-1}$ ) was observed at a magnetic field of 44 mT with the tissue-paper cantilever. A hysteresis is also observed where the recovered bending angle under no applied magnetic field is around 12° as shown in Figure 7b. The cleanroom paper-based cantilevers, with and without parylene coating, were tested in a liquid environment and it is found that the parylene coating protects the ferrofluid from leaking as shown in Figure 7c and maintains the stiffness of the cantilever. The results show that the cantilever actuators based on cleanroom and filter papers produced the greatest force ( $>40$  mg force), whereas the tissue-paper based cantilevers generated the largest deflection (40° tip angle); nevertheless, the main challenge is to achieve shape-recovering under no external

field.<sup>[117]</sup> Olsson et al. demonstrated soft actuation in magnetic actuators based on bacterial cellulose nanofibril aerogel. The porous aerogel is synthesized from bacterial cellulose hydrogel through a freeze-drying process; next, the obtained aerogel is dipped into aq.  $\text{FeSO}_4/\text{CoCl}_2$  solution at room temperature as shown in Figure 7d. The solution precipitates nonmagnetic metal oxides/hydroxides on a template when heated at 90 °C. The precipitated precursor is then dipped into  $\text{NaOH}/\text{KNO}_3$  solution at 90 °C to convert the metals into ferrite crystal nanoparticles. As a result, highly flexible magnetic aerogels are obtained which can withstand large deformations as shown in last step of Figure 7d. The magnetic aerogel is shown to deflect upward (moves far from the water droplet) and downward (touches the water droplet) when a 40 mT household magnet moves upward and downward, respectively, as shown in Figure 7e. The magnetic aerogel which is stiff (tensile modulus of 3 GPa), solid and flexible is also shown to be able to absorb the water droplet, whereas 95% of water droplet can be released again due to its high compressible property (90% strain, modulus of 0.15 MPa under compression).<sup>[119]</sup>

### 2.3. Thermally Responsive Actuators

Thermally responsive actuators include those activated by infrared (IR), NIR, thermal radiation, and Joule heating. In addition, they can be remotely activated by heat application (e.g., via lasers). Thermal stimulation also provides a safer trigger than UV light or electric field for specific applications such as biomedical applications. However, these actuators tend to be slower and less efficient than actuators using other stimuli. The use of thinner films, higher power, and materials that can absorb more heat would increase the efficiency and the response time. In the following, SMAs, shape memory polymers (SMPs), and liquid crystal elastomers (LCEs) as thermally responsive materials used for actuation are reviewed.

#### 2.3.1. Shape Memory Alloys

SMAs are a class of material that can be deformed and return to original “memorized” shape under loading/thermal cycles due to an innate ability to undergo reversible changes in their crystal structure. They can be created by alloying a variety of elements with each material having advantages and disadvantages depending on the application. Iron-based or copper-based SMAs, such as Fe–Mn–Si, Cu–Zn–Al, and Cu–Al–Ni are more common being low-cost and commercially available. However, NiTi-based SMAs are preferred for most applications because of their higher stability and practicability.<sup>[120,121]</sup> The application of this class of materials is straight-forward. However, in the martensite crystal state (Young’s modulus of 23.2 GPa), the material can be deformed into any shape by applying an external force. When the material temperature rises above a certain threshold (by external or internal Joule heating), the material changes to the austenite crystal state (Young’s modulus of 49.5 GPa) and returns to its “memorized” original shape before it was deformed. In addition, the SMA will exert a constant force to regain its original form.<sup>[122,123]</sup>

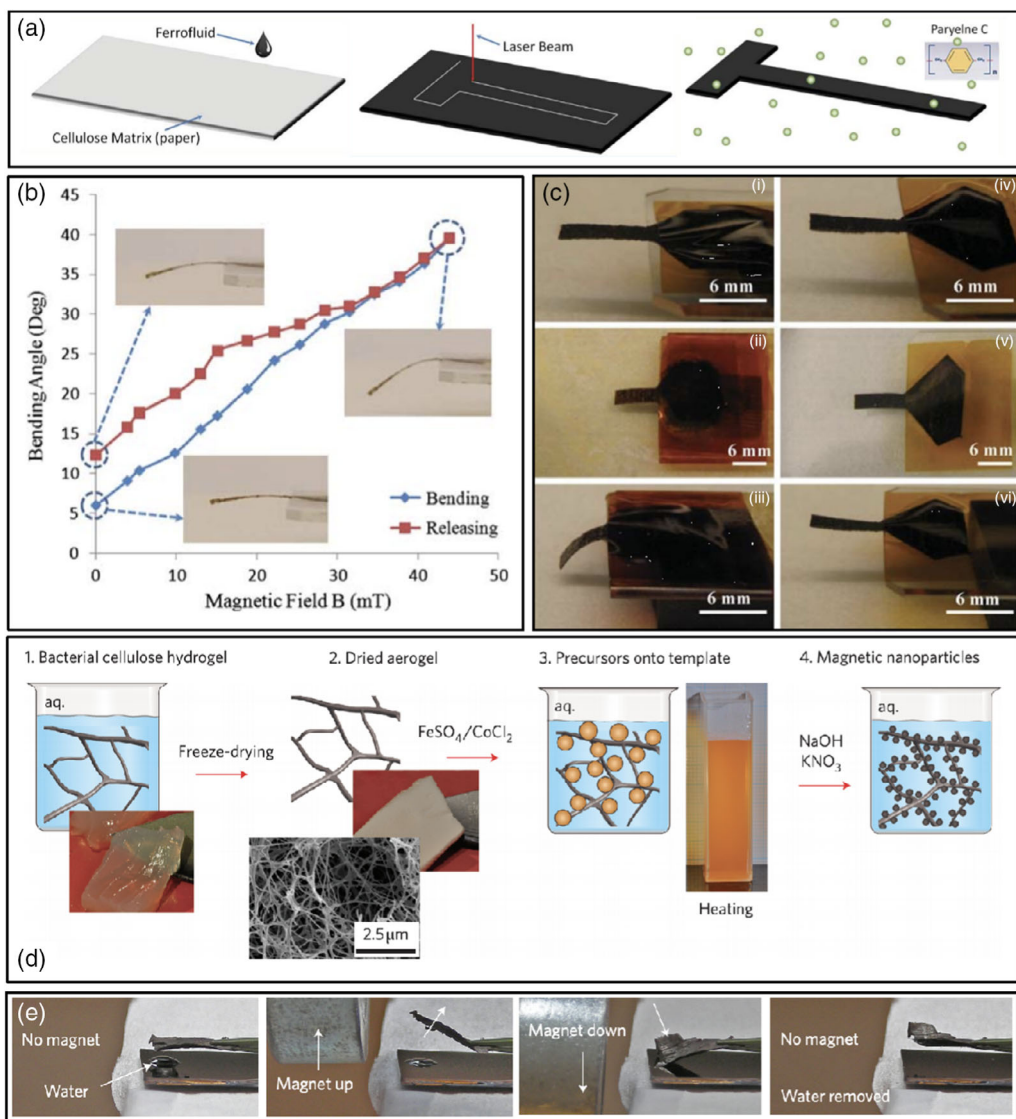


**Figure 7.** a) Fabrication flow of magnetic cantilevers: Coating of ferrofluid on cellulose Matrix (paper) which is LASER micromachined to obtain the cantilever structure. Reproduced with permission.<sup>[117]</sup> Copyright 2011, IEEE. b) Bending and releasing angle of versus applied external magnetic fields of soft tissue-paper-based cantilever ( $0.8 \text{ mm} \times 8 \text{ mm} \times 25 \mu\text{m}$ ). Reproduced with permission.<sup>[117]</sup> Copyright 2011, IEEE. c) Cleanroom ferropaper cantilevers ( $0.8 \text{ mm} \times 8 \text{ mm} \times 180 \mu\text{m}$ ) (i, ii, iii) without and (iv, v, vi) with parylene-C coating to test the water soaking. Reproduced with permission.<sup>[117]</sup> Copyright 2011, IEEE. d) Fabrication flow of synthesis of magnetic aerogel. e) Capability of the magnetic aerogel to absorb a water droplet. Reproduced with permission.<sup>[119]</sup> Copyright 2010, Nature Research.

A SMA-based soft robot inspired by the locomotion of an inchworm has been demonstrated which consists of three different parts: the body, the back foot, and the front foot. Each foot is divided into three segments, and each segment has a different friction coefficient to implement the anchor and sliding movement. The SMA wires are embedded longitudinally in a soft polymer to act as a muscle to generate contractions for the inchworm during locomotion. In fact, the SMAs were prestrained by 3% and encapsulated with a silicone elastomer with a Young's modulus of 1.8 MPa. Eight SMA wires are used as the active components and distributed into four groups: SMA-front, SMA-back, SMA-left, and SMA-right. The bending properties of the

structure are influenced by many factors; one of which is the eccentricity of the SMA wires. The design of the overall structure is shown in detail in **Figure 8a**. For linear locomotion of the robot, all four SMA wires in the body are actuated simultaneously using currents up to 1 A. To achieve turning motion, the SMA wires are actuated on only one side of the body SMA-left or SMA-right wires. Using this technique, the robot can achieve a linear stride length of 54 mm (with a speed of  $3.6 \text{ mm s}^{-1}$ ), which is nearly a third of its body length with a linear locomotion efficiency of around 97%. Also, the efficiency of the turning linear locomotion is 39.7%. Future work should focus on improving the mobility of the robot using an independent control system.

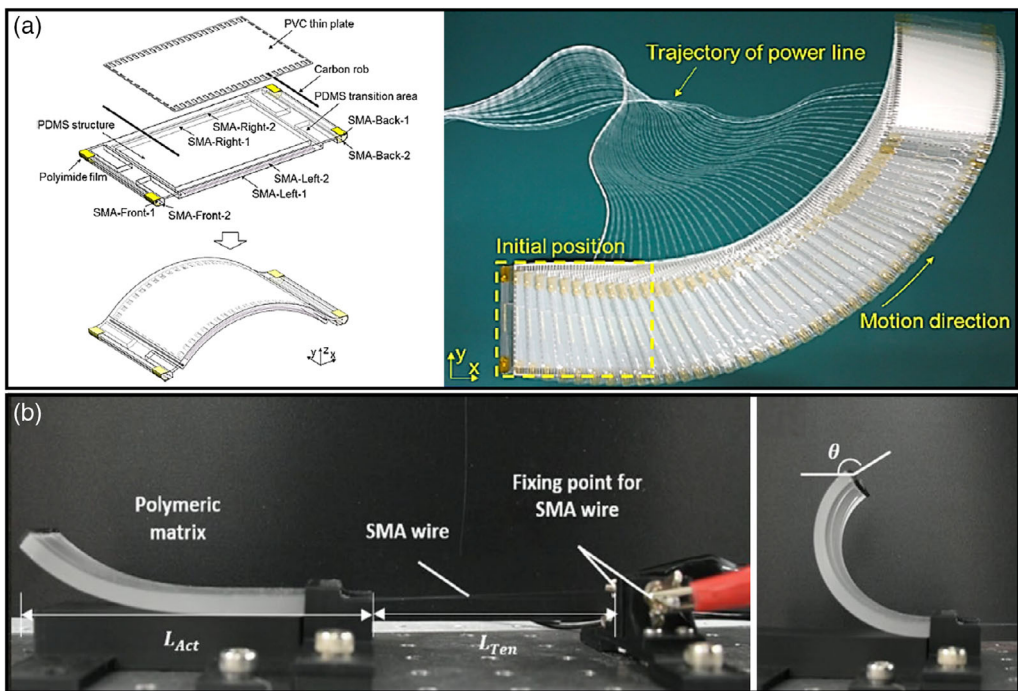


**Figure 8.** Examples of SMA wires based actuators. a) The overall structure of the inchworm-inspired robot including its components and turning locomotion for forty periods, turning angle of 90°. Reproduced with permission.<sup>[124]</sup> Copyright 2014, IOP Science. b) The setup for actuator used as a soft gripper made from SMA wire embedded in PDMS soft body. Reproduced with permission.<sup>[125]</sup> Copyright 2019, Nature Research.

Nevertheless, due to its thickness and simplicity, the robot could be useful in rescue missions where humans or larger robots are not capable to access.<sup>[124]</sup>

Another method for achieving soft actuation is reported, where SMA wires were inserted into a thin sheet of flexible plastic plate and installed in a soft body made of polydimethylsiloxane (PDMS), to make what is called “five-armed actinomorphic soft robot”. The flexible plates act as arms; they perform a 2D reciprocal bending motion when heating the SMA wires and can recover their initial position due to the restoring force of the plastic plates. The final structure appears as if one end is constrained and the other end is free to deflect. This soft robot is able to crawl on terrestrial ground (speed of 140 mm s<sup>-1</sup>), swim (speed of 67 mm s<sup>-1</sup>), and grip fragile objects (up to 0.91 kg, which is 15 times its weight) using a heating voltage of 30 V.<sup>[126]</sup>

Moreover, modules based on soft hinge actuators have been transformed from a compact configuration into a deployed quadrate configuration through the actuation of the soft hinge actuators. The soft module consists of two self-actuating soft hinge actuators with embedded SMA wires, and the actuators are connected end-to-end using compliant soft joints. Magnets are also embedded within the structure, acting as connectors, to efficiently assemble and disassemble the 3D-printed parts to form complex soft deployable structures. The biggest advantage of this technique is the ability to minimize the required storage space (up to 750% compression in length) because the structure can be assembled and disassembled. In contrast, the actuating time for the SMAs is around 8 s at 0.9 A, and then it takes 45 s for free cooling of the SMA to make it ready for

the next actuation. Using this technique, a 200 g soft robot is demonstrated which can move at a speed of up to 11.3 m h<sup>-1</sup> and with a leg-lifting force of 0.45 N.<sup>[127]</sup>

Another strategy is based on embedding a free-sliding SMA wire in a soft body made of PDMS, as shown in Figure 8b, which then act as tendons and increase both the bending angle and the bending force of the actuator. At a heating current of 0.95 A, the wire can completely deform in 1 s. One of the applications of this technique is that it can be used as a gripper with a pulling force of 30 N (up to 1.5 kg). The module was tested up to 100 cycles with a heating current of 0.95 A and a robust performance is reported. However, the main drawback of this technique is that the actuator is slow and the grasping force is too low for industrial uses.<sup>[125]</sup>

Sandwiching a U-shaped SMA wire between two thermal elastomer layers has also been reported as a method to achieve actuation. One of the layers is stretched (up to 50%), whereas the other is unstretched, which in turn leads to producing an actuator that is capable of a fast transition between a soft curled unactuated state (due to the stretched and unstretched thermal elastomers) and a rigid straight-like actuated state. The thermal conductive rubbers allow for fast heat transfer, which is a great advantage of this actuator. The resulting actuator is 3.7 g and provides a force of 0.2 N when stimulated 7.4 V with 3 s needed to switch between the different actuation states. A cycling test up to 150 cycles is conducted to confirm the mechanical resilience and reliability of the system. Accordingly, this will allow the actuator to act as an “artificial muscle” for a variety of tethered and untethered soft robotic systems capable of fast dynamic locomotion.<sup>[128]</sup>

### 2.3.2. Shape Memory Polymers

SMPs are a class of smart materials, most of which are thermally responsive, and they can be programmed to remember a temporary shape and revert back to the permanent shape upon the application of a specific stimulus, such as heat or light.<sup>[129–131]</sup> The advantages of SMPs include the following: high elastic deformation, low density, low cost, and ease of manufacturing.<sup>[132]</sup> The most common types of SMPs developed for biomedical applications are PU and thermoplastic polyurethane (TPU).<sup>[132,133]</sup>

Self-folding has been reported using SMPs. In fact, self-folding is an approach used to convert 2D patterns on flat materials/substrates into 3D systems/architectures. Traditional patterning methods which show high throughput, including photolithography and inkjet printing, result in 2D patterns; however, being able to transform the 2D patterns into 3D architectures is appealing for various applications such as packaging and mechanical actuation. Self-folding is considered an assembly technique that converts prepatterned 2D structures into a desired 3D architecture by folding it with high reliability.<sup>[134]</sup> This technique has been used in the development of various devices including but not limited to, sensors, drug delivery containers, reconfigurable device, and solar cells.<sup>[135–140]</sup> To achieve self-folding, hinges are defined on planar surfaces which would bend and fold when external stimuli are applied. Self-folding has been achieved via different techniques, such as intrinsic stress in a thin film<sup>[141–145]</sup> or an extrinsic stress produced by an external stimulus such as magnetic,<sup>[146,147]</sup> thermal and photo-stimulation, or pneumatic, chemical, and swelling stimulations.<sup>[148–150]</sup> Nevertheless, most of the reported self-folding-based soft robots have been achieved using thermal actuation which is considered an appealing approach due to ease and the accessibility of thermal stimulators, such as light and thermal radiation. In this case, the hinges can be realized using SMPs which assume distinct preprogrammed states when the temperature exceeds a threshold value.<sup>[151–154]</sup> Alternative strategies use different material stacks for the hinges than the substrate; as a result, only the hinges contract upon heating. An example includes using polyimide-based hinges which contract when heated above 500 °C.<sup>[155]</sup> Another example includes using multi-layers of materials with different thermal expansion coefficients.<sup>[156–158]</sup> Nevertheless, the development of such methods necessitate multiple fabrication techniques to include hinges with varying materials from the substrate. It should be noted that the folding patterns can be predicted by simulating them using mathematical models.<sup>[159–161]</sup>

Self-folding using SMPs has also been reported where the actuator is composed of SMPs, paper, and resistive circuits to achieve localized addressable folding, as shown in **Figure 9a**. The SMP contracts by almost 50% when heated up to 95 °C (heating current up to 2 A). This technique can be used to create 3D structures;<sup>[162]</sup> however, its main limitations include the composite thickness and the hinge torque. Self-folding has also been achieved using thin pre-strained polystyrene (PS) sheets using microwaves as a heating source (250 W for 3 s). When the PS sheets are pre-strained and there is a pattern of graphene ink on its surface, the graphene will absorb the microwaves and causes the polymer to warm up directly below the hinges causing the polymer sheet to fold. The idea behind this approach is that

when the local temperature in the inked region exceeds the glass-transition temperature of polymer, 103 °C, the strain in the inked regions of the film relaxes gradually across the sheet thickness which causes the PS sheet to fold. This method is also applicable for triggering remote folding because the microwaves can deliver large amounts of energy remotely. In addition, this technique folds polymers accurately and quickly, which can be a huge advantage for applications which are time sensitive.<sup>[164]</sup> Liu et al. achieved a different self-folding technique, where a patterned black ink and an inexpensive IR light bulb (intensity of 988 mW cm<sup>-2</sup>) for stimulation are used. This ultimately will heat localized regions on the PS, which will cause the predefined inked regions to relax and shrink. Such self-folding techniques can be useful for applications in packaging and assembly. In addition, they can be used as containers for drug delivery.<sup>[165]</sup>

Bistable SMP has been demonstrated in the application of a muscle to propel a swimming soft robot. Figure 9b shows the components of a single actuator which include the outer shell, floaters, fins, bistable element, and shape memory muscle. The outer shell covers the bistable element to ensure a linear actuation and provide stability for the robot. For the vertical direction, the floaters ensure that the SMP strips are fully submerged in water. The groove in the floaters provides the pivot point for the fins which are attached to the bistable element with elastomeric joints to provide flexibility. Before deploying the robot, the printed SMP muscle is heated past its glass-transition temperature ( $T_g$ ) and mechanically deformed to the programmed shape. The recovery force of the muscle is in the range from 0.2 to 2.1 N. There are three states of actuation; the first is when the robot is deployed in the water and the temperature of the water is equal to or larger than the transition temperature, the SMP relaxes. In the second state, the SMP recovers its original shape. After actuation, the system transitions into the third state. The forward motion of the robot occurs in the transition between states I and III. While in the second state, the shape memory muscle moves the bistable element and drives the fins backward until they are perpendicular to the direction of motion. Immediately after, the bistable element snaps to its second position. This drives the fins rapidly and causes the propulsion to the robot which can be used for delivery application.<sup>[163]</sup>

### 2.3.3. Liquid Crystal Elastomers

The combination of rubber elasticity with the orientational order of liquid crystals leads to a unique class of materials called LCEs which are promising for applications that require stimulus response.<sup>[166–168]</sup> LCE-based actuators have been reported in active hinges to interconnect polymeric tiles. The soft composite matter is composed of LCE bilayers with orthogonal director alignment and different nematic-to-isotropic transition temperatures ( $T_{NI}$ ). The printed LCE hinges are capable of a large and reversible bending response upon heating them past their respective actuation temperatures. In addition, the programmable LCE hinges can be actuated at different temperatures. Nevertheless, the hinges are not applicable when a large torque output is required.<sup>[167]</sup> Soft tubular actuators have also been reported which are actuated by applying electric potential that heats the wires embedded in the LCE. The actuator is capable

of bending, expansion, and contraction (40% homogenous contraction) while the maximal work density of the actuator could reach  $150 \text{ kJ m}^{-3}$  under an applied stress of 0.31 MPa. One advantage of this technique is that it can be controlled by a low electric voltage (1 to 3 V). In contrast, this technique has shown a much slower speed and a lower energy efficiency compared with most DEAs.<sup>[154]</sup> Light has been used to remotely control tubular LCE-based soft robots/actuators as well. The actuator can achieve complex locomotion including bending and elongation (up to 600%) and can be programmed to have new modes of locomotion. To develop the actuator, a single LCE is synthesized with allyl sulfide groups in the backbone. The photo-induced topological change enables the flexible control of alignment in both the longitudinal and peripheral directions of tubes. **Figure 10a** shows an example of the different achieved motions. A promising repeatability of actuation was reported even after performing 1000 cycles. Furthermore, omnidirectional bending of the actuator with polydopamine (PDA) coating could be controlled remotely by IR light.<sup>[169]</sup> Moreover, Yang et al. have prepared a light-sensitive composite by dispersing CNTs into LCEs with exchangeable links (xLCEs). Upon light irradiation (808 nm, intensity  $0.84 \text{ W cm}^{-2}$ ) which results in a temperature rise up to  $160^\circ\text{C}$ , flat films can be converted into dynamic 3D structures. When the light is off, the film bends toward the bottom part that is not exposed to light. As shown in Figure 10b, a chair shape is formed when the four chair legs are programmed to bend downward and the back bends upward and extends vertically. The

actuator is also shown to lift objects that are 1000 times heavier than itself. It is worth mentioning that the assembling and the actuation can be performed at low temperatures (e.g.,  $-130^\circ\text{C}$ ).<sup>[170]</sup>

Self-folding has also been reported using LCEs. In fact, in controlled self-folding methods, rigid electronic components could be integrated on the planar surfaces to achieve complete stand-alone soft-robots. However, fully soft systems that have been reported to date are generally irreversible<sup>[171,172]</sup> or geometrically limited<sup>[173]</sup> or connected to rigid energy sources.<sup>[174]</sup> New strategies are required for the development of untethered soft robots which can achieve repetitive actuation,<sup>[175]</sup> self-propulsion, and self-morphing<sup>[176]</sup> when exposed to an external stimulus. Kotikian et al. reported an untethered soft robot that is reversible and shape-morphs in addition to propelling itself when exposed to a thermal stimulus.<sup>[177]</sup> To achieve this, LCE elastomer-based hinges were used to generate active 3D structures that show wide and repeatable deformations. Using this strategy, the angles of the hinges, the orientation of the folding, and the geometry of the actuator can be programmed. Folding angles of  $180^\circ$  were reported. By embedding LCEs with two distinct nematic-to-isotropic transition temperature ( $T_{NI}$ , low and high  $T_{NI}$ ), a soft robot was demonstrated which can fold and unfold sequentially when exposed to different temperatures. An origami-based structure was reported which could assume three distinct stable configurations in response to different thermal exposures. The LCE hinges were also able to contract by up to 50% and lift

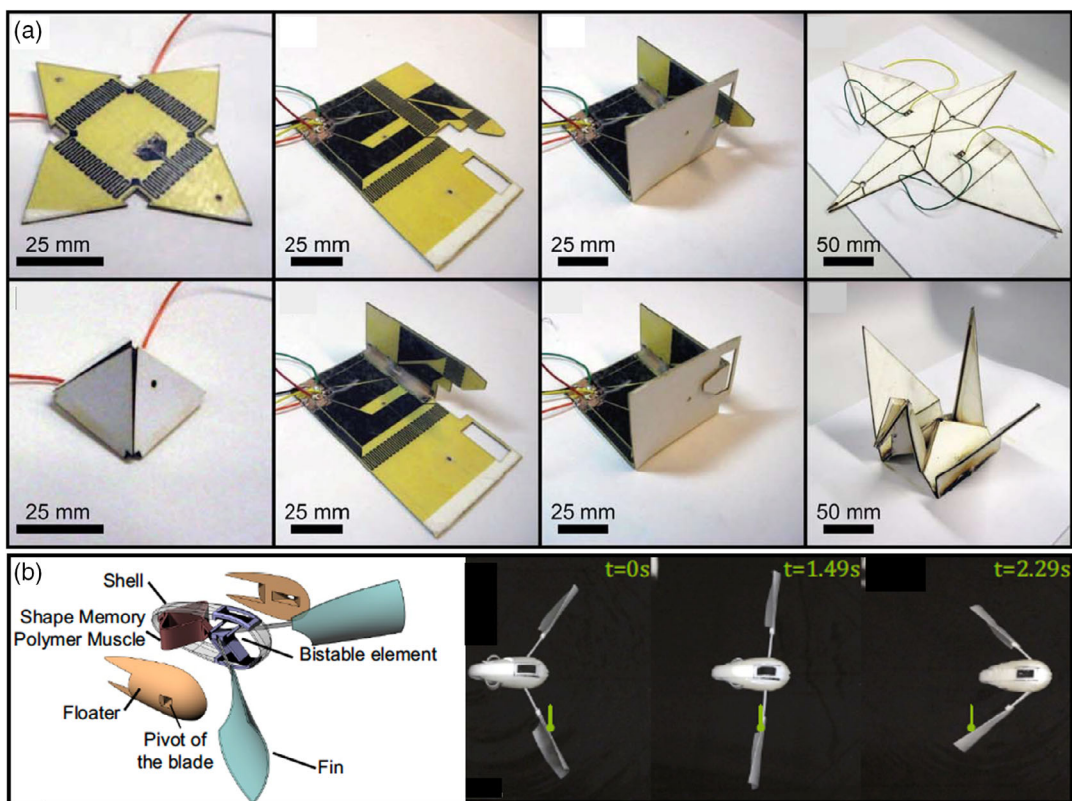


**Figure 9.** Soft robots using SMPs. a) Self-folding pyramid by activating the four hinges simultaneously via 2A supplied current. A crane is also created with a combination of sequential and simultaneous folding. Reproduced with permission.<sup>[162]</sup> Copyright 2013, RSC. b) The parts and the different states of a swimming soft robot. Reproduced with permission.<sup>[163]</sup> Copyright 2018, United States National Academy of Sciences.

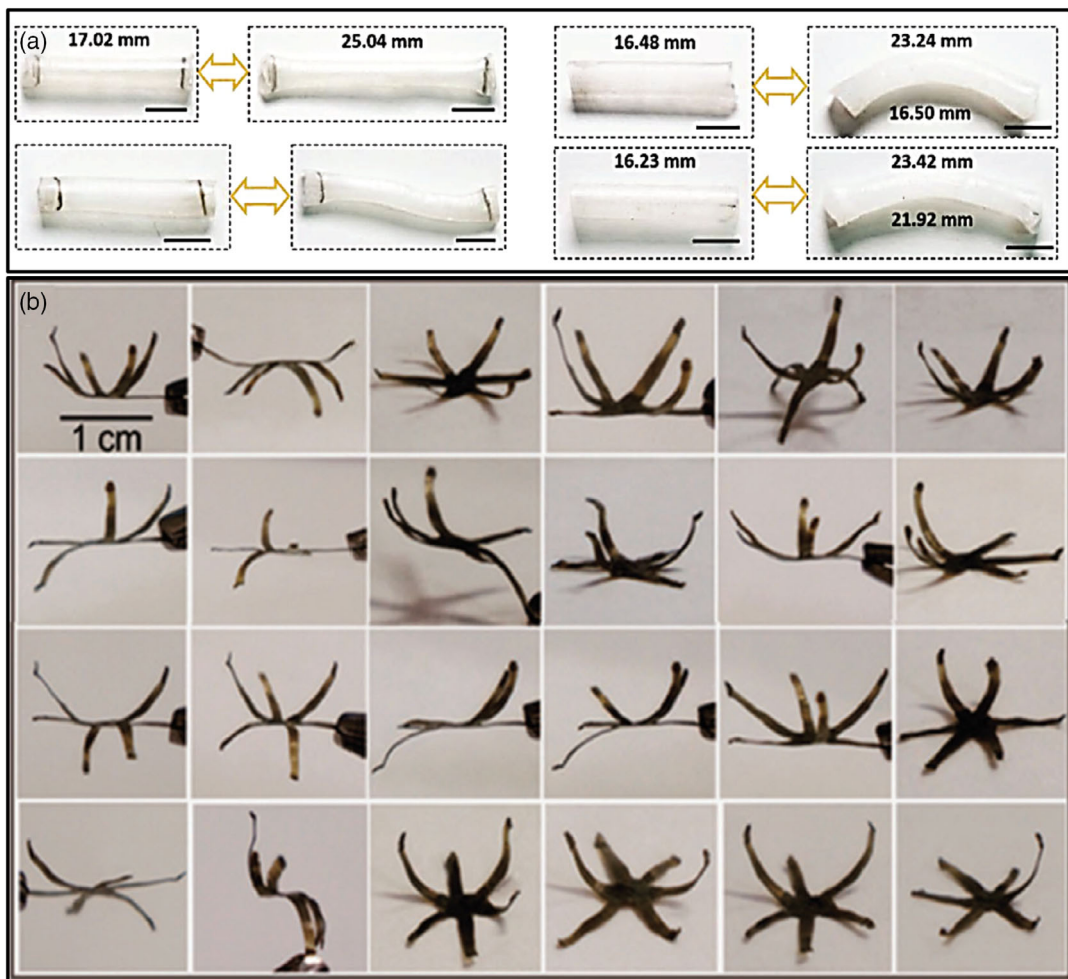


**Figure 10.** Demonstration of movement using LCE. a) Examples of photo-induced complex motions achieved using a single LCE synthesized with allyl sulfide groups in the backbone LCE. Reproduced with permission.<sup>[169]</sup> Copyright 2018, Wiley. b) Light irradiation actuation of a single LCE actuator film into 20 different shapes. Reproduced with permission.<sup>[170]</sup> Copyright 2016, ACS.

objects which were more than 450 times heavier than the hinges (energy density of  $29 \text{ J kg}^{-1}$ ). The printed tiles showed a stiffness of around 766 MPa which enabled a structural robustness under applied loading settings. Moreover, a rolling reconfigurable pentagonal prism was achieved using this technique which can exhibit self-propulsion with a speed of  $0.12 \text{ cm s}^{-1}$ , as shown in Figure 11a. Under complete folding state, the sustained torque of the LCE hinges was  $0.3 \text{ mN cm}$ .

Finally, it should be noted that shrinkable polymer has also been used to achieve actuation and self-folding. Shrinkable polymers contract by a specific percentage (as large as 95% of the original size) when heated up to a threshold value. Gomez and Shin achieved self-folding using easily obtainable and low-cost materials including a shrinkable polymer (modulus of elasticity of 3 MPa) and copper foil. By predesigning the 1 mm hinges, cubic and pyramidal structures were achieved when stimulated at a temperature of  $70^\circ\text{C}$ , as shown in Figure 11b. A  $90^\circ$  folding was possible using 1 mm wide hinges in 12 s of heat exposure. The fabrication in this case was low cost without the need for multiple layers and complex steps. Nevertheless, the

polymer requires either manual or external intervention to recover the initial expanded state.<sup>[179]</sup>

#### 2.3.4. Synthetic Hydrogels

Hydrogels consist of a 3D network of polymer networks with a large percentage of water (up to 99 wt%). Due to this characteristic, hydrogels are capable of substantially shrinking (greater than ten times in volume) as the water percentage in the hydrogel changes, which may take place when exposed to various stimuli including light, temperature, pH, among others.<sup>[180]</sup> Moreover, the sensitivity of hydrogels to biologically relevant stimuli makes them particularly appealing for biomedical applications including tissue engineering and drug delivery.<sup>[178]</sup> One of most commonly used stimuli-responsive hydrogels is poly nisopropylacrylamide (pNIPAM) which has been demonstrated as a soft actuator in various applications such as grippers<sup>[181,182]</sup> and propellers.<sup>[183,184]</sup> In fact, at temperatures of sub  $32^\circ\text{C}$ , pNIPAM-AAc shows a hydrophilic nature and shrinks in water; while at higher temperatures, the hydrogel becomes hydrophobic and expands as it

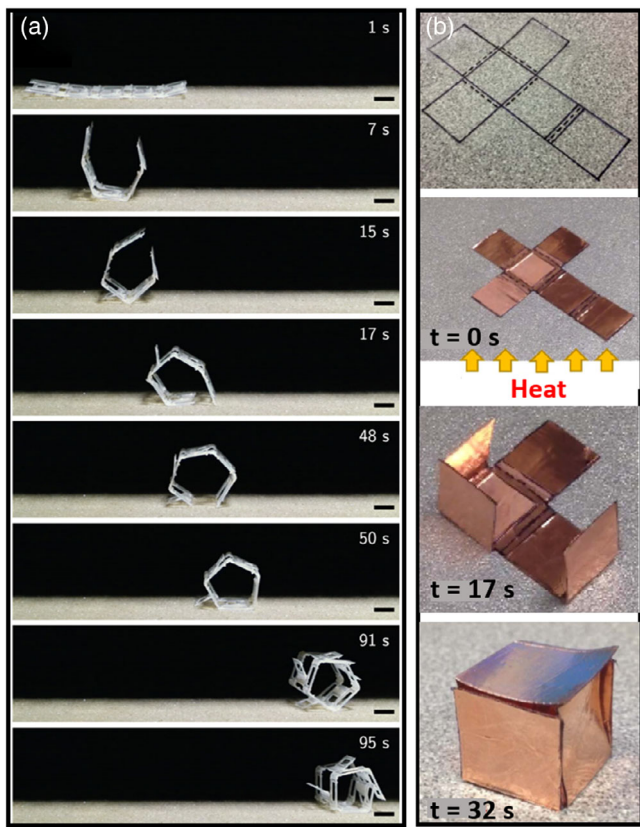


**Figure 11.** Self-folding actuation using thermal stimulus. a) Self-propelling rollbot is shown in its printed configuration and its rolling configuration, in which the low TNI LCE hinges induced folding into a pentagonal prism and the high TNI LCE hinges propelled the rollbot when heated above their actuation temperature. Scale bars, 1 cm. Reproduced with permission.<sup>[177]</sup> Copyright 2019, AAAS. b) Patterned outline on PVC shrink wrap with hinge gaps of 1 mm width between each square and subsequent addition of three-layers of copper foil tape, followed by heating on a hot plate at  $\approx 70^{\circ}\text{C}$ , leading to actuation and self-folding into a cubic shape. Reproduced with permission.<sup>[178]</sup> Copyright 2017, ACS.

dehydrates. Although this makes pNIPAM sound as an ideal hinge material in soft actuators, it generally has a low modulus/stiffness which limits its range of applications.

Gracias and co-workers have worked extensively on several approaches to overcome this limitation for a wide range of biomedical applications. One solution is based on the combination of poly(propylenefumarate) (PPF) with pNIPAM, where PPF is a biodegradable hydrogel with a three orders of magnitude larger modulus than that of most of the existing hydrogels.<sup>[185–188]</sup> As a result, the authors showed a robust gripping device which is several hundreds of microns in size and which can latch onto tissues and cells at the same temperature of the human body for drug delivery application as shown in Figure 12a. In fact, the authors developed a photolithographic technique which allowed the precise shaping of the stiff material such that sharp tips are created which can harmlessly dig into the tissue to secure the position of the theragrippers and deliver the drug. It is worthy to note that the processing methodology is compatible with real drugs. As a proof of concept, the authors showed the application of the

grippers in delivering an anti-inflammatory drug over a week. The mechanical robustness of the system is also studied under a constant fluidic flow, and it was shown that the gripper can remain attached to the tissue up to 20 days before getting carried away. The grippers were also injected into a pig's esophagus through a catheter in an endoscope port; the grippers were initially cold ( $4^{\circ}\text{C}$ ) and as soon as their temperature reached the body temperature within 5 min, the grippers were already in the stomach and closed while digging into the tissue of the stomach. Finally, even though the grippers were not recovered, the authors note that it is expected that they would be fully shed through the natural mucus turnover.<sup>[189]</sup> It is worthy to note that the authors demonstrated a similar micro-gripper structure (pNIPAM and PPF) which can be actuated using both thermal and magnetic stimuli as the hydrogel was filled with magnetic nanoparticles allowing the guidance of the gripper using magnetic fields and temperature, simultaneously.<sup>[191]</sup>

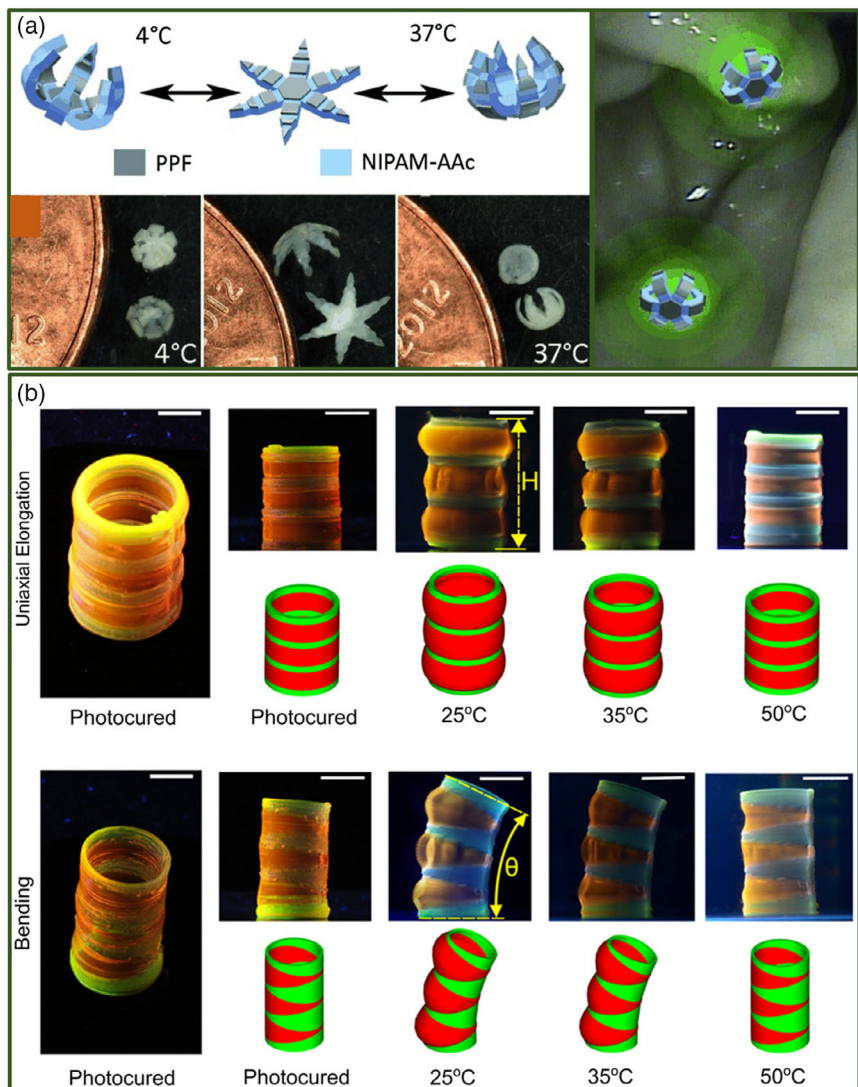
The same group has also shown the ability to customize and tune the soft actuators based on pNIPAM when coupled with 3D and 4D printing techniques. Tubular segmented architectures based on 3D-printed gel tubes composed of alternating pNIPAM and a passive stimuli nonresponsive gel (polyacrylamide) were developed. To achieve this, the 3D printer syringes were filled with both hydrogel inks. Different designs were studied to achieve various actuated states upon exposure to higher temperatures ( $>25^{\circ}\text{C}$ ) with elongations up to 38% and expansions up to 75%. However, at a temperature of  $50^{\circ}\text{C}$ , the 3D tubular structures recovered the original shapes as shown in Figure 12b. Nevertheless, it is worthy to note that the structures were placed in heated water for 24 h to reach the equilibrium state.<sup>[190]</sup>

## 2.4. Photo-Responsive Actuation

Light-stimulated soft actuators are appealing because of their wireless advantage and ability to control them even when small in size.<sup>[192,193]</sup> Photo-responsive materials are based on photochromic molecules which capture optical signals and convert them into different property modifications.<sup>[194]</sup> These molecules can be integrated into various soft actuators including gels, polymers, and fluids. In this section, we divide the photo-responsive actuators based on the light spectrum needed for actuation, visible light (e.g., sunlight) or NIR, which also determines the suitable applications.

### 2.4.1. Visible-Light-Driven Actuators

The capability to stimulate actuators by sunlight enables the development of soft robots that can operate in the natural environment without excess energy consumption.<sup>[195–199]</sup> The currently available photo-responsive actuators are mainly based on liquid crystal polymer networks (LCNs)<sup>[200–202]</sup> or carbon-based materials.<sup>[203–208]</sup> LCN-based actuators normally necessitate a high intensity ( $>1\text{ W cm}^{-2}$ ) of light while showing limited deformations.<sup>[207,208]</sup> For instance, Meijer and co-workers demonstrated a light-stimulated plastic mill which can transform high-intensity light of  $0.5\text{ W cm}^{-2}$  to a nonstop rotational movement as a result of the quick photothermal isomerization around the C–N bond of hydrazones.<sup>[208]</sup> Furthermore, carbon-based



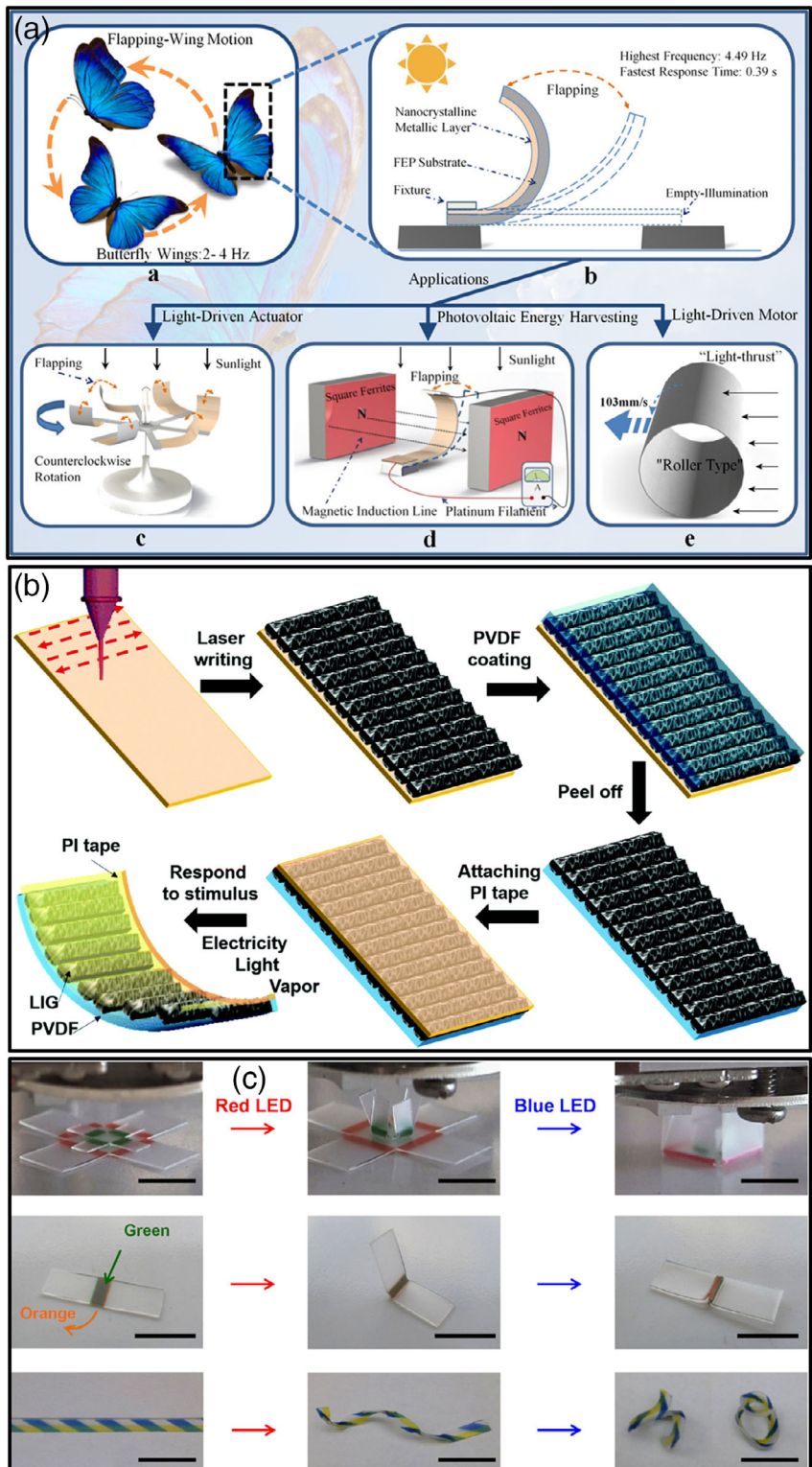
**Figure 12.** a) Schematic of theragrippers with flexible thermo-responsive pNIPAM hinges and rigid PPF panels. The grippers open and close reversibly at the temperature of the human body. Theragrippers are initially closed at 4 °C; they start opening once the solution temperature rises up and lastly closes in the opposite direction at 37 °C. A conceptual illustration of theragrippers secured on a colon wall is also shown where the grippers release a fluorescent drug to desired areas. Reproduced with permission.<sup>[189]</sup> Copyright 2014, Wiley. b) 4D-printed thermo-responsive tubes with horizontal, periodically spaced segments and the resulting elongation/expansion and architecture at different temperatures. The structures were placed in heated water for 24 h to reach the equilibrium state. The scale bars are 1 cm. Reproduced with permission.<sup>[190]</sup> Copyright 2019, ACS.

photo-responsive materials also require high intensities of light while showing simple and small deformations which result in low speeds of locomotion ( $\approx 1.6 \text{ cm s}^{-1}$ ).<sup>[195]</sup>

If nonstop motion of the photoresponsive actuator is needed for a specific application, generally, a periodic loading of light would be needed such that the actuator can deform under illumination and then return to its original state when the illumination is off. This may limit applications under sunlight as it would be difficult to turn the illumination on and off periodically. To overcome this challenge, Dong et al. reported a continuous flapping-wing actuation under sunlight using a nanocrystalline-based metal polymer bilayer. The structure transforms sunlight into a mechanical energy without the need for any added devices. The bilayers used exhibit a significantly large

mismatch in their thermal expansion coefficients; as a result, under sunlight ( $100 \text{ mW cm}^{-2}$ ), bending is achieved and then released due to a self-shadowing effect, as shown in Figure 13a. Using this technique, the highest frequency of 4.49 Hz with a light response time of 0.39 s was reported. It should be noted that a frequency of 2.7 Hz is enough to achieve a flying motion similar to that of butterflies.<sup>[209]</sup>

Inspired by botanical systems where the microstructures are concurrently created and aligned in a single bottom-up process, Deng et al. reported self-morphing soft actuators using laser-induced graphene (LIG) structures developed in a bottom-up approach and which resemble the aligned microstructures of plant cellulose fibrils. The LIG structures are used to dictate the shape of the soft actuator, based on LIG layers and a polymer,



**Figure 13.** Sunlight-driven photo-responsive soft actuators. a) Schematic diagram of continuous flapping wing motion under sunlight. The diagram of a light-driven whirling structure, photoelectric conversion, and a roller-type motor are also shown. Reproduced with permission.<sup>[209]</sup> Copyright 2020, ACS. b) Schematic of the fabrication process of the LIG-based soft actuators. Optical and electron images of a patterned Mizzou tiger logo composed of LIG are also shown. Reproduced with permission.<sup>[210]</sup> Copyright 2018, RSC. c) Sequential self-folding in printed ink-based hinges when exposed to different wavelengths of light. Scale bars 10 mm. Reproduced with permission.<sup>[211]</sup> Copyright 2017, AAAS.

when light stimulated under a 150 W lamp. A bending curvature of  $1.8 \text{ cm}^{-1}$  is reached within 5 s, while 5.5 s are needed for the actuator to recover its original flat shape. In fact, the LIG does not only absorb and respond to light but also electricity, organic vapor, and moisture. As a result, different programmable shapes can be achieved as shown in Figure 13b.<sup>[210]</sup>

Sequential self-folding has also been achieved in printed 2D shapes using visible light. Liu et al. demonstrated hinges on polymeric sheets which were prepared using printed inks having various light absorptivity; as a result, a 3D sequentially folded structure can be realized when light with different wavelengths (red 660 nm, blue 530 nm, and green 470 nm LEDs, intensity  $\approx 0.5 \text{ W cm}^{-2}$ ) is shone on the 2D structure as shown in Figure 13c. The hinges completely fold after an exposure duration of at least 40 s. The development technique is very simple and appealing as it requires a single type of stimuli (light) in addition to a single substrate which is patterned using a desktop printer. Nevertheless, the demonstrated technique allows for a single event of folding and unfolding. However, repeatable deformations could be achieved using reversible SMAs.<sup>[211]</sup>

Not only artificial/synthetic materials and polymers have been used in the development of photo-responsive soft actuators but also biological cells. In fact, nature provides numerous biological cells which can display well-established motion patterns. As a result, these cells have been integrated with artificial materials to achieve biohybrid systems. The used biological cells include motile cells which are capable of swimming (e.g., spermatozoa and bacteria), contractile cells which are capable of generating tensions with desired directions (e.g., skeletal muscle and cardiac cells), and immune cells having inherent chemotaxis capability (e.g., white blood cells).<sup>[212–214]</sup>

As a matter of fact, contractile cells including skeletal muscle cells and cardiomyocytes are capable of generating contractions and directional tensions which were explored as soft actuators in biohybrid micro-robots. Williams et al. demonstrated artificial flagellar swimmers via selectively culturing cardiomyocytes on PDMS filaments including long slim tails and short stiff heads.<sup>[215]</sup> The cardiomyocytes contract intermittently and bend the filament which results in the forward propulsion of the biohybrid swimmer. To enable wireless optical actuation, the

muscle cells are genetically modified to show photo-sensitive ion channels. In fact, biohybrid soft robots have been developed using both optogenetic skeletal muscle and cardiac cells which show tunable contraction based on light stimulus. The optical control over the cells represents a spatiotemporally well-defined stimulus that allows the local contraction of the patterned biological cells on the synthetic substrate and its subsequent deformation to result in propulsion and motion. Synthetic batoid-like fish was demonstrated by selectively patterning the optically responsive cardiomyocytes on an elastomer-based body having an encapsulated gold skeleton, as shown in Figure 14.<sup>[216]</sup> The authors showed the controlled motion of the structure using optical actuation which leads to periodical contraction of the elastomer. An average speed of  $1.5 \text{ mm s}^{-1}$  (15 times longer than its body length) was shown, which was maintained for 6 days with a maximum of 20% degradation. It is also possible to control the speed and direction of the motion by regulating the synchrony and frequency of the light directed on both fins of the structure.<sup>[216]</sup>

#### 2.4.2. NIR-Driven Actuators

In the past few years, NIR light-responsive soft actuators have gained a great deal of attention specifically due to the ability of the long-wavelength NIR light to penetrate through biomaterials with low losses. As a result, NIR became the best biocompatible wireless actuation method for biomedical devices.<sup>[217–219]</sup> Nevertheless, the potential of NIR-stimulated actuators was hindered mainly because of low actuation speeds and degraded mechanical characteristics resulting from poor fabrication technique. In specific, NIR-stimulated soft actuators, which include LCEs<sup>[220–226]</sup> and polymer-based materials,<sup>[227–229]</sup> are generally developed by doping polymers with various photothermal reagents, including CNTs, metal nanoparticles, and graphene.<sup>[229–231]</sup> The photothermal agents absorb the NIR light and transform photon energy into thermal energy that results in the modification of the polymer properties such as phase transition, swelling, or thermal expansion.<sup>[232–234]</sup> The main disadvantage of this development technique is the poor solubility of the reagents within the polymers. Reducing the amount of photothermal reagents results in poor actuation speed,

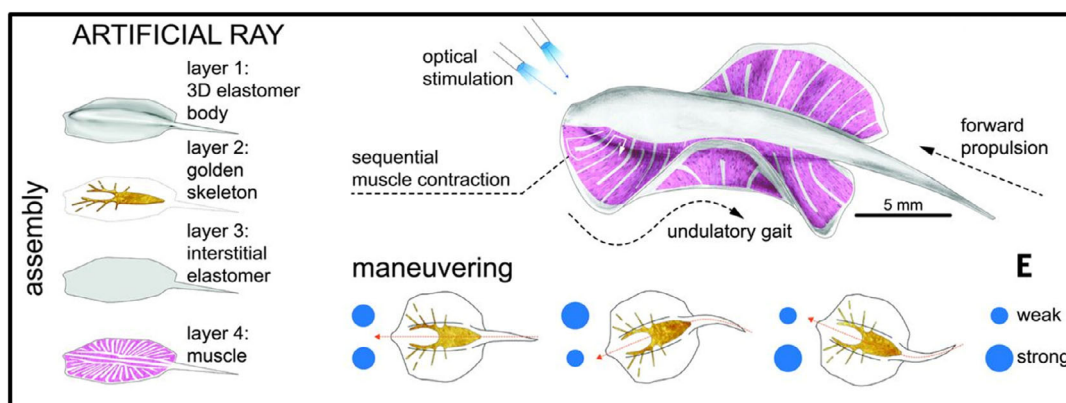


**Figure 14.** Tissue-engineered ray based on an elastomeric body with photo-responsive biological cells. Upon optical stimulation, periodical muscle contraction takes place which results in the propulsion and the swimming of the ray. The direction of the motion can also be controlled by modulating the light pulses on the right and left fins of the ray. Reproduced with permission.<sup>[216]</sup> Copyright 2016, AAAS.

whereas increasing the amount leads to an inhomogeneous doping with degraded mechanical properties of the soft actuator.

To this end, research has been conducted on enhancing the solubility of the reagent via different optimization techniques; nevertheless, a maximum dispersion concentration of around 5 wt% was still limiting the NIR-stimulated actuators.<sup>[229]</sup> To overcome this challenge, Liu et al. reported a two-step acyclic diene metathesis *in situ* polymerization/cross-linking approach to generate single-axially aligned main-chain LCEs with chemically bonded NIR absorbing four-alkenyl-tailed croconaine-core cross-linkers. As a result of the excellent photothermal conversion characteristic of the developed soft actuator, its temperature can increase from 18 °C up to 260 °C in just 8 s when exposed to an 808 nm (0.83 W cm<sup>-2</sup>) NIR wavelength. The mechanical property of the actuator was also confirmed when it was found to be able to lift up objects 5600 times heavier than itself where it shrinks by up to 110% of its original length, as shown in Figure 15a.<sup>[235]</sup> Moreover, Tian et al. reported a PDA-coated LCE-based NIR-stimulated elastomer with fast response. As a result of the photothermal effect of the PDA covering and the thermal sensitivity of LCE, the actuator exhibited large contractions under NIR light (3.1 W cm<sup>-2</sup>), where the maximum generated stress can reach up to 1.5 MPa with an estimated work density of around 10 kJ m<sup>-3</sup>. It is also worthy to mention that not only contraction can be achieved but also rolling and bending. The response time of the actuator can reach down to 0.1 s which is faster than the human muscle actuation speed, as shown in Figure 15b. Using this approach, the authors demonstrated a swimmer robotic system which swims via bending and unbending motions controlled using an NIR laser.<sup>[236]</sup>

## 2.5. Pressure-Driven Actuation

Soft actuators driven by pressure are classified as compliant mechanisms. Compliant mechanisms need to pattern their

stiffness properties spatially to provide efficient actuation, and they can be stimulated by external forces or pressure to generate the desired deformations. Although a wide range of compatible mechanisms exist, works on high-precision machines and MEMS have been well analyzed and reviewed<sup>[237–239]</sup> with a key focus on the topological optimization of continuum structures.<sup>[240–249]</sup> Miniaturized hydraulic pressure-driven soft actuators are also gaining a lot of interest even though they are less common than the thermally and electrically stimulated NEMS and MEMS devices.<sup>[250,251]</sup> Such soft actuators have shown the ability to produce good intensities of forces even at small scales. In this field, researchers are focusing on simplifying the manufacturing process of miniaturized inflatable chambers, achieving more accurate locomotion, in addition to generating higher forces.<sup>[252,253]</sup> Moreover, although pressure-driven actuators can generate high forces with a potential of being lightweight, they generally need to be connected to a quite large-sized external and rigid pump. In the following, different pneumatic-based and hydraulic-based actuators along with their applications will be discussed.

### 2.5.1. Pneumatic Actuators

Pneumatic actuators, also commonly referred to as pneumatic cylinders, air cylinders or air actuators, are highly efficient and safe sources for controlling motion by transforming energy into either linear or rotational motion using pressurized gas or air. They are specifically suitable for application in repetitive opening and closing of valves, areas of extreme temperature, or in industrial applications where the alternative electric or magnetic actuators could cause interference or hazard (for example, fire ignition from electricity). Pneumatic actuators are widely used for controlling valves that conduct fluid movement in process and chemical industries.<sup>[254]</sup> Nevertheless, most pneumatically stimulated soft robots are difficult to miniaturize as they need to be connected to rigid control and power systems to provide adequate forces required for locomotion.

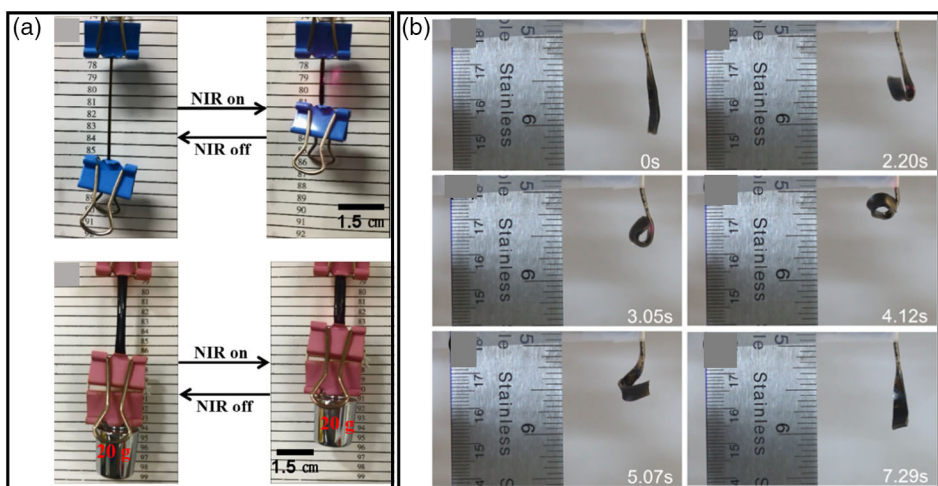


**Figure 15.** NIR photo-responsive soft actuators using LCE. a) Photo of a LCE ribbon before and after NIR (808 nm) illumination and photo of a LCE film (4.3 mg) lifting up a load ( $\approx$ 24.44 g) under NIR illumination. Reproduced with permission.<sup>[229]</sup> Copyright 2013, APS. b) Rolling up of PDA-coated mono-domain LCE film with light scanning on the surface of a film from bottom to top. At 4.12 s, the laser was turned off and the PDA coated LCE film recovered back to its original flat shape within 3 s. Reproduced with permission.<sup>[231]</sup> Copyright 2016, ACS.

A pneumatically stimulated implantable reservoir has been reported by Dolan et al. The millimeter-scale dynamic soft reservoir (DSR) uses mechanical oscillation to modify the biotic–abiotic interface biomechanics by interrupting the flow of fluid and peri-implant tissue cell activity. An implanted pump would periodically stimulate the system and was demonstrated in a rat. As the stimulating reservoir is pressurized throughout the stimulation line, the chamber increases in volume and consequently in pressure. This results in downward deflection of the middle and the lower membranes. The membrane deflection causes strain (up to 8.6%) which leads to the movement of the fluid at the tissue interface which is interfering with the cell activity. This approach makes use of the precise mechanical stimulation to provoke a desired biological response which would also reduce the fibrotic encapsulation of the implantable medical system.<sup>[255]</sup>

Yang et al. reported the development of reconfigurable and multifunctional metallic backbones which are pneumatically stimulated. The metallic backbones are used in the development of origami robots with on-board wireless communication and strain-sensing abilities. The developed origami based on Pt are further stabilized using a thin elastomer that are reconfigurable and act as the backbones in the origami robot. The planar Pt–elastomer composite (Young's modulus of around 10 MPa) was shown to withstand large and repetitive deformations where the elastomer was tested under a bending angle of 180°, twisting angle of 360° twisting, and stretchability of 30% (and up to 175%

strain). The developed reconfigurable backbones based on Pt–elastomer are thinner, more flexible, and more power efficient in comparison with traditional materials, such as plastics, papers, and other metal sheets. Moreover, using this technique, a soft robot that could crawl at a speed of  $0.2 \text{ cm s}^{-1}$  was reported.<sup>[256]</sup> Su et al. demonstrated an airtight bending actuator which can withstand high pressures of air during actuation which is needed for achieving large bending angles and large forces. This was achieved by the combination of multiple rigid and flexible components which enhanced the mechanism robustness of the system, as shown in **Figure 16**. To achieve this, a nonexpanding layer was inserted between two expanding Ecoflex-based layers. Using a combination of rigid and stretchable materials, the authors developed lightweight and small-scale actuators that show complex motions such as twisting.<sup>[257]</sup>

### 2.5.2. Hydraulic Actuators

Hydraulic actuation is generally achieved by inserting and pumping fluids into designed chambers which can be used to generate a desired movement, such as bending, twisting, etc. Similar to pneumatic actuators, most hydraulically stimulated soft robots are difficult to miniaturize as they need to be connected to rigid control and power systems to provide adequate compression force for locomotion. Katschmann et al. demonstrated a fluidic

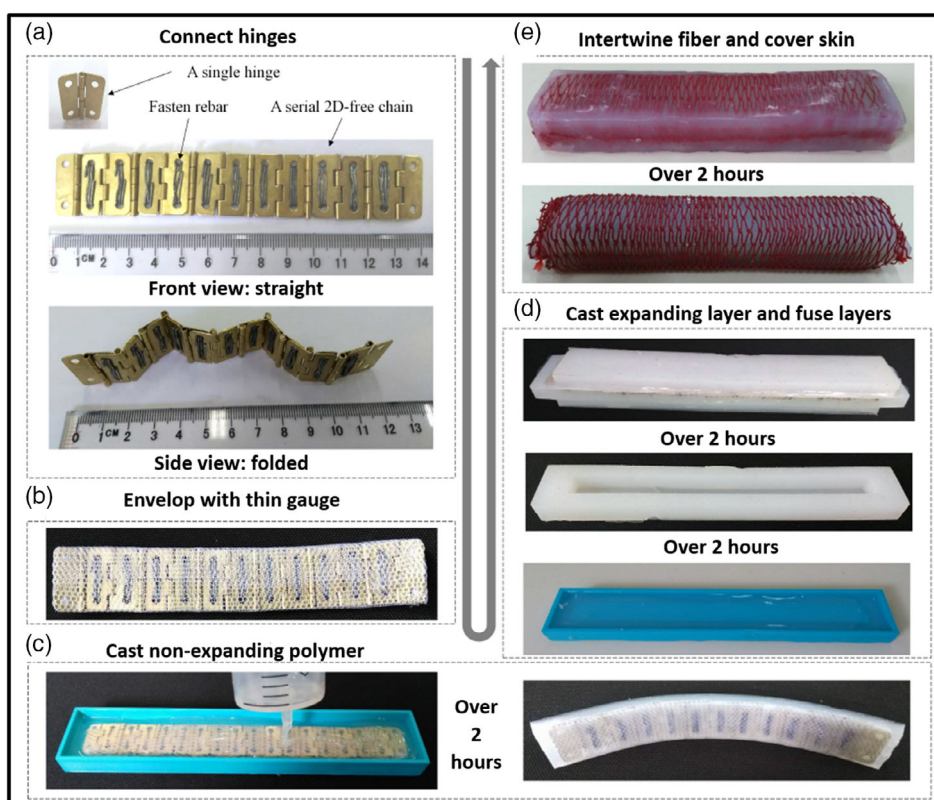


**Figure 16.** Fabrication process flow of the pneumatic actuator which can withstand high pressures of air during actuation. This was achieved by the combination of multiple rigid and flexible components. The process flow includes the following steps: a) connect hinges, b) envelop with thin gauge, c) cast non-expanding polymer, d) cast expanding layer and fuse layers, and e) intertwine fiber and cover skin. Reproduced with permission.<sup>[252]</sup> Copyright 2014, Mary Ann Liebert, Inc., publishers.

elastomer-based soft fish tail to enable swimming of a 1.65 kg fish-like robot, as shown in **Figure 17a**. The design mimics the rear part of a fish, including the caudal fin and the posterior peduncle. Using hydraulic actuation of two lateral cavities available on both sides, the tail continuously bends along the center layer, which is made of a stiff and nonstretchable material. The actuator is based on equally distributed ribs with empty space between them, connected via a channel in the center that is accessible by an inlet in the front to allow the insertion of fluid. The rib design enables the thin external skin to inflate or deflate depending on the hydraulic pressure, which can be either positive or negative. The inflation and deflation movements lead to the bending of the central nonstretchable layer, and thus the swimming motion with a speed of  $0.1 \text{ m s}^{-1}$ . A gear pump is used to pump the fluid in and out of the ribs which was controlled wirelessly through a microcontroller. This demonstration shows that complex motions can be achieved by designing fluidic chambers for application in underwater robots.<sup>[258]</sup> Sinatra et al. demonstrated a hydraulically actuated system for application in noninvasive grasping of marine organisms. Their 123 g grasping system was based on six composite “finger” actuators connected to a “palm” that was 3D printed. Each actuator was based on an elastic but mechanically robust silicone layer, in addition to flexible polymeric nanofibers which were used as the strain-limiting layer. In fact, the failure pressure of nanofiber-reinforced actuators was considerably larger than that of pure silicone based actuators. Therefore, controlling the nanofiber elastic modulus, fiber layer thickness and orientation play a role in defining the bending and curvature characteristic of the actuator. Moreover, the gripper system is shown to be stimulated using low hydraulic pressures compared with ambient ( $6.9\text{--}41.4 \text{ kPa}$ ) and resulting in a pull force of  $0.77 \text{ N}$  and a retraction speed of  $0.050 \text{ m s}^{-1}$ .<sup>[260]</sup> Galloway et al. demonstrated a hydraulically stimulated soft robot for gripper application as well, as shown in **Figure 17b**. The grippers are monolithic structures and are coupled to a palm. The soft actuators, which were reinforced using PneuNets (pneumatic networks) and fibers, showed a robust performance at underwater depths greater than 800 m. Pneumatic networks are a network of custom-designed chambers to generate specific motions by controlling, for example, chamber size, chamber

angle, and chamber distribution. The reported actuators are found to operate at high pressures (up to  $170 \text{ kPa}$ ). Two distinct architectures of soft actuators were embedded in the robot, including a boa-type actuator ( $2 \text{ kPa}$  applied pressure, holding force of  $16 \text{ N}$ ) used to reach constricted areas by changing its shape reversibly from a straight beam to a helical architecture, and also a bellows-type actuator ( $7 \text{ kPa}$  applied pressure, holding force of  $44 \text{ N}$ ) that can generate asymmetric motion through unfolding of the surplus material embedded in the bellows.<sup>[259]</sup>

## 2.6. Explosive-Based Actuators

Another approach to generate motion is through the use of explosive-based actuators. In fact, explosive chemical reactions could produce pulses of high-temperature gas for PneuNet actuation. Different methods have been reported to build such a soft robot, including multi-material 3D printing.<sup>[261]</sup> For instance, Shepherd et al. developed an approach to enable a robot to jump more than 30 times its height (around 30 cm) in less than  $0.2 \text{ s}$  (speed  $3.6 \text{ m s}^{-1}$ ). PneuNet actuation was achieved by the explosive chemical reactions between hydrocarbons and an electrical spark which caused the soft robot to jump. One limitation in this approach was the inability to control the orientation or direction of the jump.<sup>[134]</sup> To overcome this constraint, Loepfe et al. demonstrated the directed jump of a  $2.1 \text{ kg}$  soft robot through the explosive combustion of butane. **Figure 18a,b** shows the combustion chamber before and during the combustion. As a result, the robot can jump 7.5 times its body height in  $20 \text{ s}$  with a linear speed of  $0.9 \text{ cm s}^{-1}$ . However, the reported robot cannot position itself for the next jump if it lands on its back.<sup>[135]</sup> Bartlett et al. reported directed jumping in 3D-printed soft robots powered by the combustion of butane and oxygen. The directed jumping (up to  $1.12 \text{ m}$  height up to 100 cycles) was achieved through the use of pneumatic legs which help the robot to tilt prior to jumping, as in **Figure 18c-f**.<sup>[262]</sup> Nevertheless, actuation based on explosive materials show a limited shelf life as chemicals need to be replenished; they are not scalable, their applications are limited, and they require very strong mechanical resilience to sustain the explosive impact event.

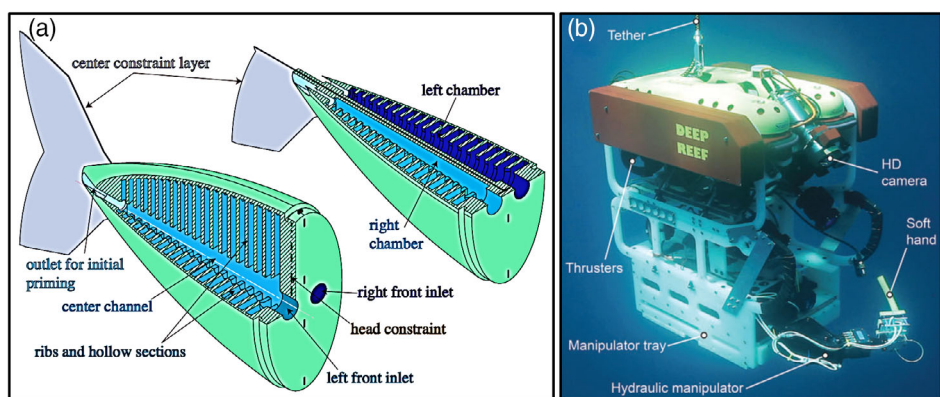


**Figure 17.** Demonstrated applications of hydraulic actuators. a) Fish soft tail as an elastomer-based hydraulic actuator consisting of two fluidic chambers. The horizontal and vertical cuts of the tail are shown. Reproduced with permission.<sup>[258]</sup> Copyright 2016, Springer. b) The Seaeye Falcon submersible (Deep Reef ROV) platform which uses a hydraulic manipulator. Reproduced with permission.<sup>[259]</sup> Copyright 2016, AAAS.

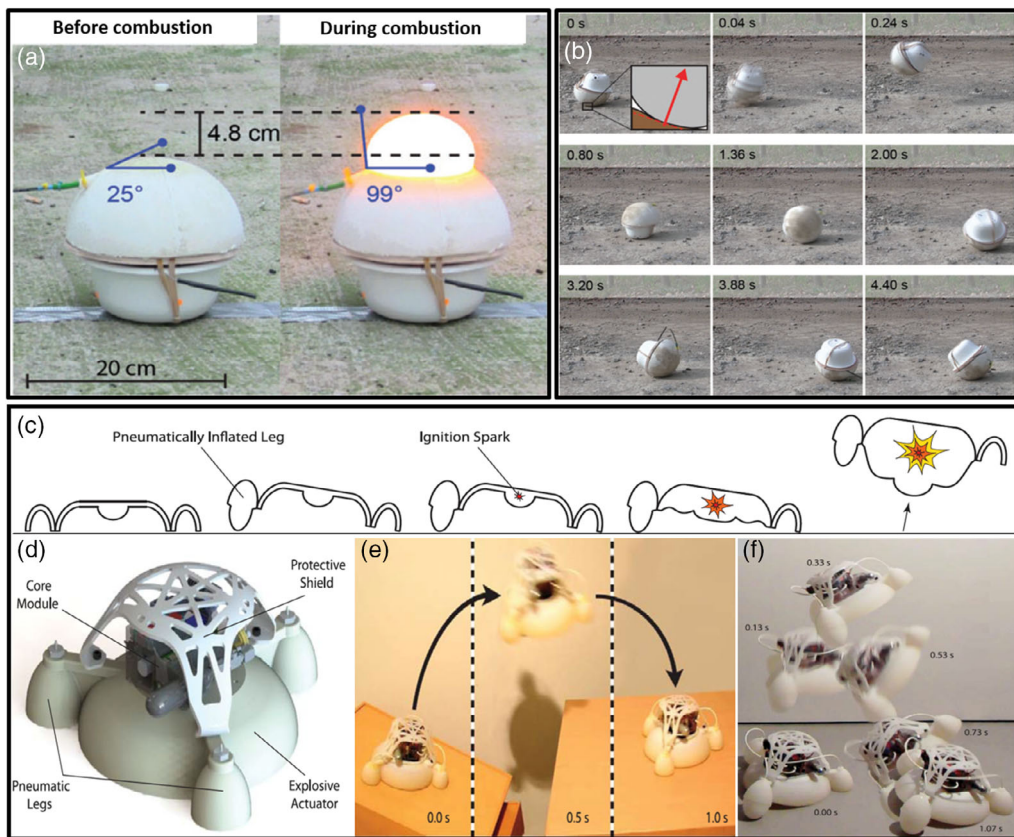


**Figure 18.** Examples of explosive-based actuated soft robots. a) Before and during photos of the combustion chamber deformation due to combustion. b) The reorientation behavior of the explosive-based soft robot is demonstrated. Reproduced with permission.<sup>[135]</sup> Copyright 2015, AAAS. c) Depiction of the soft robot jumping procedure using pneumatic actuated legs to define direction. d) Representation of the soft robot components. e,f) The soft robot is shown when jumping in specific and desired directions. Reproduced with permission.<sup>[262]</sup> Copyright 2015, AAAS.

### 3. Electrodes for Soft Actuators

The optimized selection of electrode materials and structures to be integrated with soft actuators depends on the actuation principle of the stimuli-responsive actuator. In general, soft actuators which can be electrically or thermally stimulated require highly flexible and stretchable electrodes which can achieve reliable and conformal contact with other parts of the actuator.<sup>[263–265]</sup> Various fabrication techniques have been studied for the development of flexible and stretchable electrodes including the geometric patterning of electrodes based on fractal designs or the deposition of the electrodes on compressed thin films. Moreover, a wide range of electrode materials have been studied including metallic films/diaphragms, carbon-based materials (carbon powders, graphene, CNTs), nanoparticles, liquid metals, ion/hydro gels, and different composite materials.<sup>[263,266–271]</sup> Carbon-based materials are most commonly used due to their conductivity even under high applied levels of stress/strain, whereas CNTs are the most common among all carbon-based materials. For instance, Zhao et al. designed rolled DEAs which utilizes CNTs-based electrodes developed using a stamping process from polytetrafluoroethylene (PTFE) filter.<sup>[56]</sup> Nagireddy et al. proposed CNTs-based multilayer-perforated electrodes for DEAs which enable a lower capacitance in the DEA as the

number of perforations is increased.<sup>[268]</sup> Wu et al. demonstrated high-performance actuators using graphite carbon nitride nanosheet-based ionic electrodes.<sup>[271]</sup> Liquid crystal materials have also been broadly explored in the development of electrodes for soft robotics due to their high electrical and thermal conductivity at normal room temperature.<sup>[272]</sup> Moreover, the electrodes should be based on a material that is effective and reliable in terms of showing a high conductivity and being insoluble and noncorrosive in humid environments.<sup>[273]</sup> Even though the materials which have been used for the electrodes fabrication are well established with an excellent performance, cost effectiveness, and energy efficiency, the stabilization, feasibility, high polarizability, and handling of electrodes are challenges which still need to be improved, which would otherwise degrade the stability and reliability of the actuators.<sup>[273]</sup>

The enhancements in flexible and stretchable conformal electronics enabled the placement of electronics on curvilinear and irregular surfaces which revolutionized human healthcare and the wearable electronic sectors.<sup>[264,265,274]</sup> The contact between actual human skin and artificial sensors/actuators e-skin generally requires excellent conformability which is the motivation behind material selection for soft actuators too.<sup>[274,275]</sup> Moreover, as the actuators would bend and stretch upon exposure to a stimulus, the electrodes should be compliant, conformable,

and stretchable. Based on the application requirements, the electrodes can also be transparent and morphological.<sup>[264,265,276,277]</sup> Finally, to increase the life span and the reliability of the soft actuators electrodes, encapsulation is usually used. Different solid and liquid materials have been used for the encapsulation of the electrodes including PDMS, Ecoflex, silicone, polyimide, and hydrogels, each of which exhibit different flexing and stretching capabilities in addition to different properties which makes them suitable for different ranges of applications (e.g., air permeability, water permeability, cost, curing temperature, etc.).<sup>[273,277–279]</sup>

## 4. Applications

Soft robotics is still considered a growing field, defining new fabrication techniques and control methods. To realize inventive systems, researchers are being inspired by nature's solutions to achieve soft and compliant joints, insect-like and fish-like robots, and so on. In this section, the application of soft robotics in three different fields, including nature-inspired robots, ring oscillator and biosensing, with specific examples will be covered.

### 4.1. Nature-Inspired Soft Robots for the Realization of Complex Motions and Tasks

Human-made robots are generally stiff so that they can achieve precise, fast, and repetitive tasks with good mechanical robustness. In contrast, most of animals are soft bodied even when they have stiff exoskeletons, such as insects. The human body for instance consists of 11% skeleton, whereas muscles contribute to around 42% of the body mass. Analyzing how animals use their soft body to perform complex motions and tasks can generate instrumental insights for the development of robotic applications in human assistance, medicine, and disaster response in unpredictable environments. As a result, the robots may be able to realize some unique tasks that are out of reach of the traditional rigid robot. Earthworm-inspired soft robots may do better jobs, for instance, in the rescue of trapped people after the earthquakes. Although animals' motion is based on an interconnection between neural and mechanical controls, soft robotics target to produce simple mechanisms using the "mechanical intelligence" of innovative combinations of soft materials.<sup>[280]</sup>

Inspired by starfish motion, Mao et al. demonstrated a starfish-like soft robot having flexible rays fostering multi-gait movement via SMA actuators.<sup>[281]</sup> As previously explained, SMA actuators are materials that can go through deformation while having the ability to return to their original shape using a heat treatment. SMA actuators offer a high cyclic energy density and a high power-to-weight ratio, enabling the actuators to generate significant displacements with simple mechanisms. Due to the large size and quite minor force characteristic of elastic materials deformation, the authors selected SMA-based springs as the actuators for the starfish-like soft-robot prototype. The deformation kinematics of the SMA springs were modeled using a reverse martensitic transformation that goes through three primary stages, as shown in **Figure 19a**. In demonstrated work, the SMA-based actuators were integrated into the flexible rays of a starfish-like soft robot having a symmetrical structure of five

rays and a soft internal skeleton. As shown in **Figure 19b**, the prototype consists of two layers—a sealing and a shaping layer. Both layers were made of silicone curing agent and colorants, built using 3D printing technology. The soft robot was encapsulated by a specific silicone rubber that allows the robot to achieve various postures and meet the essential flexible deformation requirements.

Locomotion and control strategy were developed to meet the force and displacement requirements. Those strategies were applied to the SMA actuators by rapid impulses of high currents and open-loop sequential control. Because of the unsealed soft rays design, the prototype was tested in terrestrial environments only, such as sand, clammy rough terrain, rough ground, and rocks. The starfish-like soft robot successfully navigated various terrains. As for the dry sand terrain, the robot could crawl smoothly with an average speed of  $130 \text{ mm min}^{-1}$ . Similarly, the robot could creep across a clammy rough terrain with an average speed of  $20.7 \text{ mm min}^{-1}$ . As shown in **Figure 19c**, the performance analysis in different terrains was given. Due to the different characteristics of each terrain, the prototype was 6.5 times quicker on sand than when it was placed on a clammy rough terrain. As for the rocky terrain, the robot successfully crossed over an obstacle that was around twice its body height of  $12.2 \text{ mm}$  and completed a rolling motion to leave the rocks. In addition to that, the results indicated that the robot could bypass enormous obstacles by managing the timing sequence of the rays multi-gait pattern. The authors discussed a few limitations of the demonstrated prototype including underwater speed, autonomy, adaptability, and modeling methodology. Nonlinear analysis of the soft rays is required to obtain an accurate locomotion analysis and achieve robustness in irregular environments.<sup>[281]</sup>

### 4.2. Ring Oscillator for Chronological Manipulations in Time and Space

A ring oscillator is a device which consists of an odd number of NOT gates integrated in a loop, where its output varies between two levels, realizing binary signal 1 and 0 or true and false. The inverters, or NOT gates, are interconnected in series where the output of the final inverter is fed back into the initial one. Preston et al. presented the development of a soft ring oscillator which produces periodic movement in soft actuators via a single source of constant pressure.<sup>[282]</sup> More specifically, the ring oscillator consists of an odd number of soft pneumatic inverters. A single soft pneumatic inverter was built using an elastomeric valve with two cylindrical chambers and an elastomeric tube that goes through both chambers. The chambers are separated by a hemispherical membrane. The valve has two states: unactuated and actuated, as it interchanges between them depending on the input pressure. The upper chamber of the inverter is connected to an adjustable input pressure while atmospheric pressure ( $\text{Patm}$ ) is applied to the bottom chamber. Initially, the membrane is in its unactuated state deflected upward, resulting in kinking the elastomer tube inside the upper chamber, allowing the  $P_{out}$  to connect to  $P_{supp}$  in the bottom chamber. Once the input pressure increases and surpasses a critical pressure ( $P_{snap-thru}$ ), the membrane is in the actuated state deflected toward the bottom chamber, causing a flow blockage in the internal tubing of the

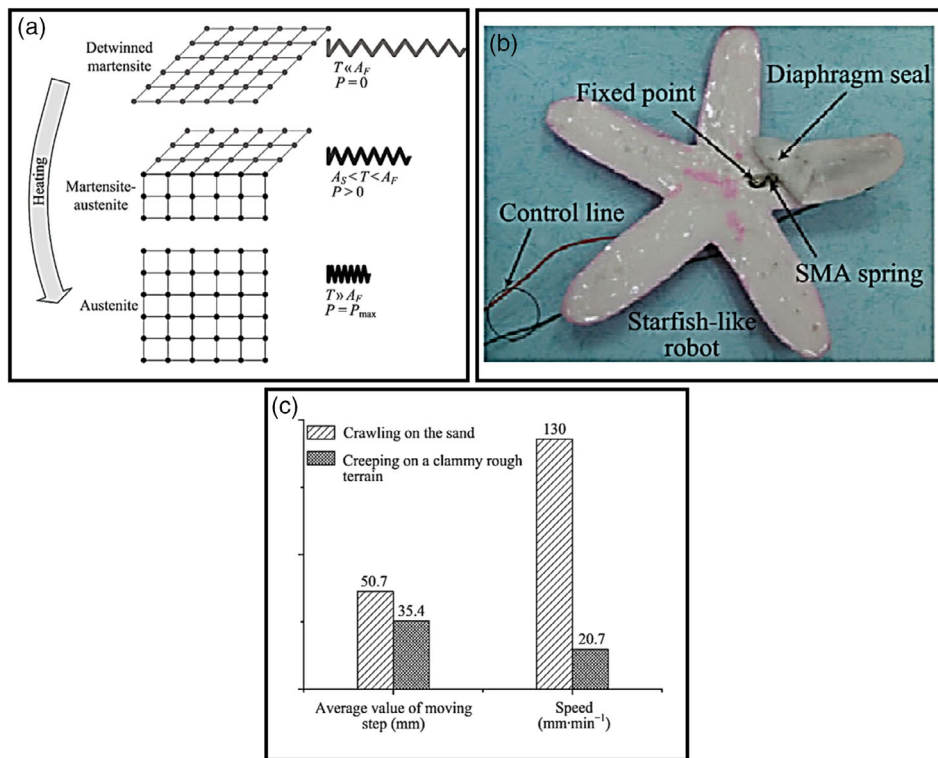


**Figure 19.** Nature-inspired soft robot using SMA actuators. a) The three primary stages of reverse transformation of SMA spring deformation. When the temperature increases, the spring causes continuous bending deformation during the total reverse transformation. In contrast, when the temperature decreases, the spring returns to its original state. b) The soft robot prototype consists of the SMA actuators and the soft silicone rays. c) The average value of moving step and speed of the prototype on sand and clammy rough terrain. Reproduced with permission.<sup>[281]</sup> Copyright 2014, Springer.

bottom chamber and the connection of  $P_{atm}$  to  $P_{out}$ , which inverts the input signal.

The authors thus developed a soft ring oscillator using three NOT gates interconnected in series. Inverters in the loop sequentially inflated and deflated, resulting in output pressures with periodic, temporally offset oscillation with  $120^\circ$  phase shift. The inverters were fabricated using Dragon Skin 10 NV,  $P_{snap-thru}$  of around 11 kPa,  $P_{snap-back}$  of around 2.5 kPa, connected to constant pressure  $P_{supp}$  of 17 kPa and with an oscillation period of 3.1 s. The dependence of the oscillation period was studied against the three system factors: the supply pressure ( $P_{supp}$ ), the pneumatic resistance, and capacitance. First, the supply pressure was increased from 11 to 20 kPa. This showed that increasing the supply pressure results in decreasing the oscillation period. Second, additional tubing with the lengths ranging from 0 to 1.27 m was added between the inverters, and this showed that increasing the tubing length increases the oscillation period. Finally, additional glass jars were added between the inverters with pneumatic capacitance change from 0 up to 315 mL; this showed that increasing the pneumatic capacitance results in increasing the oscillation period.

The authors showed several applications of the soft ring oscillator to drive motion. In one, a ball was moved around a track consisting of an array of chambers connected to the ring oscillator outputs in a recurring pattern. Serial inflation and deflation of the chambers allowed the forward movements of

the ball. In another motion application, a soft and hexagonal-shaped robot which rolls with a flexible foam-based border was built using a soft ring oscillator. Figure 20a shows the soft robot rolling from one side of the structure to the adjacent as double-balloon actuators added on each front consecutively inflate and deflate. In addition to movement, the ring oscillator can be used to control chronological manipulations in time and space. As shown in Figure 20b, size-based particle sorting was implemented by controlling an elastomeric stage using a soft ring oscillator. In addition, soft medical or therapeutic devices can be designed using a soft ring oscillator. One application demonstrates a mechanotherapeutic system using textile which can wrap around the lower leg and provide upward-propagating pressure through the inflation of the internal pneumatic chambers. Finally, a soft ring oscillator can be also used to control liquid flow. Nevertheless, the main challenge was in the inverter fabrication. Casting the inverters in 3D using molds that were previously printed and manually assembling the parts is not efficient. This process can be shortened using direct 3D printing or roll-to-roll manufacturing of a flat 2D version of the elastomeric inverters.<sup>[282]</sup>

#### 4.3. Biosensing

The future generation of soft robots will be extremely improved when synthetic biology is integrated with soft materials.

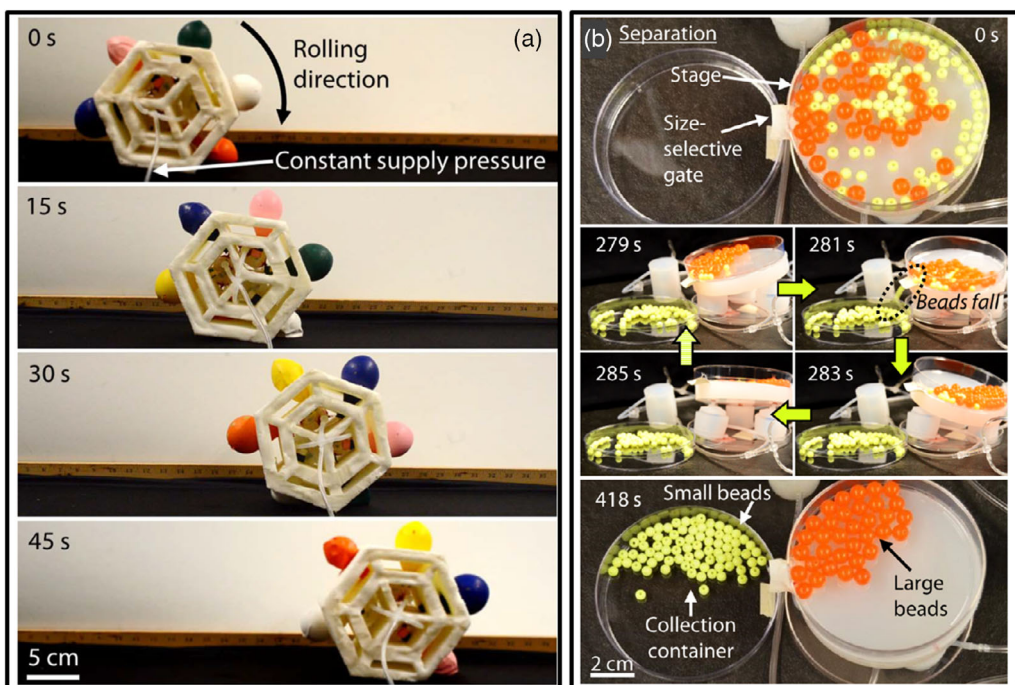


**Figure 20.** Example applications using ring oscillators. a) Double-balloon actuators mounted on each face of the hexagon cause it to tip from one face to another during inflation and roll with only a single, constant-pressure input required. b) Separation of particles by size. The three temporally coordinated output pressures from the ring oscillator enable separation. The stage motion can separate particles of different sizes when a size-selective gate is placed on the side of the stage. Reproduced with permission.<sup>[282]</sup> Copyright 2019, AAAS.

Synthetic biology enables the realization of bioinspired systems which exhibit the functionality of different biological structures with different dimensions. Such developments complement the current inventions in the soft robotics field where soft materials are able to achieve flexible, lightweight, and multifunctional complete systems with excellent mechanical resilience for mimicking natural biological tissues and organisms.<sup>[280,283–288]</sup> Up to date, the building blocks for soft robots mainly consist of elastomers, metal alloys, fluids, and other inorganic materials. The resulting systems include artificial muscle actuators which can be stimulated either pneumatically, or when exposed to heat using SMAs and DEAs.<sup>[285]</sup> Artificial skins have also been demonstrated which can sense various parameters such as pressure and heat.<sup>[284]</sup> Moreover, elastic matters have been used during the development of soft robots that mimic natural biological organisms<sup>[289–291]</sup> and bioinspired grippers.<sup>[292–294]</sup> More recently, biohybrid materials, which integrate biological cells with soft materials, have been used as soft actuators. The resulting soft robots are able to swim or crawl, due to the contractile cells integrated on a polymeric or 3D-printed substrate,<sup>[295,296]</sup> sense and achieve computations.<sup>[297,298]</sup> The biohybrid materials promise a miniaturized soft actuator capable of chemical signal detection.<sup>[299–301]</sup> Thus, such materials are promising components to be integrated into compliant bioinspired devices as it increases their functionality in a reduced area. Nevertheless, the main challenge for the integration between biological cells and soft robots is the unavailability of a flexible and small-scale interfacial communication protocol or module between the cells, the electronics, and the environment. The main role of this

module would be to protect the cells and hinder their escape from the system, enable the exchange of the electrical or chemical signals detected from the environment, and to convert these collected signals to cellular and to electronic signals. Recently, a biosensing module integrating biological *E. coli* cells with a soft gripper was reported by Justus et al. for application in detecting chemicals available in the environment, such as IPTG.<sup>[301]</sup> A flexible light-emitting-diode circuit was used in this case to convert the cellular signal into an electronic signal, whereas a PneuNet hydraulic actuator was used to convert the electronic signal into a mechanical one where the gripper would move. Three different soft materials have been used in the development of the soft gripper membranes and on which the cells were cultured, including PDMS, polyethersulfone (PES), and polycarbonate track etch (PCTE). PCTE and PES membranes provided better uniformity in terms of pore sizes and distributions, which resulted in enhanced permeation of the chemical; however, they lacked optical transparency and elastomeric properties compared with PDMS, as shown in Figure 21.<sup>[301]</sup>

## 5. Future Perspectives and Conclusion

Robotic actuation necessitates proper interactions between the environment and a body. Traditionally, robots use nondeformable components and accurate controls to exert forces and manage the movement of the system. Soft robots are challenging this traditional strategy, which is based on rigid bodies, and are coherently defining new principles for achieving robotic actuation with

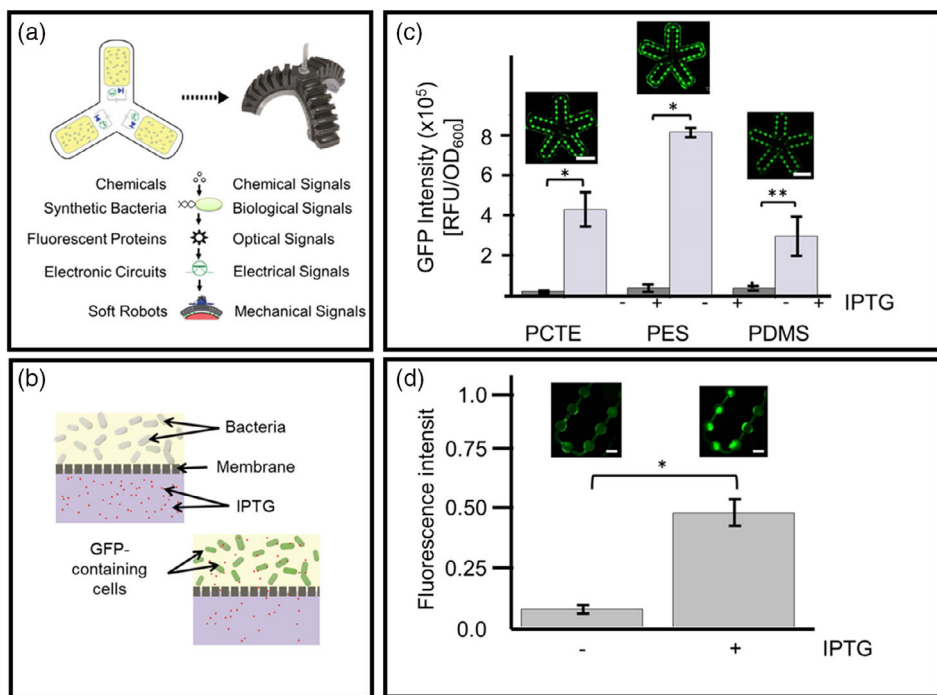


**Figure 21.** Integrating chemical-responsive synthetic cells and flexible materials for a biosensing soft robot. a) Genetically modified *E. coli* housed in fluidic wells and channels within a PDMS polymer mold. This approach enables an integrated soft robotic system featuring pneumatic actuation and embedded electronics with feedback from engineered cells. b) The sealing membranes have pores that allowed chemical stimuli while rejecting bacteria to maintain biosensing capabilities. c) To have control over the engineered cell interface, various membrane compositions were integrated with the device and evaluated for permeability, including PCTE, PES, and PDMS. Scale bars, 2 cm. d) Induced chemosensitive bacteria were introduced into a patterned PDMS layer sealed by a transparent PDMS membrane and imaged using a laser scanner to observe the fluorescent signal from within the device. Scale bars, 3 mm. Reproduced with permission.<sup>[30]</sup> Copyright 2019, AAAS.

soft bodies. In this article, we reported some of the actuation mechanisms used in soft robots which range from the micrometer scale to the centimeter scale and larger. The most recent or most notable results were reported with a focus on the underlying principles behind the movements achieved in the soft robots in addition to the soft robotics application. A wide range of materials have been reviewed which can be stimulated either electrically, magnetically, pneumatically, hydraulically, or thermally. Other materials were responsive to pressure differentials and chemicals. The discussed soft actuators were based on either polymers, fluids, papers, inorganic material or even hybrid materials which integrate biological cells and matter. Each of these materials showed advantages and disadvantages in addition to being promising for a specific range of applications as summarized in Table 1 and 2.

To date, the majority of soft robots consist of pneumatic networks integrated within polymeric materials to achieve actuation or propulsion. Nevertheless, most of the soft robots which use pneumatic actuation need to be tethered to a rigid energy source and control systems to provide proper forces for the desired motions. Self-actuating materials which respond to an external stimulus, such as light, temperature, or electric field, have shown potential in wireless and scaled soft robotics applications, however, they have limitations that still need to be overcome. For instance, electrically responsive actuators generally need to be connected to rigid energy sources, SMPs and SMAs necessitate manual reprogramming to enable repetitive actuation, multi-

layer materials which experience differential growth are costly, whereas to date, DEA-based soft actuators require high driving voltages (several hundreds of volts) which poses a safety concern when embedding DEAs in wearable electronics or soft robots. The reduction of the driving voltage is thus necessary for soft actuators based on DEAs to be a viable solution for a wide range of applications. Moreover, actuators based on hydrogels need to be integrated with pneumatic systems to generate quick and large forces. The development of soft robots which are untethered and can accomplish complex tasks is still challenging. For instance, soft robots based on pneumatic actuation generally experience wide deformations throughout their entire structural frame. Foreseeing the kinematics of such systems is not simple as nonlinear elastic models that meet the requirements of a wide set of boundary conditions are needed. These difficulties become more complex when the integration and development of control systems is preferred. Nevertheless, in most of the categories, actuator nonlinearities are being explored and exploited for the amplification of the force output and response time.

Currently, the biggest driving force behind the soft robotics field is for application in biomedical systems needed for surgery, treatment, and accurate manipulation of soft natural materials. As a result, research on soft actuators that are biocompatible and biodegradable are gaining a lot of attention. Moreover, as the desired soft actuators are scaling down, most of the electronic components are being integrated off-board, including sensors,

**Table 1.** Comparison between the performances of the different types of actuators discussed in this review article.

Type of actuators			Advantages	Limitations/Challenges
Electrically responsive	External physical stimulation	Dielectric elastomer	Soft, flexible and stretchable Scalable High energy density High power-to-weight ratio Stores and recovers kinetic energy Suitable for high force applications, Large operation bandwidth High efficiency of power conversion Quiet, clean, and creates no pollution Less expensive and easy for maintenance Suitable for small/medium industrial applications Easy to implement the remote controllable system No limitation of separation between energy source and system Efficient controllability Generally connected to rigid components which enables an easier recovering of the actuator initial state	Slow response time Low payload capacity due to softness Large displacement, Requirement of high drive voltage Large actuating force is difficult to achieve Rigid and bulky Limited flexibility and scalability of the full system Possibility of infection Potential of increasing the pain at other places Loss in therapy effect
Magnetic			Linear effect Highly precise output Quick response Capability to penetrate most materials	Large dimensions, non-scalability of the required magnetic coils Complex manufacturing process
Thermal	Shape memory alloy		Flexible in nature High energy density Low actuation temperature Provides large frequency response Scalable Low cost Biodegradable Low density Highly elastic deformable Sustain broad range of temperature drift Excellent thermal and electrical conductivity, Low viscosity	Hysteresis Low efficiency High power consumption Pre-programming motion through high temperature annealing Generally rigid components to recover the original shape are needed Requirement of systematic synthesizing and processing methods
	Shape memory polymer		Excellent performance of soft robots due to zero stiffness and high stretchability Low voltage	Slower and less efficient than DEAs Liquid metals need to be in aqueous state for most of driving methods Challenges in the development of the liquid metal soft robots for remote controlling and soft robotics Liquid metal based flexible electronics and actuators cannot be integrated with rigid chips Development of driving method/mechanism for large liquid metal robots is needed
	Liquid metal		Large shrinkage in volume Sensitive to biologically relevant stimuli Responsive to various stimuli Environmental-friendly	Low modulus, low stiffness Limited applications
Photo-responsive	Synthetic hydrogel		Full possibility of remote controlling	Requirement of sophisticated materials of highly organized and polarized array of molecules High intensities of light are required

**Table 1.** Continued.

Type of actuators	Advantages			Limitations/Challenges	
	Ease in controlling and tuning the strength of the response			Limited deformations	
	Excellent resolution and fast response time				
	Scalable				
Pressure driven	Pneumatic	Affordable		Compressibility of air is needed	
		Fast working cycle		Not suitable for high loads	
		Insensitive to temperature drift		Limitation in separation between energy source and system	
		No need for mechanical transmission		Requirement of auxiliary energy source for maintenance	
		High actuating forces		Large scale	
	Hydraulic	High stability		Expensive in controlling	
		High stroking velocity		Leakage causes degradation in performance	
		Suitable for high loads		Temperature↑ ⇒ Viscosity↓ which sluggish the performance	
		High actuating force		Limitation in separation between energy source and system	
		Stiff and incompressible source		Large scale	
Explosive		Fast actuation		Limited lifespan,	
		Beneficial for unusual environment-like space		Requirement of explosive materials	
		Large jumps are possible		Not very safe for handling and deployment	
		Useful for defense applications		Nonfragment and debris operation	
				Large scale	

**Table 2.** Comparison between selected stimuli-responsive soft robots characteristics.

Type of actuators		Driving signal	Mode of actuation	Speed of soft robot [mm s <sup>-1</sup> ]	Weight [g]	Ref.
Electrically responsive	External physical stimulation	Dielectric elastomer Piezoelectric	450 V >60 V, 200 Hz	Forward movement Climbing, forward and backward movement	30 Bidirectional; 200	1 0.024
		Mechanical/ motor	6 V	Crawling	200	135
		Neuro-stimulation based	Rectangular biphasic pulses with 150 µA current amplitude, 50 Hz frequency and 80 µs pulse width	Deformation and/or strain	–	[74]
Magnetic			9 mT rotating field at 20 Hz	Crawling	3.38	–
Thermal	Shape memory alloy		30 V heating voltage	Crawling, swimming	140	[116]
	Shape memory polymer		2 A current	Self-folding	75 s (response time)	–
	Liquid metal		200 °C	Crawling	1.2	[126]
	Hydrogels		>25 °C	Elongation	24 h (response time)	0.022
Photo-responsive			Sunlight, 100 mW cm <sup>-2</sup>	Flapping wing	0.39 (response time), 4.49 Hz flapping frequency	0.733
			NIR, 808 nm (0.83 W cm <sup>-2</sup> )	Shrinking	8 s (response time)	[209]
Pressure driven	Pneumatic		Air-pressure of 11.9 kPa	Twisting and crawling	2	–
	Hydraulic		Fluid-pressure of 41.4 kPa	Gripping	50	[256]
Explosive			Butane combustion	Jumping	9	123
					2100	[135]

energy and control systems, whereas remotely actuated materials are being used that can be programmed to achieve complex movements for increased functionality. To this end, LCEs and magnetic

actuators programming have shown remarkable demonstrations with great potential for further development. Moreover, using the soft actuators with self-sensing abilities can potentially lead to

inexpensive soft robots that can interact with the environment through detection and actuation. Nevertheless, more effort is needed for miniaturizing some of the electronic components required for on-board applications, such as softer and smaller pumps which are capable of providing high pressures for pneumatic and hydraulic actuators, in addition to smaller devices that are able to generate high voltages needed for some of the electrically activated elastomers. To solve the minimized area challenge of rigid components, a reversible stretchable platform has been demonstrated for a stretchable display application. The 3D-printed stretchable platform utilized the concept of the multilevel arrangement of LEDs, which are mechanically guided by joint pins/links to move out of plane and fill the evolved gap, as shown in **Figure 22**.<sup>[302]</sup> Such techniques can be promising for robotics applications where a larger number of electronic components could be embedded into a smaller footprint area.

In addition, to achieve fully compliant and standalone soft robots, the integration of flexible electronic devices is essential. To this end, many CMOS-based logic and memory devices in addition to energy sources have been reported.<sup>[303–310]</sup> The flexing of the CMOS devices has been demonstrated using either back-etching the substrate or using XeF<sub>2</sub>-based etching technique, whereas the flexing of large-scale monocrystalline silicon solar cells has been reported using a corrugation technique, as shown in **Figure 23a,b**. In all of these methods, the electric performance of the devices is reported to be maintained after flexing while exhibiting strong mechanical robustness. Moreover, as we

have reported in this Review article, many of the soft components included in a soft robot are 3D printed. Therefore, the integration of the flexible electronics into the 3D-printed system with high reliability and mechanical resilience is needed. A “pause-embed-resume” method has been developed by our group for this purpose where we show the integration of flexible MOSCAP devices into a 3D-printed head and human femur. To achieve this, the 3D-printing process was paused in the middle of the fabrication process; then flexible MOSCAP devices were robotically positioned inside the 3D package using specially designed robotic arms, and finally the printing process was resumed. The 3D-printed systems were prepared using NinjaFlex material, enabling outstanding flexibility under bending and compressive conditions. The electric performance of the embedded MOSCAPs was retained, as shown in **Figure 23c,j**. Such approaches can potentially enable the development of standalone soft robotic devices which are fully compliant and with high performance.

Finally, due to the wide range of actuation materials and stimuli, there is still no standard protocol to follow or standard parameters to report when characterizing the soft actuators. Some of the important parameters that need to be reported for a better understanding and benchmarking of the soft actuators include: generated force, strain and stress within the material, response time, sensitivity to noise, size, reliability (in terms of cycling tests), and shelf life. In addition, parameters related to the stimuli are needed, such as frequency and amplitude of the driving signal in addition to its size and distance from the soft actuators.

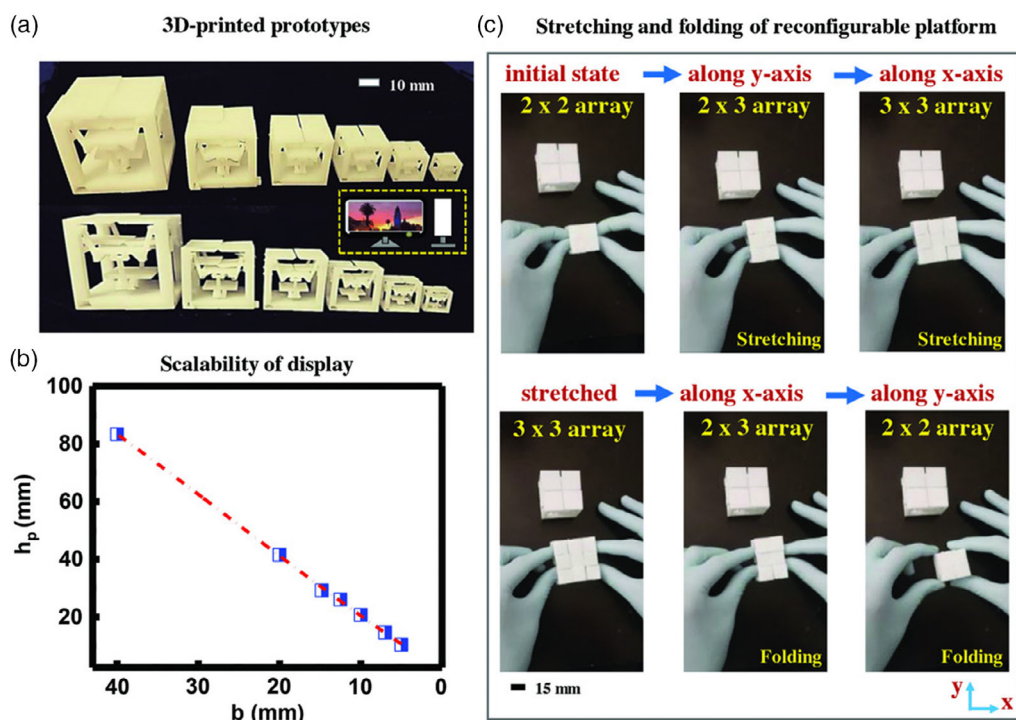


**Figure 22.** Proof-of-concept of the reconfigurable and expandable display by using the 3D-printed platforms. a) 3D printed and assembled platforms with different sizes ranging from  $b = 40$  to 5 mm. For comparison, the front and cross-section view of common display device is shown in inset. b) A linear relationship between the height of platform  $h_p$  and size of square island  $b$  to exhibit the scalability of the design. c) Reversible stretching and folding progression of the reconfigurable platform to demonstrate the transformation of the original 2 × 2 array (4 islands) into a 2 × 3 array (6 islands), and then into a 3 × 3 array (9 islands), respectively and vice versa for folding. Reproduced with permission.<sup>[302]</sup> Copyright 2018, Wiley.

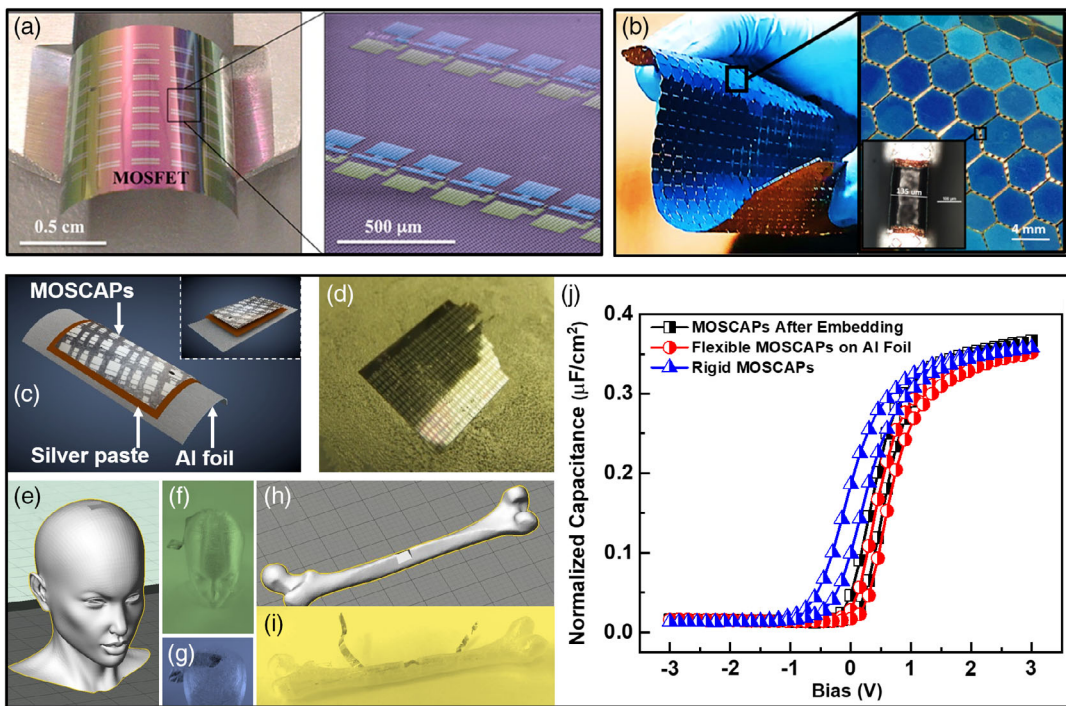


**Figure 23.** Demonstrated application and performance of flexible electronic devices. a) Flexible MOSFET devices fabricated using  $\text{XeF}_2$  etching technique. Reproduced with permission.<sup>[303]</sup> Copyright 2014, ACS. b) Ultra-flexible monocrystalline silicon solar cells with 19% efficiency fabricated using a corrugation technique. Reproduced with permission.<sup>[307]</sup> Copyright 2020, ACS. c) Schematic of MOSCAP devices bounded to Al foil using silver paste. d) Flexible MOSCAPs placed on aluminum foil. e) 3D model of human head. f,g) 3D-printed head with embedded high-performance electronics. h) 3D model of human femur. i) 3D-printed femur with embedded MOSCAPs. j) Performance of MOSCAP devices through different stages of the embedding process.

## Acknowledgements

The authors acknowledge generous support of the King Abdullah University of Science and Technology (KAUST). The authors acknowledge Dr. Joanna M. Nassar, Dr. Galo A. Torres, Dr. Mohamed T. Ghoneim, Andres A. Aguirre-Pablo, Davide Priante, Dr. Jhonathan P. Rojas, Sigurdur T. Thoroddsen, and Prof. Boon S. Ooi who contributed to the “pause-embed-resume” data. The authors thank Kelly Rader for proof reading this manuscript.

## Conflict of Interest

The authors declare no conflict of interest.

## Keywords

dielectric elastomers, self-folding, shape memory alloys, soft actuators, soft robotics

Received: June 12, 2020

Revised: July 8, 2020

Published online: August 23, 2020

[1] T. Mirfakhrai, J. D. W. Madden, R. H. Baughman, *Mater. Today* **2007**, 10, 30.

- [2] F. Rosso, G. Marino, A. Giordano, M. Barbarisi, D. Parmeggiani, A. Barbarisi, *J. Cell Physiol.* **2005**, 203, 465.
- [3] D. Morales, E. Palleau, M. D. Dickey, O. D. Velev, *Soft Matter* **2014**, 10, 1337.
- [4] M. T. Tolley, R. F. Shepherd, B. Mosadegh, K. C. Galloway, M. Wehner, M. Karpelson, R. J. Wood, G. M. Whitesides, *Soft Rob.* **2014**, 1, 213.
- [5] S. Seok, C. D. Onal, K.-J. Cho, R. J. Wood, D. Rus, S. Kim, *IEEE ASME Trans. Mechatron.* **2013**, 18, 1485.
- [6] C. Majidi, *Soft Rob.* **2014**, 1, 5.
- [7] D. Rus, M. T. Tolley, *Nature* **2015**, 521, 467.
- [8] S. Fusco, H.-W. Huang, K. E. Peyer, C. Peters, M. Häberli, A. Ulbers, A. Spyrogianni, E. Pellicer, J. Sort, S. E. Pratsinis, B. J. Nelson, M. S. Sakar, S. Pané, *ACS Appl. Mater. Interfaces* **2015**, 7, 6803.
- [9] K. K. Westbrook, H. J. Qi, J. *Intell. Mater. Syst. Struct.* **2008**, 19, 597.
- [10] M. Amjadi, M. Turan, C. P. Clementson, M. Sitti, *ACS Appl. Mater. Interfaces* **2016**, 8, 5618.
- [11] R. B. Mishra, S. M. Khan, S. F. Shaikh, A. M. Hussain, M. M. Hussain, in *Proc. 3rd IEEE Int. Conf. on Soft Robotics (RoboSoft)*, IEEE, Piscataway, NJ **2020**, p. 194.
- [12] X. Liu, J. Liu, S. Lin, X. Zhao, *Mater. Today* **2020**, 36, 102.
- [13] L. Hines, K. Petersen, G. Lum, M. Sitti, *Adv. Mater.* **2016**, 29, 1603483.
- [14] L. Sun, Y. Yu, Z. Chen, F. Bian, F. Ye, L. Sun, Y. Zhao, *Chem. Soc. Rev.* **2020**, 49, 4043.
- [15] X. Huang, M. Ford, Z. Patterson, M. Zarepoor, C. Pan, C. Majidi, *J. Mater. Chem. B* **2020**, 8, 4539.
- [16] A. Ghosh, C. Yoon, F. Ongaro, S. Scheggi, F. Selaru, S. Misra, D. Gracias, *Front. Mech. Eng.* **2017**, 3, 7.

- [17] M. Cianchetti, C. Laschi, A. Menciassi, P. Dario, *Nat. Rev. Mater.* **2018**, *3*, 143..
- [18] C. Hu, S. Pané, B. Nelson, *Annu. Rev. Control Rob. Auton. Syst.* **2018**, *1*, 53.
- [19] J. Shintake, V. Cacucciolo, D. Floreano, H. Shea, *Adv. Mater.* **2018**, *30*, 1707035.
- [20] J. McCracken, B. Donovan, T. White, *Adv. Mater.* **2020**, *32*, 1906564.
- [21] O. Erol, A. Pantula, W. Liu, D. Gracias, *Adv. Mater. Technol.* **2019**, *4*, 1900043.
- [22] M. Dickey, *Adv. Mater.* **2017**, *29*, 1606425.
- [23] C. Jones, J. Steed, *Chem. Soc. Rev.* **2016**, *45*, 6546.
- [24] L. Jing, K. Li, H. Yang, P. Chen, *Mater. Horizons* **2020**, *7*, 54.
- [25] W. Xu, D. Gracias, *ACS Nano* **2019**, *13*, 4883.
- [26] K. E. Petersen, *Proc. IEEE* **1982**, *70*, 420.
- [27] S. Kota, G. K. Ananthasuresh, S. B. Crary, K. D. Wise, *J. Mech. Design* **1994**, *116*, 1081.
- [28] G. K. Ananthasuresh, L. L. Howell, *J. Mech. Design* **2005**, *127*, 736.
- [29] S. M. Khan, R. B. Mishra, N. Qaiser, A. M. Hussain, M. M. Hussain, *AIP Adv.* **2020**, *10*, 015009.
- [30] F. Iida, C. Laschi, *Proc. Comput. Sci.* **2011**, *7*, 99.
- [31] R. B. Mishra, S. F. Shaikh, A. M. Hussain, M. M. Hussain, *AIP Adv.* **2020**, *10*, 055112.
- [32] A. M. Hussain, M. T. Ghoneim, J. P. Rojas, H. Fahad, *J. Sens.* **2019**, *2019*, 828394.
- [33] K. Takemura, F. Yajima, S. Yokota, K. Edamura, *Sens. Actuators, A Phys.* **2008**, *144*, 348.
- [34] R. Goyal, *Int. J. Sci. Eng. Res.* **2019**, *10*, 39.
- [35] R. Pelrine, R. D. Kornbluh, Q. Pei, S. Stanford, S. Oh, J. Eckerle, R. J. Full, M. A. Rosenthal, K. Meijer, in *Proc. SPIE*, San Diego, CA **2002**.
- [36] X. Niu, M. Zhang, J. Wu, W. Wen, P. Sheng, *Soft Matter* **2009**, *5*, 576.
- [37] G. H. Kwon, J. Y. Park, J. Y. Kim, M. L. Frisk, D. J. Beebe, S. H. Lee, *Small* **2008**, *4*, 2148.
- [38] E. W. H. Jager, O. Inganäs, I. Lundström, *Science* **2000**, *288*, 2335.
- [39] R. V. Raghavan, J. Qin, L. Y. Yeo, J. R. Friend, K. Takemura, S. Yokota, K. Edamura, *Sens. Actuators, B Chem.* **2009**, *140*, 287.
- [40] P. Brochu, Q. Pei, *Macromol. Rapid Commun.* **2010**, *31*, 10.
- [41] Q. M. Zhang, H. Li, M. Poh, F. Xia, Z. Y. Cheng, H. Xu, C. Huang, *Nature* **2002**, *419*, 284.
- [42] G. H. Kwon, J. Y. Park, J. Y. Kim, M. L. Frisk, D. J. Beebe, S.-H. Lee, *Small* **2008**, *4*, 2148.
- [43] J. Shintake, PhD thesis, École Polytechnique Fédérale de Lausanne, **2016**.
- [44] K. Jung, J. C. Koo, J. Do Nam, Y. K. Lee, H. R. Choi, *Bioinspir. Biomim.* **2007**, *2*, 42.
- [45] J. Shintake, S. Rosset, B. Schubert, D. Floreano, H. Shea, *Adv. Mater.* **2016**, *28*, 231.
- [46] R. Pelrine, R. Kornbluh, Q. Pei, J. Joseph, *Science* **2000**, *287*, 836.
- [47] M. Niklaus, S. Rosset, P. Dubois, H. Shea, *Proc. Chem.* **2009**, *1*, 702.
- [48] S. Shian, D. R. Clarke, *Soft Matter* **2016**, *12*, 3137.
- [49] E. Torenbeek, *Synthesis of Subsonic Airplane Design*, Springer, Berlin **1982**.
- [50] D. D. Chin, L. Y. Matloff, A. K. Stowers, E. R. Tucci, D. Lentink, *J. R. Soc. Interface* **2017**, *14*, 201702405.
- [51] A. Hedenström, G. Norevik, K. Warfvinge, A. Andersson, J. Bäckman, S. Åkesson, *Curr. Biol.* **2016**, *26*, 3066.
- [52] M. Duduta, D. R. Clarke, R. J. Wood, in *Proc. IEEE Int. Conf. Robotics and Automation*, IEEE, Piscataway, NJ **2017**.
- [53] Q. Pei, R. Pelrine, S. Stanford, R. Kornbluh, M. Rosenthal, K. Meijer, R. Full, *Smart Structures and Materials 2002: Industrial and Commercial Applications of Smart Structures Technologies*, Vol. 4698, SPIE, Bellingham, WA **2002**, pp. 246–253.
- [54] Q. Pei, R. Pelrine, S. Stanford, R. Kornbluh, M. Rosenthal, *Synth. Met.* **2003**, *135*, 129.
- [55] R. Sarban, R. W. Jones, B. R. Mace, E. Rustighi, *Mech. Syst. Signal Process.* **2011**, *25*, 2879.
- [56] H. Zhao, A. M. Hussain, M. Duduta, D. M. Vogt, R. J. Wood, D. R. Clarke, *Adv. Funct. Mater.* **2018**, *28*, 1804328.
- [57] E. Acome, S. K. Mitchell, T. G. Morrissey, M. B. Emmett, C. Benjamin, M. King, M. Radakovitz, C. Keplinger, *Science* **2018**, *359*, 61.
- [58] X. Ji, X. Liu, V. Cacucciolo, M. Imboden, Y. Civet, A. El Haitami, S. Cantin, Y. Perriard, H. Shea, *Sci. Robot.* **2019**, *4*, 6451.
- [59] Y. Wu, J. K. Yim, J. Liang, Z. Shao, M. Qi, J. Zhong, Z. Luo, X. Yan, M. Zhang, X. Wang, R. S. Fearing, R. J. Full, L. Lin, *Sci. Robot.* **2019**, *4*, 1594.
- [60] J.-W. Sohn, S.-B. Choi, *Int. J. Mech. Syst. Eng.* **2017**, *3*, 122.
- [61] K. Y. Ma, P. Chirarattananon, S. B. Fuller, R. J. Wood, *Science* **2013**, *340*, 603.
- [62] M. H. Sadraey, *Aircraft Design: A Systems Engineering Approach*, Wiley, Hoboken, NJ **2012**.
- [63] E. Chang, L. Y. Matloff, A. K. Stowers, D. Lentink, *Sci. Robot.* **2020**, *5*, 1246.
- [64] S. Micera, J. Carpaneto, S. Raspopovic, *IEEE Rev. Biomed. Eng.* **2010**, *3*, 48.
- [65] E. Biddiss, T. Chau, *Prosthet. Orthot. Int.* **2007**, *31*, 236.
- [66] B. Siciliano, O. Khatib, *Springer Handbook of Robotics*, Springer, Berlin/Heidelberg, Germany **2008**.
- [67] J. A. Cheney, N. Konow, K. M. Middleton, K. S. Breuer, T. J. Roberts, E. L. Giblin, S. M. Swartz, *Bioinspiration Biomimetics* **2014**, *9*, 025007.
- [68] J. W. Bahlman, S. M. Swartz, K. S. Breuer, *Bioinspiration Biomimetics* **2013**, *8*, 16009.
- [69] A. Ramezani, S. J. Chung, S. Hutchinson, *Sci. Robot.* **2017**, *2*, 2505.
- [70] S. Li, R. Katzschatmann, D. Rus, in *IEEE Int. Conf. Intelligent Robots and Systems*, IEEE, New York **2015**.
- [71] M. Calisti, A. Arienti, F. Renda, G. Levy, B. Hochner, B. Mazzolai, P. Dario, C. Laschi, presented at *Proc. on IEEE Int. Conf. on Robotics and Automation*, Chengdu, China, **2012**.
- [72] G. S. Dhillon, K. W. Horch, *IEEE Trans. Neural Syst. Rehabil. Eng.* **2005**, *13*, 468.
- [73] K. Horch, S. Meek, T. G. Taylor, D. T. Hutchinson, *IEEE Trans. Neural Syst. Rehabil. Eng.* **2011**, *19*, 483.
- [74] L. Zollo, G. Di Pino, A. L. Ciancio, F. Ranieri, F. Cordella, C. Gentile, E. Noce, R. A. Romeo, A. D. Bellingegni, G. Vadalà, S. Miccinilli, A. Mioli, L. Diaz-Balzani, M. Bravi, K. P. Hoffmann, A. Schneider, L. Denaro, A. Davalli, E. Gruppioni, R. Sacchetti, S. Castellano, V. Di Lazzaro, S. Sterzi, V. Denaro, E. Guglielmelli, *Sci. Robot.* **2019**, *4*, 9924.
- [75] T. G. Thuruthel, B. Shih, C. Laschi, M. T. Tolley, *Sci. Robot.* **2019**, *4*, 1488.
- [76] P. R. Ouyang, R. C. Tjiptoprodjo, W. J. Zhang, G. S. Yang, *Int. J. Adv. Manuf. Technol.* **2008**, *38*, 463.
- [77] J. B. Hopkins, M. L. Culpepper, *Precis. Eng.* **2010**, *34*, 259.
- [78] S. Raspopovic, M. Capogrossi, F. M. Petrini, M. Bonizzato, J. Rigosa, G. Di Pino, J. Carpaneto, M. Controzzi, T. Boretius, E. Fernandez, G. Granata, C. M. Oddo, L. Citi, A. L. Ciancio, C. Cipriani, M. C. Carrozza, W. Jensen, E. Guglielmelli, T. Stieglitz, P. M. Rossini, S. Micera, *Sci. Transl. Med.* **2014**, *6*, 222.
- [79] D. W. Tan, M. A. Schiefer, M. W. Keith, J. R. Anderson, J. Tyler, D. J. Tyler, *Sci. Transl. Med.* **2014**, *6*, 257.
- [80] C. M. Oddo, S. Raspopovic, F. Artoni, A. Mazzoni, G. Spigler, F. Petrini, F. Giambattistelli, F. Vecchio, F. Miraglia, L. Zollo, G. Di Pino, D. Camboni, M. C. Carrozza, E. Guglielmelli, P. M. Rossini, U. Faraguna, S. Micera, *Elife* **2016**, *8*, 09148.
- [81] M. Ortiz-Catalan, B. Häkansson, R. Bråemark, *Sci. Transl. Med.* **2014**, *6*, 257.

- [82] T. S. Davis, H. A. C. Wark, D. T. Hutchinson, D. J. Warren, K. O'Neill, T. Scheinblum, G. A. Clark, R. A. Normann, B. Greger, *J. Neural Eng.* **2016**, *13*, 036001.
- [83] T. Pistohl, D. Joshi, G. Ganesh, A. Jackson, K. Nazarpour, *IEEE Trans. Neural Syst. Rehabil. Eng.* **2015**, *23*, 498.
- [84] M. Schiefer, D. Tan, S. M. Sidek, D. J. Tyler, *J. Neural Eng.* **2015**, *13*, 016001.
- [85] D. Farina, O. Aszmann, *Sci. Transl. Med.* **2014**, *6*, 257.
- [86] C. Genna, C. M. Oddo, C. Fanciullacci, C. Chisari, H. Jörntell, F. Artoni, S. Micera, *Brain Topogr.* **2017**, *30*, 473.
- [87] G. Granata, R. Di Iorio, R. Romanello, F. Iodice, S. Raspopovic, F. Petrini, I. Strauss, G. Valle, T. Stieglitz, P. Čvančara, D. Andreu, J. L. Divoux, D. Giraud, L. Wauters, A. Hiairrassary, W. Jensen, S. Micera, P. M. Rossini, *Clin. Neurophysiol.* **2018**, *129*, 1117.
- [88] A. M. De Nunzio, S. Dosen, S. Lemling, M. Markovic, M. A. Schweisfurth, N. Ge, B. Graumann, D. Falla, D. Farina, *Exp. Brain Res.* **2017**, *235*, 2547.
- [89] C. M. Oddo, A. Mazzoni, A. Spanne, J. M. D. Enander, H. Mogensen, F. Bengtsson, D. Camboni, S. Micera, H. Jörntell, *Sci. Rep.* **2017**, *7*, 45898.
- [90] P. M. Rossini, S. Micera, A. Benvenuto, J. Carpaneto, G. Cavallo, L. Citi, C. Cipriani, L. Denaro, V. Denaro, G. Di Pino, F. Ferreri, E. Guglielmelli, K. P. Hoffmann, S. Raspopovic, J. Rigos, L. Rossini, M. Tombini, P. Dario, *Clin. Neurophysiol.* **2010**, *121*, 777.
- [91] S. N. Flesher, J. L. Collinger, S. T. Foldes, J. M. Weiss, J. E. Downey, E. C. Tyler-Kabara, S. J. Bensmaia, A. B. Schwartz, M. L. Boninger, R. A. Gaunt, *Sci. Transl. Med.* **2016**, *8*, 361.
- [92] E. D'Anna, G. Valle, A. Mazzoni, I. Strauss, F. Iberite, J. Patton, F. M. Petrini, S. Raspopovic, G. Granata, R. Di Iorio, M. Controzzi, C. Cipriani, T. Stieglitz, P. M. Rossini, S. Micera, *Sci. Robot.* **2019**, *4*, 8892.
- [93] N.-T. Nguyen, *Microfluid. Nanofluid.* **2012**, *12*, 1.
- [94] E. Diller, J. Zhuang, G. Zhan Lum, M. R. Edwards, M. Sitti, *Appl. Phys. Lett.* **2014**, *104*, 174101.
- [95] T. Qiu, S. Palagi, P. Fischer, presented at 2015 37th Annual Int. Conf. of the IEEE Engineering in Medicine and Biology Society (EMBC), IEEE, Piscataway, NJ, **2015**.
- [96] T. Qiu, T.-C. Lee, A. G. Mark, K. I. Morozov, R. Münster, O. Mierka, S. Turek, A. M. Leshansky, P. Fischer, *Nat. Commun.* **2014**, *5*, 5119.
- [97] G. Z. Lum, Z. Ye, X. Dong, H. Marvi, O. Erin, W. Hu, M. Sitti, *Proc. Natl. Acad. Sci. USA* **2016**, *113*, E6007.
- [98] E. Diller, J. Giltinan, G. Z. Lum, Z. Ye, M. Sitti, presented at *Robotics: Science and Systems*, Rome, Italy, July **2014**.
- [99] S. Fusco, H.-W. Huang, K. E. Peyer, C. Peters, M. Häberli, A. Ulbers, A. Spyrogianni, E. Pellicer, J. Sort, S. E. Pratsinis, B. J. Nelson, M. S. Sakar, S. Pané, *ACS Appl. Mater. Interfaces* **2015**, *7*, 6803.
- [100] E. Diller, J. Giltinan, G. Z. Lum, Z. Ye, M. Sitti, *Int. J. Rob. Res.* **2016**, *35*, 114.
- [101] M. P. Kummer, J. J. Abbott, B. E. Kratochvil, R. Borer, A. Sengul, B. J. Nelson, *IEEE Trans. Robot.* **2010**, *26*, 1006.
- [102] S. Tasoglu, E. Diller, S. Guven, M. Sitti, U. Demirci, *Nat. Commun.* **2014**, *5*, 3124.
- [103] E. Diller, S. Miyashita, M. Sitti, *RSC Adv.* **2012**, *2*, 3850.
- [104] E. Diller, C. Pawashe, S. Floyd, M. Sitti, *Int. J. Rob. Res.* **2011**, *30*, 1667.
- [105] P. Garstecki, P. Tierno, D. B. Weibel, F. Saguès, G. M. Whitesides, *J. Phys.: Condens. Matter* **2009**, *21*, 204110.
- [106] S. Miyashita, E. Diller, M. Sitti, *Int. J. Rob. Res.* **2013**, *32*, 591.
- [107] E. Diller, J. Giltinan, M. Sitti, *Int. J. Rob. Res.* **2013**, *32*, 614.
- [108] E. Diller, S. Floyd, C. Pawashe, M. Sitti, *IEEE Trans. Rob.* **2012**, *28*, 172.
- [109] S. Floyd, E. Diller, C. Pawashe, M. Sitti, *Int. J. Rob. Res.* **2011**, *30*, 1553.
- [110] C. Pawashe, S. Floyd, M. Sitti, *Appl. Phys. Lett.* **2009**, *94*, 164108.
- [111] H.-W. Huang, M. S. Sakar, K. Riederer, N. Shamsudhin, A. Petruska, S. Pan, B. J. Nelson, in *2016 IEEE Int. Conf. on Robotics and Automation (ICRA)*, IEEE, Piscataway, NJ **2016**.
- [112] Z. Ye, S. Règnier, M. Sitti, *IEEE Trans. Rob.* **2014**, *30*, 3.
- [113] J. Kim, S. E. Chung, S.-E. Choi, H. Lee, J. Kim, S. Kwon, *Nat. Mater.* **2011**, *10*, 747.
- [114] M. Khoo, C. Liu, *Sens. Actuators, A* **2001**, *89*, 259.
- [115] Y. Kim, G. Parada, S. Liu, X. Zhao, *Sci. Robotics* **2019**, *4*, 7329.
- [116] T. Xu, J. Zhang, M. Salehizadeh, O. Onaizah, E. Diller, *Sci. Robotics* **2019**, *4*, 4494.
- [117] Z. Ding, P. Wei, G. Chitnis, B. Ziae, *J. Microelectromech. Syst.* **2011**, *20*, 59.
- [118] Q. Zhao, J. W. C. Dunlop, X. Qiu, F. Huang, Z. Zhang, J. Heyda, J. Dzubiella, M. Antonietti, J. Yuan, *Nat. Commun.* **2014**, *5*, 1.
- [119] R. T. Olsson, M. A. S. Azizi Samir, G. Salazar-Alvarez, L. Belova, V. Ström, L. A. Berglund, O. Ikkala, J. Nogues, U. W. Gedde, *Nat. Nanotechnol.* **2010**, *5*, 584.
- [120] K. E. Wilkes, P. K. Liaw, *J. Med.* **2000**, *52*, 45.
- [121] J. Cederström, J. Van Humbeeck, *Le J. Phys. IV* **1995**, *5*, 333.
- [122] J. Mohd Jani, M. Leary, A. Subic, M. A. Gibson, *Mater. Des.* **2014**, *56*, 1078.
- [123] H. Rodrigue, W. Wang, M. W. Han, T. J. Y. Kim, S. H. Ahn, *Soft Robot.* **2017**, *4*, 3.
- [124] W. Wang, J. Y. Lee, H. Rodrigue, S. H. Song, W. S. Chu, S. H. Ahn, *Bioinspiration Biomimetics* **2014**, *9*, 046006.
- [125] J. H. Lee, Y. S. Chung, H. Rodrigue, *Sci. Rep.* **2019**, *9*, 11251.
- [126] H. Jin, E. Dong, M. Xu, C. Liu, G. Alici, Y. Jie, *Smart Mater. Struct.* **2016**, *25*, 085026.
- [127] W. Wang, N. G. Kim, H. Rodrigue, S. H. Ahn, *Mater. Horizons* **2017**, *4*, 367.
- [128] X. Huang, K. Kumar, M. K. Jawed, A. Mohammadi Nasab, Z. Ye, W. Shan, C. Majidi, *Adv. Mater. Technol.* **2019**, *4*, 1800540.
- [129] A. Lendlein, S. Kelch, *Angew. Chem., Int. Ed. Engl.* **2002**, *41*, 2035.
- [130] T. Xie, *Polymer* **2011**, *52*, 4985.
- [131] C. Liu, H. Qin, P. T. Mather, *J. Mater. Chem.* **2007**, *17*, 1543.
- [132] W. Small IV, P. Singhal, T. S. Wilson, D. J. Maitland, *J. Mater. Chem.* **2010**, *20*, 3356.
- [133] A. Lendlein, M. Behl, B. Hiebl, C. Wischke, *Expert Rev. Med. Devices* **2010**, *7*, 357.
- [134] R. F. Shepherd, A. A. Stokes, J. Freake, J. Barber, P. W. Snyder, A. D. Mazzeo, L. Cademartiri, S. A. Morin, G. M. Whitesides, *Angew. Chem., Int. Ed.* **2013**, *125*, 2964.
- [135] M. Loepfe, C. M. Schumacher, U. B. Lustenberger, W. J. Stark, *Soft Robot.* **2015**, *2*, 33.
- [136] T. G. Leong, A. M. Zarafshar, D. H. Gracias, *Small* **2010**, *6*, 792.
- [137] N. Bassik, G. M. Stern, D. H. Gracias, *Appl. Phys. Lett.* **2009**, *95*, 091901.
- [138] J. H. Cho, S. Hu, D. H. Gracias, *Appl. Phys. Lett.* **2008**, *93*, 043505.
- [139] J. Chen, M. Yang, Q. Zhang, E. Cho, C. Cobley, C. Kim, C. Glaus, L. Wang, M. Welch, Y. Xia, *Adv. Funct. Mater.* **2010**, *20*, 3684.
- [140] W. Small IV, P. Singhal, T. Wilson, D. Maitland, *J. Mater. Chem.* **2010**, *20*, 3356.
- [141] X. Guo, H. Li, B. Yeop Ahn, E. Duoss, K. Hsia, J. Lewis, R. Nuzzo, *Proc. Natl. Acad. Sci.* **2009**, *106*, 20149.
- [142] E. Hawkes, B. An, N. Benbernou, H. Tanaka, S. Kim, E. Demaine, D. Rus, R. Wood, *Proc. Natl. Acad. Sci.* **2010**, *107*, 12441.
- [143] T. Leong, P. Lester, T. Koh, E. Call, D. Gracias, *Langmuir* **2009**, *25*, 8747.
- [144] P. Tyagi, N. Bassik, T. Leong, J.-H. Cho, B. Benson, D. Gracias, *J. Microelectromech. Syst.* **2009**, *18*, 784.
- [145] T. Leong, B. Benson, E. Call, D. Gracias, *Small* **2008**, *4*, 1605.
- [146] W. Arora, A. Nichol, H. Smith, G. Barbastathis, *Appl. Phys. Lett.* **2006**, *88*, 053108.

- [147] J. W. Judy, R. S. Muller, *J. Microelectromech. Syst.* **1997**, *6*, 249.
- [148] Y. W. Yi, C. Liu, *J. Microelectromech. Syst.* **1999**, *8*, 10.
- [149] Y. W. Lu, C. J. Kim, *Appl. Phys. Lett.* **2006**, *89*, 164101.
- [150] J. Leng, D. Zhang, Y. Liu, K. Yu, X. Lan, *Appl. Phys. Lett.* **2010**, *96*, 111905.
- [151] A. Lendlein, H. Jiang, O. Jünger, R. Langer, *Nature* **2005**, *434*, 879.
- [152] H. Jiang, S. Kelch, A. Lendlein, *Adv. Mater.* **2006**, *18*, 1471.
- [153] J. Leng, X. Wu, Y. Li, *J. Appl. Polym. Sci.* **2009**, *114*, 2455.
- [154] A. Lendlein, S. Kelch, *Angew. Chem., Int. Ed.* **2002**, *41*, 2034.
- [155] L. Ionov, *Soft Matter* **2011**, *7*, 6786.
- [156] K. Lee, H. Koerner, R. Vaia, T. Bunning, T. White, *Soft Matter* **2011**, *7*, 4318.
- [157] N. Liu, Q. Xie, W. Huang, S. Phee, N. Guo, *J. Micromech. Microeng.* **2008**, *18*, 027001.
- [158] T. Ebefors, E. Kälvesten, G. Stemme, *Sens. Actuators, A* **1998**, *67*, 199.
- [159] J. Luo, J. He, Y. Fu, A. Flewitt, S. Spearing, N. Fleck, W. Milne, *J. Micromech. Microeng.* **2005**, *15*, 1406.
- [160] J. Luo, R. Huang, J. He, Y. Fu, A. Flewitt, S. Spearing, N. Fleck, W. Milne, *Sens. Actuators A, Phys.* **2006**, *132*, 346.
- [161] G. Stoychev, N. Puretskiy, L. Ionov, *Soft Matter* **2011**, *7*, 3277.
- [162] S. M. Elton, M. T. Tolley, B. Shin, C. D. Onal, E. D. Demaine, D. Rus, R. J. Wood, *Soft Matter* **2013**, *9*, 7688.
- [163] T. Chen, O. R. Bilal, K. Shea, C. Daraio, *Proc. Natl. Acad. Sci. USA* **2018**, *115*, 5698.
- [164] D. Davis, R. Mailen, J. Genzer, M. D. Dickey, *RSC Adv.* **2015**, *5*, 89254.
- [165] Y. Liu, J. K. Boyles, J. Genzer, M. D. Dickey, *Soft Matter* **2012**, *8*, 1764.
- [166] R. S. Kularatne, H. Kim, J. M. Boothby, T. H. Ware, *J. Polym. Sci. Part B Polym. Phys.* **2017**, *55*, 395.
- [167] A. Kotikian, C. McMahan, E. C. Davidson, J. M. Muhammad, R. D. Weeks, C. Daraio, J. A. Lewis, *Sci. Robot.* **2019**, *4*, 7044.
- [168] Q. He, Z. Wang, Y. Wang, A. Minori, M. T. Tolley, S. Cai, *Sci. Adv.* **2019**, *5*, 5746.
- [169] X. Qian, Q. Chen, Y. Yang, Y. Xu, Z. Li, Z. Wang, Y. Wu, Y. Wei, Y. Ji, *Adv. Mater.* **2018**, *30*, 1801103.
- [170] Y. Yang, Z. Pei, Z. Li, Y. Wei, Y. Ji, *J. Am. Chem. Soc.* **2016**, *138*, 2118.
- [171] S. Zakharchenko, N. Puretskiy, G. Stoychev, M. Stamm, L. Ionov, *Soft Matter* **2010**, *6*, 2633.
- [172] A. Grimes, D. Breslauer, M. Long, J. Pegan, L. Lee, M. Khine, *Lab Chip* **2008**, *8*, 170.
- [173] P. T. Mather, X. Luo, I. A. Rousseau, *Annu. Rev. Mater. Res.* **2009**, *39*, 445.
- [174] H. Yabu, Y. Matsuo, K. Ijiro, F. Nishino, T. Takaki, M. Kuwahara, M. Shimomura, *ACS Appl. Mat. Int.* **2009**, *2*, 23.
- [175] M. Lee, M. Huntington, W. Zhou, J. Yang, T. Odom, *Nano Lett.* **2011**, *11*, 311.
- [176] J. E. Mark, *Physical Properties of Polymers Handbook*, Springer, New York **2007**.
- [177] A. Kotikian, C. McMahan, E. Davidson, J. Muhammad, R. Weeks, C. Daraio, J. Lewis, *Sci. Robot.* **2019**, *4*, 7044.
- [178] S. J. Jeon, A. W. Hauser, R. C. Hayward, *Acc. Chem. Res.* **2017**, *50*, 161.
- [179] A. Gomez, M. Shin, *J. Mech. Sci. Technol.* **2018**, *32*, 3107.
- [180] L. Ionov, *Mater. Today* **2014**, *17*, 494.
- [181] E. Wang, M. S. Desai, S. W. Lee, *Nano Lett.* **2013**, *13*, 2826.
- [182] J. C. Breger, C. Yoon, R. Xiao, H. R. Kwag, M. O. Wang, J. P. Fisher, T. D. Nguyen, D. H. Gracias, *ACS Appl. Mater. Interfaces* **2015**, *7*, 3398.
- [183] V. Magdanz, G. Stoychev, L. Ionov, S. Sanchez, O. G. Schmidt, *Angew. Chem., Int. Ed.* **2014**, *53*, 2673.
- [184] H. W. Huang, M. S. Sakar, A. J. Petruska, S. Pane, B. J. Nelson, *Nat. Commun.* **2016**, *7*, 12263.
- [185] A. Haesslein, H. Ueda, M. C. Hacker, S. Jo, D. M. Ammon, R. N. Borazjani, J. F. Kunzler, J. C. Salamone, A. G. Mikos, *J. Control. Release* **2006**, *114*, 251.
- [186] J. P. Fisher, T. A. Holland, D. Dean, P. S. Engel, A. G. Mikos, *J. Biomater. Sci. Polym. Ed.* **2001**, *12*, 673.
- [187] J. P. Fisher, D. Dean, A. G. Mikos, *Biomaterials* **2002**, *23*, 4333.
- [188] J. Choi, K. Kim, T. Kim, G. Liu, A. Bar-Shir, T. Hyeon, M. T. McMahon, J. W. M. Bulte, J. P. Fisher, A. A. Gilad, *J. Control. Release* **2011**, *156*, 239.
- [189] K. Malachowski, J. Breger, H. Kwag, M. Wang, J. Fisher, F. Selaru, D. Gracias, *Angew. Chem., Int. Ed.* **2014**, *126*, 8183.
- [190] J. Liu, O. Erol, A. Pantula, W. Liu, Z. Jiang, K. Kobayashi, D. Chatterjee, N. Hibino, L. Romer, S. Kang, T. Nguyen, D. Gracias, *ACS Appl. Mater. Interfaces* **2019**, *11*, 8492.
- [191] J. Breger, C. Yoon, R. Xiao, H. Kwag, M. Wang, J. Fisher, T. Nguyen, D. Gracias, *ACS Appl. Mater. Interfaces* **2015**, *7*, 3398.
- [192] F. Ercole, T. P. Davis, R. A. Evans, *Polym. Chem.* **2010**, *1*, 37.
- [193] J. Wei, Y. Yu, *Soft Matter* **2012**, *8*, 8050.
- [194] H. Y. Jiang, S. Kelch, A. Lendlein, *Adv. Mater.* **2006**, *18*, 1471.
- [195] X. Zhang, Z. Yu, C. Wang, D. Zarrouk, J. W. T. Seo, J. C. Cheng, A. D. Buchan, K. Takei, Y. Zhao, J. W. Ager, J. Zhang, M. Hettick, M. C. Hersan, A. P. Pisano, R. S. Fearing, A. Javey, *Nat. Commun.* **2014**, *5*, 1.
- [196] T. Lan, Y. Hu, G. Wu, X. Tao, W. J. Chen, *Mater. Chem. C* **2015**, *3*, 1888.
- [197] S. Lu, B. Panchapakesan, *Nanotechnology* **2005**, *16*, 2548.
- [198] J. Deng, J. Li, P. Chen, X. Fang, X. Sun, Y. Jiang, W. Weng, B. Wang, H. Peng, *J. Am. Chem. Soc.* **2016**, *138*, 225.
- [199] D. Kim, H. S. Lee, J. Yoon, *Sci. Rep.* **2016**, *6*, 20921.
- [200] L. Chen, M. Weng, P. Zhou, L. Zhang, Z. Huang, W. Zhang, *Nanoscale* **2017**, *9*, 9825.
- [201] Y. Hu, J. Liu, L. Chang, L. Yang, A. Xu, K. Qi, P. Lu, G. Wu, W. Chen, Y. Wu, *Adv. Funct. Mater.* **2017**, *27*, 1704388.
- [202] K. W. Kwan, S. J. Li, N. Y. Hau, W. D. Li, S. P. Feng, A. H. W. Ngan, *Sci. Robot.* **2018**, *3*, 4051.
- [203] R. Yin, W. Xu, M. Kondo, C.-C. Yen, J. L. Mamiya, T. Ikeda, Y. Yu, *J. Mater. Chem.* **2009**, *19*, 3141.
- [204] C. Li, Y. Liu, X. Huang, H. Jiang, *Adv. Funct. Mater.* **2012**, *22*, 5166.
- [205] O. M. Wani, H. Zeng, A. Priimagi, *Nat. Commun.* **2017**, *8*, 15546.
- [206] M. Rogóz, H. Zeng, C. Xuan, D. S. Wiersma, P. Wasylczyk, *Adv. Opt. Mater.* **2016**, *4*, 1689.
- [207] A. H. Gelebart, D. J. Mulder, M. Varga, A. Konya, G. Vantomme, E. W. Meijer, R. L. B. Selinger, D. J. Broer, *Nature* **2017**, *546*, 632.
- [208] J. J. Wie, M. R. Shankar, T. J. White, *Nat. Commun* **2016**, *7*, 13260.
- [209] X. Dong, J. Xu, X. Xu, S. Dai, X. Zhou, C. Ma, G. Cheng, N. Yuan, J. Ding, *ACS Appl. Mater. Interfaces* **2020**, *12*, 28.
- [210] H. Deng, C. Zhang, J. Su, Y. Xie, C. Zhang, J. Lin, *J. Mater. Chem. B* **2018**, *6*, 5415.
- [211] Y. Liu, B. Shaw, M. Dickey, J. Genzer, *Sci. Adv.* **2017**, *3*, e1602417.
- [212] R. Kamm, R. Bashir, N. Arora, R. Dar, M. Gillette, L. Griffith, M. Kemp, K. Kinlaw, M. Levin, A. Martin, T. McDevitt, R. Nerem, M. Powers, T. Saif, J. Sharpe, S. Takayama, S. Takeuchi, R. Weiss, K. Ye, H. Yevick, M. Zaman, *APL Bioeng.* **2018**, *2*, 040901.
- [213] A. Cangialosi, C. Yoon, J. Liu, Q. Huang, J. Guo, T. Nguyen, D. Gracias, R. Schulman, *Science* **2017**, *357*, 1126.
- [214] H. Wang, M. Pumera, *Adv. Funct. Mater.* **2018**, *28*, 1705421.
- [215] B. J. Williams, S. V. Anand, J. Rajagopalan, M. T. A. Saif, *Nat. Commun.* **2014**, *5*, 3081.
- [216] S.-J. Park, M. Gazzola, K. S. Park, S. Park, V. D. Santo, E. L. Blevins, J. U. Lind, P. H. Campbell, S. Dauth, A. K. Capulli, F. S. Pasqualini, S. Ahn, A. Cho, H. Yuan, B. M. Maoz, R. Vijaykumar, J.-W. Choi, K. Deisseroth, G. V. Lauder, *Science* **2016**, *353*, 158.
- [217] J. L. Drury, D. J. Mooney, *Biomaterials* **2003**, *24*, 4337.

- [218] C. L. Randall, E. Gultepe, D. H. Gracias, *Trends Biotechnol.* **2012**, 30, 138.
- [219] M. Ma, L. Guo, D. G. Anderson, R. Langer, *Science* **2013**, 339, 186.
- [220] H. Yu, T. Ikeda, *Adv. Mater.* **2011**, 23, 2149.
- [221] C. Loewenberg, M. Balk, C. Wischke, M. Behl, A. Lendlein, *Acc. Chem. Res.* **2017**, 50, 723.
- [222] H. Ko, A. Javey, *Acc. Chem. Res.* **2017**, 50, 691.
- [223] X. Zhang, C. Pint, M. Lee, B. Schubert, A. Jamshidi, K. Takei, H. Ko, A. Gillies, R. Bardhan, J. Urban, M. Wu, R. Fearing, A. Javey, *Nano Lett.* **2011**, 11, 3239.
- [224] C. Li, Y. Liu, X. Huang, H. Jiang, *Adv. Funct. Mater.* **2012**, 22, 5166.
- [225] R. R. Kohlmeyer, J. Chen, *Angew. Chem., Int. Ed.* **2013**, 52, 9234.
- [226] Y. Zhao, L. Song, Z. Zhang, L. Qu, *Energy Environ. Sci.* **2013**, 6, 3520.
- [227] E. Wang, M. S. Desai, S. W. Lee, *Nano Lett.* **2013**, 13, 2826.
- [228] Y. Yang, W. Zhan, R. Peng, C. He, X. Pang, D. Shi, T. Jiang, Z. Lin, *Adv. Mater.* **2015**, 27, 6376.
- [229] J. S. Evans, Y. Sun, B. Senyuk, P. Keller, V. M. Pergamenshchik, T. Lee, I. I. Smalyukh, *Phys. Rev. Lett.* **2013**, 110, 187802.
- [230] X. Liu, R. Wei, P. T. Hoang, X. Wang, T. Liu, P. Keller, *Adv. Funct. Mater.* **2015**, 25, 3022.
- [231] X. Liu, X. Wang, T. Liu, P. Keller, *Macromolecules* **2016**, 49, 8322.
- [232] K. K. Hon, D. Corbett, E. M. Terentjev, *Eur. Phys. J. E* **2008**, 25, 83.
- [233] Z. Qin, J. C. Bischof, *Chem. Soc. Rev.* **2012**, 41, 1191.
- [234] A. Gandini, *Prog. Polym. Sci.* **2013**, 38, 1.
- [235] L. Liu, M. Liu, L. Deng, B. Lin, H. Yang, *J. Am. Chem. Soc.* **2017**, 139, 11333.
- [236] H. Tian, Z. Wang, Y. Chen, J. Shao, T. Gao, S. Cai, *ACS Appl. Mater. Interfaces* **2018**, 10, 37760.
- [237] L. L. Howell, *Compliant Mechanisms*, Wiley, New York, USA **2001**.
- [238] S. T. Smith, *Flexures: Elements of Elastic Mechanisms*, CRC Press, Boca Raton, FL **2000**.
- [239] D. L. Blanding, *Exact Constraint: Machine Design Using Kinematic Principles*, ASME Press, New York **1999**.
- [240] O. Sigmund, K. Maute, *Struct. Multidiscip. Optim.* **2013**, 48, 1031.
- [241] M. Y. Wang, X. Wang, D. Guo, *Comput. Methods Appl. Mech. Eng.* **2003**, 192, 227.
- [242] M. P. Bendsøe, N. Kikuchi, *Comput. Methods Appl. Mech. Eng.* **1988**, 71, 197.
- [243] C. J. Kim, Y. M. Moon, S. Kota, *J. Mech. Des. Trans. ASME* **2008**, 130, 022308.
- [244] X. Huang, Y. M. Xie, *Struct. Multidiscip. Optim.* **2010**, 41, 671.
- [245] M. P. Bendsoe, O. Sigmund, *Topology Optimization: Theory, Methods, and Applications*, Springer-Verlag, Heidelberg, Germany **2003**.
- [246] Y. M. Xie, G. P. Steven, *Evolutionary Structural Optimization*, Springer-Verlag, London, UK **1997**.
- [247] M. T. Pham, T. J. Teo, S. H. Yeo, *Precis. Eng.* **2017**, 47, 131.
- [248] G. Z. Lum, T. J. Teo, G. Yang, S. H. Yeo, M. Sitti, *Precis. Eng.* **2015**, 39, 125.
- [249] G. Z. Lum, T. J. Teo, S. H. Yeo, G. Yang, M. Sitti, *Precis. Eng.* **2015**, 42, 195.
- [250] R. D. Kornbluh, R. Pelrine, H. Prahlad, R. Heydt, *MEMS/MOEMS Components and Their Applications* (Eds: S. W. Janson, A. K. Henning), SPIE, San Jose, CA **2004**, p. 13.
- [251] N. C. Tsai, C. Y. Sue, *Sens. Actuators, A Phys.* **2007**, 134, 555.
- [252] M. Wehner, M. T. Tolley, Y. Mengüç, Y. L. Park, A. Mozeika, Y. Ding, C. Onal, R. F. Shepherd, G. M. Whitesides, R. J. Wood, *Soft Robot.* **2014**, 1, 263.
- [253] M. De Volder, D. Reynaerts, *J. Micromech. Microeng.* **2010**, 20, 043001.
- [254] How Pneumatic Actuators Work: Pneumatic Actuator Uses & Applications, <https://www.semcor.net/blog/advantages-of-pneumatic-actuators/> (accessed: April 2020).
- [255] E. B. Dolan, C. E. Varela, K. Mendez, W. Whyte, R. E. Levey, S. T. Robinson, E. Maye, J. O'Dwyer, R. Beatty, A. Rothman, Y. Fan, J. Hochstein, S. E. Rothenbucher, R. Wylie, J. R. Starr, M. Monaghan, P. Dockery, G. P. Duffy, E. T. Roche, *Sci. Robot.* **2019**, 4, 7043.
- [256] H. Yang, B. S. Yeow, Z. Li, K. Li, T.-H. Chang, L. Jing, Y. Li, J. S. Ho, H. Ren, P.-Y. Chen, *Sci. Robot.* **2019**, 4, 7020.
- [257] M. Su, R. Xie, Y. Zhang, X. Kang, D. Huang, Y. Guan, H. Zhu, *Appl. Sci.* **2019**, 9, 2999.
- [258] R. K. Katzschnmann, A. D. Marchese, D. Rus, *Springer Tracts in Advanced Robotics*, Springer, Berlin **2016**, pp. 405–420.
- [259] K. C. Galloway, K. P. Becker, B. Phillips, J. Kirby, S. Licht, D. Tchernov, R. J. Wood, D. F. Gruber, *Soft Robot.* **2016**, 3, 23.
- [260] N. R. Sinatra, C. B. Teeple, D. M. Vogt, K. K. Parker, D. F. Gruber, R. J. Wood, *Sci. Robot.* **2019**, 4, 5425.
- [261] M. Jin, X. Zhang, *Mech. Mach. Theory* **2016**, 95, 42.
- [262] N. W. Bartlett, M. T. Tolley, J. T. B. Overvelde, J. C. Weaver, B. Mosadegh, K. Bertoldi, G. M. Whitesides, R. J. Wood, *Science* **2015**, 349, 161.
- [263] S. Rosset, H. R. Shea, *Appl. Phys. A: Mater. Sci. Process.* **2013**, 110, 281.
- [264] J. A. Rogers, T. Someya, Y. Huang, *Science* **2010**, 327, 1603.
- [265] J. A. Rogers, *Science* **2010**, 341, 968.
- [266] Y. Yang, Y. Wu, C. Li, X. Yang, W. Chen, *Adv. Intell. Syst.* **2020**, 2, 1900077.
- [267] V. Cacucciolo, J. Shintake, Y. Kuwajima, S. Maeda, D. Floreano, H. Shea, *Nature* **2020**, 572, 516.
- [268] S. R. Nagireddy, K. K. S. Charan, R. B. Mishra, A. M. Hussain, *MRS Adv.* **2020**, 5, 765.
- [269] M. D. Dickey, *Adv. Mater.* **2017**, 29, 1606425.
- [270] O. Kim, H. Kim, U. H. Choi, M. J. Park, *Nat. Commun.* **2016**, 7, 1.
- [271] G. Wu, Y. Hu, Y. Liu, J. Zhao, X. Chen, V. Whoehling, C. Plesse, G. T. M. Nguyen, F. Vidal, W. Chen, *Nat. Commun.* **2015**, 6, 1.
- [272] C. B. Eaker, M. D. Dickey, *Appl. Phys. Rev.* **2016**, 3, 031103.
- [273] P. Rinne, I. Pöldsalu, U. Johanson, T. Tamm, K. Pöhako-Esko, A. Punning, D. V. D. Ende, A. Aabloo, *Smart Mater. Struct.* **2019**, 28, 074002.
- [274] J. H. Kim, S. R. Kim, H. J. Kil, Y. C. Kim, J. W. Park, *Nano Lett.* **2018**, 18, 4531.
- [275] H. Wang, M. Totaro, L. Beccai, *Adv. Sci.* **2018**, 5, 1800541.
- [276] X. Wang, R. Guo, J. Liu, *Adv. Mater. Technol.* **2019**, 4, 1800549.
- [277] C. Keplinger, J. Y. Sun, C. C. Foo, P. Rothemund, G. M. Whitesides, Z. Suo, *Science* **2013**, 341, 984.
- [278] T. Kim, D. M. Kim, B. J. Lee, J. Lee, *Sensors* **2019**, 19, 4250.
- [279] K. Li, X. Cheng, F. Zhu, L. Li, Z. Xie, H. Luan, Z. Wang, Z. Ji, H. Wang, F. Liu, Y. Xue, C. Jiang, X. Feng, L. Li, J. A. Rogers, Y. Huang, Y. Zhang, *Adv. Funct. Mater.* **2019**, 29, 1806630.
- [280] S. Palagi, P. Fischer, *Nat. Rev. Mater.* **2018**, 3, 113.
- [281] S. Mao, E. Dong, H. Jin, M. Xu, S. Zhang, J. Yang, K. Low, J. *Bionic Eng.* **2014**, 11, 400.
- [282] D. J. Preston, H. J. Jiang, V. Sanchez, P. Rothemund, J. Rawson, M. P. Nemitz, W.-K. Lee, Z. Suo, C. J. Walsh, G. M. Whitesides, *Sci. Robot.* **2019**, 4, 5496.
- [283] S. Bauer, S. Bauer-Gogonea, I. Graz, M. Kaltenbrunner, C. Keplinger, R. Schwödiauer, *Adv. Mater.* **2014**, 26, 149.
- [284] M. L. Hammock, A. Chortos, B. C.-K. Tee, J. B. H. Tok, Z. A. Bao, *Adv. Mater.* **2013**, 25, 5997.
- [285] F. Ilievski, A. D. Mazzeo, R. F. Shepherd, X. Chen, G. M. Whitesides, *Angew. Chem., Int. Ed. Engl.* **2011**, 50, 1890.
- [286] S. Kim, C. Laschi, B. Trimmer, *Trends Biotechnol.* **2013**, 31, 287.
- [287] S. I. Rich, R. J. Wood, C. Majidi, *Nat. Electron.* **2018**, 1, 102.
- [288] M. Calisti, M. Giorelli, G. Levy, B. Mazzolai, B. Hochner, C. Laschi, P. Dario, *Bioinspir. Biomim.* **2011**, 6, 036002.

- [289] H.-T. Lin, G. G. Leisk, B. Trimmer, *GoQBot. Bioinspir. Biomim.* **2011**, 6, 026007.
- [290] R. V. Martinez, J. L. Branch, C. R. Fish, L. Jin, R. F. Shepherd, R. M. D. Nunes, Z. Suo, G. M. Whitesides, *Adv. Mater.* **2013**, 25, 205.
- [291] R. Deimel, O. Brock, *Int. J. Robot. Res.* **2016**, 35, 161.
- [292] X. Zhou, C. Majidi, O. M. O'Reilly, *Int. J. Solids Struct.* **2015**, 64, 155.
- [293] A. W. Feinberg, A. Feigel, S. S. Shevkoplyas, S. Sheehy, G. M. Whitesides, K. K. Parker, *Science* **2007**, 317, 1366.
- [294] J. C. Nawroth, H. Lee, A. W. Feinberg, C. M. Ripplinger, M. L. McCain, A. Grosberg, J. O. Dabiri, K. K. Parker, *Nat. Biotechnol.* **2012**, 30, 792.
- [295] C. Cvetkovic, R. Raman, V. Chan, B. J. Williams, M. Tolish, P. Bajaj, M. S. Sakar, H. H. Asada, M. T. A. Saif, R. Bashir, *Proc. Natl. Acad. Sci. USA* **2014**, 111, 10125.
- [296] Y. Ding, F. Wu, C. Tan, *Life* **2014**, 4, 1092.
- [297] M. B. Elowitz, S. Leibler, *Nature* **2000**, 403, 335.
- [298] A. S. Khalil, J. J. Collins, *Nat. Rev. Genet.* **2010**, 11, 367.
- [299] C. M. Tan, S.-J. Lo, P. R. LeDuc, C.-M. Cheng, *Lab Chip* **2012**, 12, 3654.
- [300] M. A. TerAvest, C. M. Ajo-Franklin, *Biotechnol. Bioeng.* **2016**, 113, 687.
- [301] K. B. Justus, T. Hellebrekers, D. D. Lewis, A. Wood, C. Ingham, C. Majidi, P. R. LeDuc, C. Tan, *Sci. Robot.* **2019**, 4, eaax0765.
- [302] N. Qaiser, S. Khan, K. Chow, M. Cordero, I. Wicaksono, M. Hussain, *Adv. Mater. Technol.* **2018**, 3, 1800344.
- [303] J. Rojas, G. Torres Sevilla, M. Ghoneim, S. Inayat, S. Ahmed, A. Hussain, M. Hussain, *ACS Nano* **2014**, 8, 1468.
- [304] G. Torres Sevilla, M. Ghoneim, H. Fahad, J. Rojas, A. Hussain, M. Hussain, *ACS Nano* **2014**, 8, 9850.
- [305] J. Rojas, G. Torres Sevilla, M. Hussain, *Sci. Rep.* **2013**, 3, 2609.
- [306] M. Ghoneim, M. Zidan, M. Alnassar, A. Hanna, J. Kosel, K. Salama, M. Hussain, *Adv. Electr. Mat.* **2015**, 1, 1500045.
- [307] N. El-Atab, W. Babatain, R. Bahabry, R. Alshanbari, R. Shamsuddin, M. Hussain, *ACS Appl. Mater. Int.* **2020**, 12, 2269.
- [308] R. R. Bahabry, A. T. Kutbee, S. M. Khan, A. C. Sepulveda, I. Wicaksono, M. Nour, N. Wehbe, A. S. Almislem, M. T. Ghoneim, G. A. Torres Sevilla, A. Syed, S. F. Shaikh, M. M. Hussain, *Adv. Ener. Mat.* **2018**, 8, 1702221.
- [309] N. El-Atab, N. Qaiser, R. Bahabry, M. Hussain, *Adv. Energy Mater.* **2019**, 9, 1902883.
- [310] N. El-Atab, R. Shamsuddin, R. Bahabry, M. M. Hussain, in *IEEE 46th Photovoltaic Specialists Conf. (PVSC)*, IEEE, Piscataway, NJ **2019**, pp. 1499–1501.



**Nazek El-Atab** received her Ph.D. degree in interdisciplinary engineering from the Masdar Institute of Science and Technology, Abu Dhabi, in 2017, funded by the Office of Naval Research Global. She is currently a post-doctoral research fellow with Professor Muhammad Mustafa Hussain at the MMH Labs at King Abdullah University of Science and Technology (KAUST), Saudi Arabia. Her current research focuses on the design and fabrication of futuristic electronics.



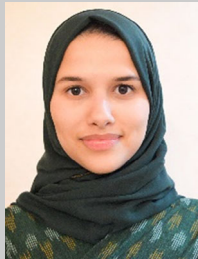
**Rishabh B. Mishra** is currently pursuing his M.Sc. degree by research in electronics and communication engineering from International Institute of Information Technology (IIIT)—Hyderabad, India. Before starting his M.Sc., he has been a research trainee in CSIR-Central Electronics Engineering Research Institute (CEERI), Pilani, India. Currently, he is a visiting student at the MMH Labs, Electrical Engineering, King Abdullah University of Science and Technology (KAUST), Saudi Arabia under the guidance of Prof. Muhammad M. Hussain. His research interests are flexible and stretchable electronics, low-cost MEMS devices, and soft sensing/actuation.



**Fhad Al-Modaf** is a junior mechanical engineering student at King Abdulaziz University (KAU), Jeddah, Saudi Arabia. Currently, he is a visiting student working under the supervision of Prof. Muhammad M. Hussain at the MMH Labs, King Abdullah University of Science and Technology (KAUST), Thuwal, Saudi Arabia. His research interests include soft robotics and programmable self-assembly.



**Lana N. Joharji** is currently an undergraduate senior student majoring in electrical and computer engineering at King Abdulaziz University (KAU), Saudi Arabia. She is also a visiting student conducting research under the supervision of Prof. Muhammad M. Hussain at the MMH Labs, King Abdullah University of Science and Technology (KAUST), Thuwal, Saudi Arabia. Her research interests include robotics, cost-efficient MEMS devices, and soft actuation.



**Aljohara A. Alsharif** is currently pursuing her B.Sc. degree in electrical and computer engineering at King Abdulaziz University (KAU), Saudi Arabia. She is also a visiting student at the MMH Labs at King Abdullah University of Science and Technology (KAUST), Saudi Arabia. Her research interests include humanoid and flexible robotics developments along with analog and digital electronic circuits analysis, design, and implementation.



**Haneen Mohammed Alamoudi** is a senior undergraduate student majoring in electrical and computer engineering at King Abdulaziz University (KAU), Saudi Arabia. Currently, she is a visiting student at the MMH Labs at King Abdullah University of Science and Technology (KAUST), Saudi Arabia. Her research interests include robotics, machine learning, and deep learning.



**Nadeem Qaiser** received his Ph.D. degree in mechanical engineering at Korea Advanced Institute of Science and Technology (KAIST), Daejeon, South Korea. His skills include the use of solid mechanics (Numerical modeling + experimental testing). Currently, he is working as a research scientist at KAUST since March 2017.



**Muhammad Mustafa Hussain** received his Ph.D. in electrical and computer engineering from the University of Texas at Austin in 2005. Currently, he is a professor of Electrical Engineering at King Abdullah University of Science and Technology (KAUST) and a professor of EECS of University of California, Berkeley. Before joining KAUST, Prof. Hussain was Program Manager of Emerging Technology Program in SEMATECH, Inc. Austin, Texas. He is the Fellow of IEEE, American Physical Society (APS), Institute of Physics, UK and Institute of Nanotechnology, UK. His research interest is to expand the horizon of complementary metal–oxide–semiconductor (CMOS) electronics and technology for futuristic applications.